

Proceedings of the
*14th International Symposium on Vibrations of
Continuous Systems*

Grundlsee, Salzkammergut, Austria

27th July to 2nd August 2025



Preface

It is with great pleasure that we present the Proceedings of the 14th International Symposium on Vibrations of Continuous Systems (ISVCS 2025), held from July 27 to August 2, 2025, in the serene and inspiring setting of Lake Grundlsee, in the Austrian Salzkammergut region. This unique Symposium continues a long-standing tradition of bringing together leading researchers and seasoned experts in the field of vibrations and dynamics of continuous systems.

Since its first edition in 1997, ISVCS has provided a distinctive platform for the open exchange of ideas, the presentation of both mature and developing research, and the fostering of collaborations in a relaxed and collegial environment. The scientific scope of the Symposium includes, but is not limited to, the vibratory behavior of structural elements such as strings, beams, membranes, plates, and shells. What sets ISVCS apart is its unique discussion-driven format, designed to promote in-depth engagement with topics and encourage participants to share not only their latest results but also their personal insights and reflections over years of work in the field. The daily schedule—technical sessions in the morning, and outdoor excursions in the afternoon, and social and scientific gatherings in the evening—facilitates both rigorous academic dialogue and the building of lasting professional relationships.

This volume includes short summaries of the technical presentations delivered at the Symposium, alongside brief biographical sketches of the participants. These contributions reflect the depth and breadth of research currently being conducted in the study of continuous systems and provide a valuable snapshot of the field as it stands today. This year marks the third edition of ISVCS held without the presence of Art Leissa, the founder of the Symposium. Art's vision and enthusiasm shaped ISVCS into the vibrant and collaborative community it has become. We remember him fondly and are proud to continue the Symposium in his spirit, welcoming new voices and encouraging the next generation of researchers to carry forward the tradition of excellence, curiosity, and collegiality.

We would like to express our sincere gratitude to all participants for their contributions and to those who have worked hard to organize and support this event. We hope that the Symposium continues to inspire constructive discussions, foster new collaborations, and deepen our collective understanding of the complex and beautiful dynamics of continuous systems.

The Organizing Committee

General Chairman Francesco Pellicano
Editorial Chairman Piotr Cupial
Local Arrangements Chairman Y. Vetyukov, J. Scheidl
Publicity Chairman S. Honda
Honorary Chairman E. Carrera

Past Symposia

The **1st** International Symposium:
The Stanley Hotel, Estes Park, Colorado, USA
August 11-15, 1997

The **2nd** International Symposium:
The Sunstar Hotel, Grindelwald, Switzerland
July 11-16, 1999

The **3rd** International Symposium:
Jackson Lake Lodge, Grand Teton National Park, Wyoming, USA
July 23-27, 2001

The **4th** International Symposium:
Keswick, Lake District, England
July 23-27, 2003

The **5th** International Symposium:
Berchtesgaden at Lake Königssee, Germany
July 25-29, 2005

The **6th** International Symposium:
PlumpJack Squaw Valley Inn, Olympic Valley, California, USA
July 23-27, 2007

The **7th** International Symposium:
Zakopane, Poland
July 19-25, 2009

The **8th** International Symposium:
Whistler, British Columbia, Canada
July 18-22, 2011

The **9th** International Symposium:
Courmayeur, Italy
July 22-26, 2013

The **10th** International Symposium:
Stanley Hotel, Estes Park, Colorado, USA,
July 26-31, 2015

The **11th** International Symposium:
the Royal Victoria Hotel, Llanberis, Snowdonia, Wales, UK,
July 16-21, 2017

The **12th** International Symposium:
the Sporthotel Panorama, Str. Sciuz, 1, 39033 Corvara In Badia BZ – Italy,
July 28 - August 2, 2019

The **13th** International Symposium:
Pomeroy, Kananaskis Mountain Lodge, Alberta, CANADA
30th July to 4th August 2023

Details of the Proceedings of the past Symposia can be found at
<http://www.isvcs.org>

Table of Contents

Presentation Summaries (Only speaker are mentioned)

01. Delamination detection using the tracking of beam's natural frequencies

Haim Abramovich..... Page 1

02. Various Dynamic Pull-in Mechanisms of Electrically Actuated MEMS/ NEMS

Igor Andrianov..... Page 5

03. Free Vibration of Axially Loaded Axial-Bending Coupled Timoshenko-Ehrenfest Beams

Ranjan Banerjee..... Page 9

04. Vibrations of Rectangular Plates with Mixed Boundary Conditions:

Moshe Eisenberger..... Page 13

05. Variable-fidelity finite elements for nonlinear steady-state responses of structures:

Matteo Filippi.....Page 16

06. The sliding beam formulation revisited: From the spaghetti problem to hot-rolled slabs:

Alexander Humer..... Page 19

07. A study on the spacing of roving body placement for natural frequency-based crack detection:

Sinniah Ilanko..... Page 23

08. Energy element method for vibration analysis of plates and solids with complex geometries:

Zhao Jing..... Page 27

09. Dynamic Analysis of Temperature-Sensitive Bi-Metallic Beams:

Moslem Molaie..... Page 31

10. Dynamic Modelling of Rigid-Flexible Coupled Beams with Flexoelectric Actuation

Fan Mu Page 34

11. Use of Non-integer Boundary Index for Vibration of Elastically Supported Continuous Systems:	
Yoshihiro Narita.....	Page 38
12. Linearized vibration analysis of fibre-reinforced multilayered soft materials by high order 2D finite elements:	
Alfonso Pagani.....	Page 42
13. Shells under Random excitation: unusual phenomena:	
Francesco Pellicano.....	Page 46
14. Dynamics of a moving bandsaw blade in a narrow lubricated gap subjected to parametric excitation in axial direction	
Jakob Scheidl.....	Page 50
15. Structural Damage Identification Leveraging High-Frequency Interrogation and Inverse Dynamic Analysis	
Jiong Tang.....	Page 53
16. Distributed Control of Multi-function Structronic Shell Systems with Piezo/Flexo-electric, Electro/Photo-strictive, LaSMP Actuators:	
Hornsen (HS) TZOU	Page 57
17. Asymptotic justification of the energy approach for estimating changes of natural frequencies of elastic structures due to damage:	
Yury Vetyukov.....	Page 61
18. Exact computation of lower bound eigenvalues of vibrating beams:	
Andrew Watson.....	Page 65
19. Influence of temperature on metamaterial structure dynamics: an experimental study:	
Antonio Zippo.....	Page 69

Biosketches of participants page

Haim Abramovich	page 72
Igor Andrianov	page 73
Ranjan Banerjee	page 74
Moshe Eisenberger	page 75
Matteo Filippi	page 76
Alexander Humer	page 77
Sinniah Ilanko	page 78
Zhao Jing	page 79
Moslem Molaie	page 81
Fan Mu	page 82
Yoshihiro Narita	page 83
Alfonso Pagani	page 84
Francesco Pellicano	page 85
Jakob Scheidl	page 86
Jiong Tang	page 87
Hornsen (HS) TZOU	page 88
Yury Vetyukov	page 89
Andrew Watson	page 90
Antonio Zippo	page 91

Delamination detection using the tracking of beam's natural frequencies

H. Abramovich and S. Penias

Faculty of Aerospace Engineering, Technion, I.I.T., 32000 Haifa, Israel

*haim@technion.ac.il, abramovich.haim@gmail.com

Abstract

The purpose of the present study was to evaluate the effect of inter-laminar delaminations in composite materials on the natural frequencies of a laminated structure. The ability to predict such changes in the natural frequencies, and to measure them, can be translated into an ability to detect delaminations in a composite structure by vibrating it and measuring its natural frequencies.

Inter-laminar delaminations can be the product of faulty manufacturing, which propagates itself in lack of adhesion between the epoxy resin and the graphite fabric. Such delamination might also be the result of time-dependent delamination because of load cycles or environmental effects. This kind of delamination can be propagated into a catastrophic failure of the aircraft itself, see also [1-5]).

In the study, a numeric analysis was performed, in which various types of delaminations existing in a composite beam were modeled and their effects on the natural frequencies were evaluated. The numerical part was followed by an experimental test series aimed at validating the proposed method.

The numerical study considered a rectangular cantilever beam with a high length to width ratio, 1:20, made from 16 Graphite-Epoxy AS4-12k/E7K8 layers, (see Fig. 1)

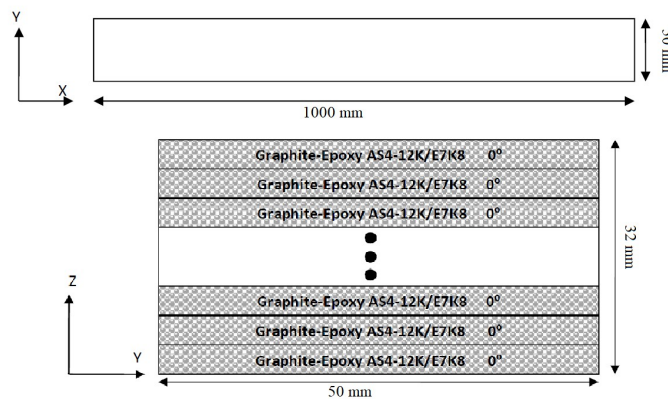


Fig. 1 Geometric dimensions and materials of the calculated beam

The beam's first 10 natural frequencies and mode shapes were numerically calculated, using the ANSYS software code. The delamination was created by changing the boundary conditions of certain elements to an "un-bounded" mode in the code. Fig. 2 presents the delamination shape which was applied between various material's layers.

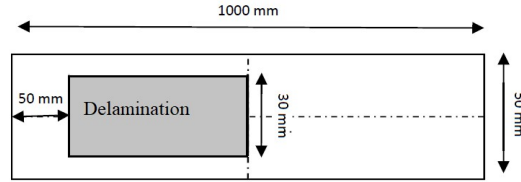


Fig. 2 Delamination shape

Numerical results show that the natural frequencies around the Z axis (sideway bending) remain the same, as expected, therefore those modes will be disregarded. As expected from the literature (see for example [6-9]), the natural modes around the X axis (torque) and the Y axis (bending) show decrease in the natural frequencies as the delamination is closer to the mid-layer of the beam (Figs. 3,4).

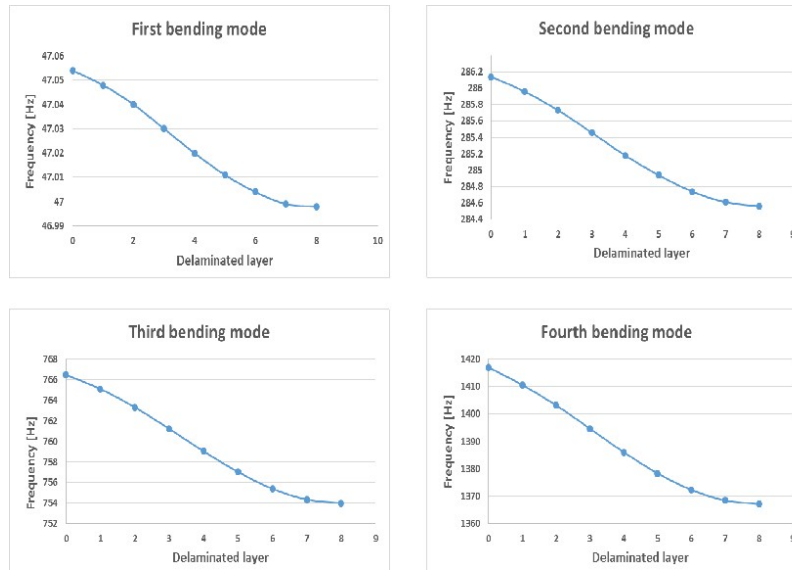


Fig. 3 The first four bending modes

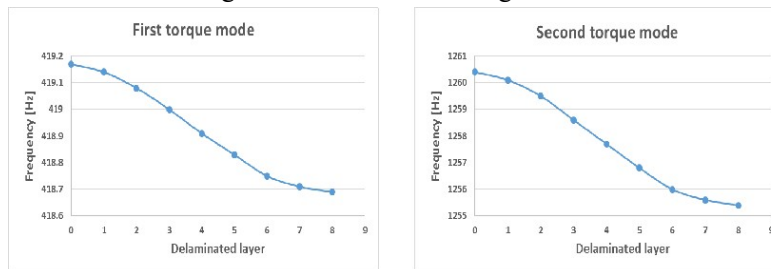


Fig. 4 The first two torsion modes

Delamination of different sizes were also considered, all symmetric in respect to the X axis. The numeric results show that, as expected, the natural frequencies in the bending and torque modes decrease with the increase in delamination size. Figures 5 and 6 show the results for delamination of various sizes and different layers, for the 4th bending mode and for the 2nd torque mode, respectively.

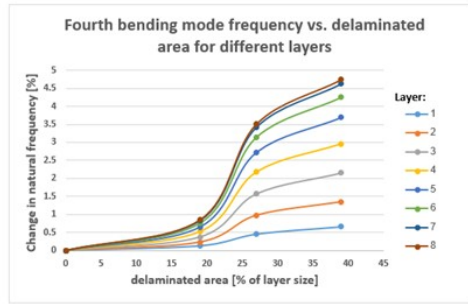


Fig. 5 Forth bending mode

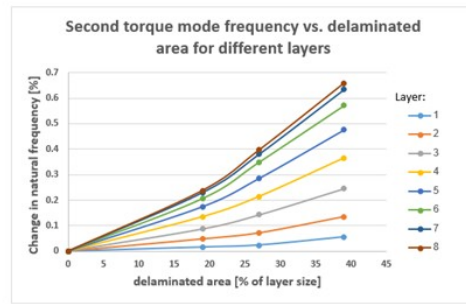


Fig. 6 Secomd torque mode

In addition, the effect of the delamination location within the layer was also investigated for different configurations, as shown in Fig. 7, yielding interesting results.

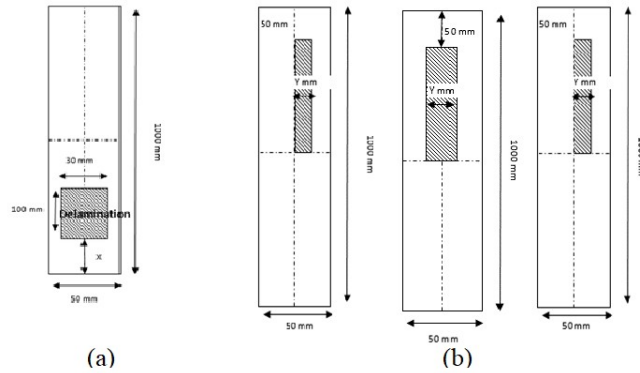


Fig. 7 (a)- position in the x direction, (b)- position in the y direction

An experimental study was also conducted on four specimens, as depicted in Fig. 8.

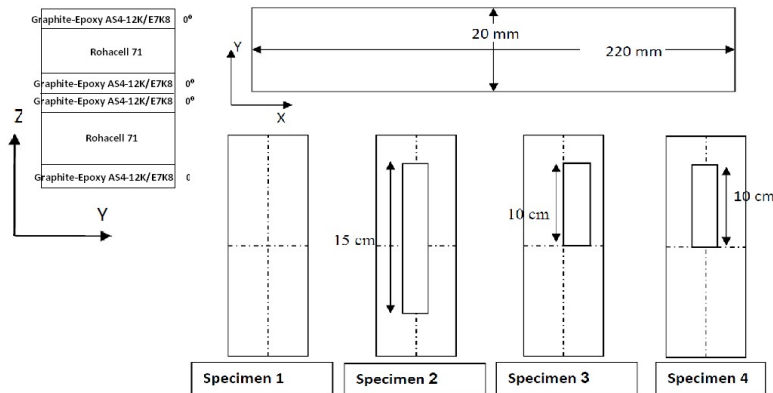


Fig. 8 The experimental specimens

The comparison of the experimental results to numerical ones shows a relatively good matching, thus increasing the confidence in the proposed method for detecting delamination in laminated composite beams using dynamic excitation.

To sum up, some interesting conclusions can be drawn:

- Effect of delamination on the bending and torque modes natural frequencies increase as the delamination is closer to the mid-layer of the beam.
- Natural bending and torque frequencies decrease as the delamination area is larger.

- c. Bending frequencies are affected by delamination's size alone. Torque frequencies are affected by the deviation of the delamination from symmetry.
- d. Change in natural bending frequencies would change with the location of the delamination on the X axis. The frequency change plot resembles the mode shape.
- e. Composite beams have significantly larger effect on natural frequencies when delamination is introduced, than isotropic materials.
- f. Clamped-clamped beams showed a more significant change in natural frequencies than cantilever and simply supported beams.

All the conclusions above show that a simple measurement of the first few beams' bending and torque natural frequencies of a beam, can give a lot of information regarding a possible delamination:

- Delaminated layer – by the change in bending modes frequencies.
- Delamination size – by change in both torque and bending modes
- Delamination location:
 - o In the X axis – by difference between various bending modes.
 - o In the Y axis – by change in torque modes

For better detection, it is suggested to clamp the beam at both sides. The present approach is valid, if the natural frequencies of the perfect beam are available.

References

- [1] Paul, D., Kelly, L., Venkayya, V. and Hess, T., Evaluation of US military aircraft structures technology, *Journal of Aircraft*, Vol. 39, No. 1, 2002, pp. 18–29.
- [2] Hojo, M., Tanaka, K., Gustafson, C.G. and Hayashi, R., Effect of stress ratio on fatigue cracks in unidirectional CFRP, *Composite Science and Technology* Vol. 29, 1987, pp. 273-292.
- [3] Kenane, M. and Benzeggagh, M.L., Mixed-mode delamination fracture toughness of unidirectional glass/epoxy composites under fatigue loading, *Composites Science and Technology* Vol. 57, 1997, pp. 597-605.
- [4] Asp, L.E., Sjogren, A. and Greenhalgh, E.S., Delamination growth and thresholds in a Carbon/Epoxy composite under fatigue loading", *Journal of Composites Technology and Research*, Vol. 23, No 2, April 2001, pp.55-68.
- [5] O'Brien, T.K., Characterization of a delamination onset and growth in a composite laminate, in *Damage in Composite Materials: Basic Mechanisms, Accumulation, Tolerance, and Characterization* Damage, ASTM STP 775, K.L. Reifsnider, Editor., American Society for Testing and Materials, 1982, 28p.
- [6] Miller, A.G., Review of limit loads of structures containing defects, *International Journal of Pressure Vessels and Piping*, Vol. 32, Issues 1-4, 1988, pp. 197-327.
- [7] Adams, R.D. and Cawley, P., A review of defect types and nondestructive testing techniques for composites and bonded joints, *NDT International*, Vol.21 No. 4, August 1988, pp. 208-222.
- [8] Scott, I.G. and Scala, C.M., A review of non-destructive testing of composite materials, *NDT International*. Vol. 15, No.2, April 1982, pp. 75-86.
- [9] Schnars, U. and Henrich, R., Applications of NDT methods on composite structures in aerospace Industry, In *Proc. Of the Conference on Damage in Composite Materials*. Stuttgart, Germany, 18-19 September 2006, pp. 1-8.

Various Dynamic Pull-in Mechanisms of Electrically Actuated MEMS/NEMS

Igor Andrianov^{*}, Lelya Khajiyeva[#], Steve Koblik[†], Galina Starushenko[§]

^{*} Chair and Institute of General Mechanics
RWTH Aachen University
Eilfschornsteinstrasse 18, D-52062,
Aachen, Germany
Igor.andrianov@gmail.com

[#] Department of Mathematical and Computer
Modelling
Al-Farabi Kazakh National University
Al-Farabi Av. 71, 050040, Almaty, Kazakhstan
Lelya.Khajiyeva@kaznu.edu.kz

[†] Independent Researcher
8110 Birchfield Drive, IN 46268,
Indianapolis, USA
Stevekoblik8110@comcast.net

[§] Department of Construction, Geotechnics and
Geomechanics
Dnipro University of Technology
Av. Dm. Yavornytskoho 19, 49005, Dnipro, Ukraine
Starushenko.H.A@nmu.one

MEMS and NEMS are now widespread in modern engineering. They combine such useful properties as small size, light weight, inexpensive operation, and low-power consumption [1-4].

MEMS and NEMS are interesting and attractive systems that offer unique and intelligent technological solutions. In this regard, the accurate modelling of the mechanical behavior of such structures is of great importance. However, the following difficulties might arise. The electric forces are inherently strongly nonlinear. The micro- and nanoscale components undergo large deflections, that is why geometric nonlinearity is significant. Therefore, the mathematical models for MEMS and NEMS contain power and non-power nonlinearities and are difficult to analyze. One of the essentially nonlinear effects is the pull-in phenomenon, i.e., collapse of the system when values of applied DC or/and AC voltages overcome some threshold [3,4]. If only DC voltage is applied and it increases monotonically, the stable equilibrium (node) and unstable equilibrium (saddle) coincide at a saddle-node bifurcation (static pull-in). Application of the AC voltage can lead to dynamic instabilities of various natures – parametric resonances, nonlinear resonance due to the forcing signal, bifurcations. Such phenomenon is called dynamic pull-in. In the papers [1,2] an effective algorithm was proposed to analyze the pull-in phenomenon for thin-walled MEMS/NEMS. In the present paper, this algorithm is used to analyze various mechanisms of the dynamic pull-in for electrically actuated rectangular micro/nanoplate (Fig. 1).

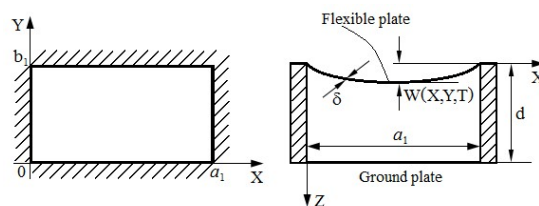


Figure 1. Top and cross-section views of a model of the parallel charged micro/nano rectangular plate.

The nonlinear vibrations of a rectangular micro/nanoplate (Fig. 1) under the action of Coulomb force can be described by the following equation:

$$\frac{\partial^2 w}{\partial t^2} + \psi \frac{\partial w}{\partial t} + \Delta_b^2 w - \left\{ B_1 \left(\int_0^1 \int_0^1 \left(\left(\frac{\partial w}{\partial x} \right)^2 + \frac{1}{b^2} \left(\frac{\partial w}{\partial y} \right)^2 \right) dx dy \right) \Delta_b w \right\} - \frac{(\alpha + \alpha_1 \sin \omega t)^2}{(1-w)^2} = 0, \quad (1)$$

where:

$$\Delta_b = \left(\frac{\partial^2}{\partial x^2} + \frac{1}{b^2} \frac{\partial^2}{\partial y^2} \right); x = X/a_1; y = Y/b_1; b = b_1/a_1; t = \frac{T}{a_1^2} \sqrt{\frac{D}{\rho \delta}}; w(x, y, t) = W(X, Y, T)/d;$$

$$B_1 = \frac{d^2}{2D} B; B = \frac{E \delta}{1-\nu^2}; D = \frac{B \delta^2}{12}; \psi = \frac{a_1^2}{\sqrt{\rho \delta D}} \Psi; \alpha = \frac{a_1^2 V_0}{d} \sqrt{\frac{\varepsilon^* \varepsilon_0}{2dD}}; \alpha_1 = \frac{a_1^2 V_1}{d} \sqrt{\frac{\varepsilon^* \varepsilon_0}{2dD}}; \omega = a_1^2 \Omega \sqrt{\frac{\rho \delta}{D}};$$

$\varepsilon^*, \varepsilon_0$ are the relative and vacuum permittivities; V_0 (V_1) is the magnitude of DC (AC) voltage; Ω is the AC frequency; Ψ is the damping coefficient; ρ is the flexible plate mass density.

We use Berger's approach for flexible plate, within this hypothesis, the influence of geometric nonlinearity is described by the expression in curly brackets in equation (1). For approximation of distributed Coulomb force we apply a parallel capacitor formula and neglect fringe field effect and Casimir/van der Waals forces.

It is assumed that the plate is clamped along the contour

$$w = 0 \text{ at } x = 0, 1; y = 0, 1; \frac{\partial w}{\partial x} = 0 \text{ at } x = 0, 1; \frac{\partial w}{\partial y} = 0 \text{ at } x = 0, 1. \quad (2)$$

To reduce the original PDE to an ODE, we use the following ansatz:

$$w(x, y, t) \approx u(t) \theta(x, y); \theta(x, y) = \sin^2(\pi x) \sin^2(\pi y). \quad (3)$$

Then we apply the Kantorovich procedure and obtain an ODE

$$\frac{d^2 u}{dt^2} + \psi \frac{du}{dt} + c_1 u + c_3 u^3 + (\alpha + \alpha_1 \sin \omega t)^2 I(u) = 0, \quad (4)$$

$$c_1 = \frac{16\pi^4}{9} \left(3 + \frac{2}{b^2} + \frac{3}{b^4} \right); c_3 = \frac{\pi^4}{4} B_1 \left(1 + \frac{1}{b^2} \right)^2; I(u) = \frac{64}{9} \int_0^1 \int_0^1 \frac{\theta(x, y) dx dy}{[1 - u \theta(x, y)]^2}.$$

Let us denote the static pull-in value as α_{pi} . Then for each $0 \leq \alpha < \alpha_{pi}$ there is a stable u_{st} and unstable u_{unst} equilibrium point. Next, we solve equation (4) for given values of DC α ($0 \leq \alpha < \alpha_{pi}$), amplitude α_1 and frequency ω of AC under zero initial conditions. Eq. (4) is solved numerically by the Runge-Kutta method over a longtime interval. We vary the amplitude α_1 and use a binary search to find the value α_{1pi} such that when $\alpha_1 < \alpha_{1pi}$ the displacement u is less than the given value u_{lim} , and for $\alpha_1 \geq \alpha_{1pi}$ the displacement u exceeds u_{lim} . Both u_{unst} and the largest permissible value $u = 1$ were used as u_{lim} . Calculations carried out with $u_{lim} = u_{unst}$ and $u_{lim} = 1.0$ coincided with an accuracy of up to 10^{-4} . The comparison with the results of calculations based on other methods, as well as with experimental results [4] shows sufficient accuracy of the proposed algorithm and the adequacy of the adopted model.

For the simulation, the physical parameters of a typical device [3] were selected: $b=1$, $B_1=6.00$, $\psi=0.100$. The static pull-in value for movable plate with these parameters is $\alpha_{pi}=14.471$. The step size of frequency ω change was chosen to be 0.01. For convenience, the discrete points are connected by continuous curves (Fig. 2-4). Periodic (stable) solutions of Eq. (4) correspond to points α_1 located below the graph $\alpha_{1pi}(\alpha, \omega)$, and non-periodic (unstable) solutions correspond to points α_1 allocated above the specified graph.

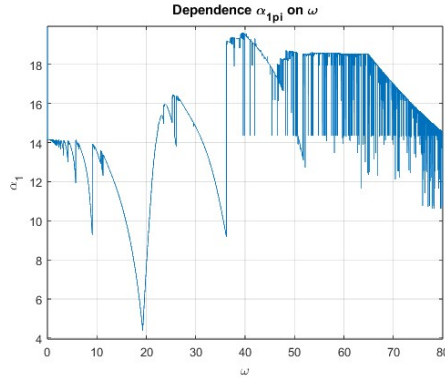


Figure 2. Dependence of the dimensionless dynamic pull-in α_{1pi} on the dimensionless frequency ω in the absence of a DC voltage ($\alpha = 0$).

At low frequencies the difference between values of dynamic and static pull-in is small. At points $\omega \approx 9.0$, $\omega \approx 19.3$, $\omega \approx 36.2$ the value of the dynamic pull-in α_{1pi} is significantly less than α_{pi} , which is explained by the presence of resonances. Let us analyze the nature of these resonances. Eq. (4) for $\alpha = 0$ can be written as follows:

$$\frac{d^2u}{dt^2} + \psi \frac{du}{dt} + c_1u + c_3u^3 = \frac{32}{9}\varphi_1\alpha_1^2(\cos 2\omega t - 1)[I(u) - 1/4] + \frac{8}{9}\varphi_2\alpha_1^2(\cos 2\omega t - 1). \quad (5)$$

The parameters φ_i take the values 0 or 1. Eq. (5) contains both force ($\varphi_1 = 0$, $\varphi_2 = 1$) and parametric ($\varphi_1 = 1$, $\varphi_2 = 0$) excitations. Let us conduct numerical experiments, by neglecting the parametric excitation in one case ($\varphi_1 = 0$, $\varphi_2 = 1$), and by discarding the force excitation ($\varphi_1 = 1$, $\varphi_2 = 0$) in the second case. The results are presented in the Figs. 3 and 4 (note that these figures do not model a real problem, but only illustrate the influence of certain factors).

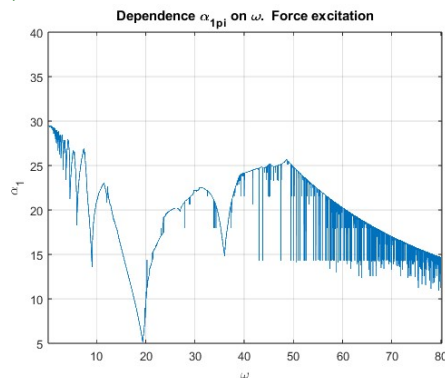


Figure 3. Numerical experiment: force excitation ($\varphi_1 = 0$, $\varphi_2 = 1$).

At the points $\omega \approx 9.1$, $\omega \approx 19.4$, $\omega \approx 36.0$ (Fig. 2) the values of the dynamic pull-in, as can be seen in Fig. 2, are significantly less than at other neighboring points. This confirms the presence of resonances caused by a driving force. We also note that the chaotic behavior of an electromechanical system at high excitation frequencies qualitatively coincides with the behavior of a force driven Duffing equation.

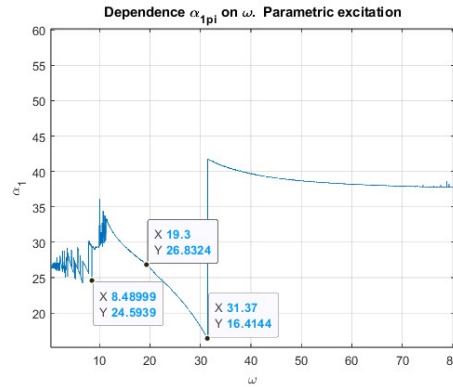


Figure 4. Numerical experiment: pure parametric excitation ($\varphi_1 = 1$, $\varphi_2 = 0$).

In Fig. 4, in the neighborhood of the point $\omega \approx 19.3$, the dynamic pull-in does not have an extremum at all. At the points $\omega \approx 8.5$ and $\omega \approx 31.4$, the dynamic pull-in reaches local minimum values $\alpha_{1pi} \approx 24.6$ and $\alpha_{1pi} \approx 16.3$. This allows us to assume the presence of parametric resonances at these points. In addition, judging by the discontinuous behavior of the solutions, these points may be bifurcation points as well.

Numerical experiments allow us to draw a conclusion about the nature of the emerging resonances. This provides useful information in practical situations. Knowing the resonant frequencies allows us to avoid them in operating electromechanical systems. This can be achieved by changing the AC voltage frequency or by modifying the parameters of the system itself. On the other hand, knowledge of the resonant frequencies allows us to design new and more effective devices [4].

This research was partly funded by the Science Committee of the Ministry of Science and Higher Education of the Republic of Kazakhstan (Grant No. AP 23490543) (for Andrianov, Khajiyeva) and was partly supported by a Simons Foundation (SF) grant (Award ID: 1160642, Project: SF Support to Researchers in Ukraine, Program: Presidential Discretionary-Ukraine Support Grants) (for Starushenko).

References

- [1] Andrianov, I.V.; Awrejcewicz, J.; Koblik, S.G.; Starushenko, G.A.: Nonlinear oscillation of a microbeam due to an electric actuation – Comparison of approximate models. ZAMM, Vol. 104, No. 2, p. e202300091, 2024.
- [2] Andrianov, I.V.; Koblik, S.G.; Starushenko, G.A.: Investigation of electrically actuated geometrically nonlinear clamped circular nanoplate. Acta Mechanica, Vol. 235, No. 2, pp. 1015–1026, 2024.
- [3] Saghir, S.; Younis, M.I.: An investigation of the static and dynamic behavior of electrically actuated rectangular microplates. International Journal of Non-Linear Mechanics, Vol. 85, pp. 81–93, 2016.
- [4] Younis, M.I.: MEMS: Linear and Nonlinear Statics and Dynamics. Springer, 2011.

Free Vibration of Axially Loaded Axial-Bending Coupled Timoshenko-Ehrenfest Beams

J Ranjan Banerjee

School of Science and Technology, City St George's, University of London
Northampton Square, London EC1V 0HB, United Kingdom

Email: j.r.banerjee@citystgeorges.ac.uk

Abstract

The free vibration analysis of an axially loaded Timoshenko-Ehrenfest beam coupled in axial and bending deformations is carried out in this paper for different boundary conditions. First, the governing differential equations of motion in free vibration are developed using Hamilton's principle and then they are solved in closed algebraic form for axial displacement, bending displacement and bending rotation. The expressions for axial force, shear force and bending moment are also obtained in explicit algebraic form. Finally, by applying the boundary conditions, the natural frequencies and mode shapes of the axially loaded axial-bending coupled Timoshenko-Ehrenfest beam are computed for an illustrative example with clamped-free (C-F), pinned-pinned (P-P) and clamped-clamped (C-C) supports at the ends. The results are discussed, and some conclusions are drawn.

1. Introduction

The free vibration behaviour of axial-bending coupled beams using Bernoulli-Euler and Timoshenko-Ehrenfest theories has been investigated by several authors [1-6], but these publications do not generally account for the case when the beam carries an axial load whose effect on the beam's free vibration characteristics can be significant. For an axial-bending coupled Timoshenko-Ehrenfest beam exhibiting free vibration, the inclusion of an axial load increases the level of complexity greatly. The problem does not appear to have been adequately dealt with in the literature. The present paper addresses this problem.

2. Theory

Figure 1 shows a uniform axial-bending coupled Timoshenko-Ehrenfest beam of length L in a right-handed Cartesian coordinate system with the Y -axis coinciding with the beam elastic axis which is the locus of shear centres of the beam cross-sections. A compressive axial load (P) considered to be positive, is assumed to act through the elastic axis of the beam as shown. Note that P can be negative so that tension is included in the theory. The coupling between axial and bending displacements will occur in a beam of this type because of the eccentricity between the centroid (G_c) and shear centre (E_s) of the beam cross-section, see Figure 1. There are many practical cross-sections for which the centroid and shear centre are non-coincident (see Figure 2 of [4]), but the inverted T section is shown in Figure 1 only for convenience. The mass axis which is the locus of the centroid of the beam cross-sections is separated by a distance z_α from the elastic axis, as shown. Now, if v_0 , w_0 and θ are axial displacement, bending displacement and bending rotation of a point on the elastic axis at a distance y from the origin in the coordinate system of Figure 1, the governing differential equations of motion in free vibration of the axially loaded axial-bending coupled Timoshenko-Ehrenfest beam can be obtained by applying Hamilton's principle and they are in the usual notation, given by

$$EA v_0'' - EA z_\alpha \theta'' - \rho A \ddot{v}_0 + \rho A z_\alpha \ddot{\theta} = 0 \quad (1)$$

$$EI_e \theta'' - \rho I_e \ddot{\theta} + \rho A z_\alpha \ddot{v}_0 - EA z_\alpha v_0'' + kAG(w_0' - \theta) = 0 \quad (2)$$

$$kAG(w_0'' - \theta') - Pw_0'' - \rho A \ddot{w}_0 = 0 \quad (3)$$

where EA , EI_e and kAG are axial, bending (about the elastic axis) and shear rigidities of the beam, ρA , ρI_e are mass per unit length and mass moment of inertia per unit length (about the elastic axis) and a prime and an over dot denote partial differentiation with respect to length y and time t , respectively.

The expressions for axial force (f), bending moment (m) and shear force (s) which result from the natural boundary conditions of the Hamiltonian formulation are given by

$$f = -EA v'_0 + EA z_\alpha \theta' \quad (4)$$

$$m = -EI_e \theta' + EA z_\alpha v'_0 \quad (5)$$

$$s = -kAG(w'_0 - \theta) + Pw'_0 \quad (6)$$

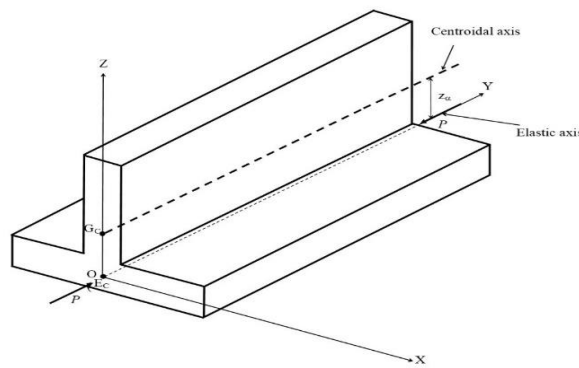


Figure 1. Coordinate system and notation for an axially loaded axial-bending coupled Timoshenko-Ehrenfest beam.

For harmonic oscillation with circular or angular frequency ω , and by introducing the non-dimensional length parameter $\xi=y/L$, Equations (1)-(3) can be solved for the amplitudes of axial displacement (V), bending displacement (W) and bending rotation (Θ) in terms of integration constants A_1 - A_6 to give

$$V(\xi) = \mu k_\alpha A_1 \sinh \alpha \xi + \mu k_\alpha A_2 \cosh \alpha \xi + \mu k_\beta A_3 \sin \beta \xi - \mu k_\beta A_4 \cos \beta \xi + A_5 \sin \gamma \xi + A_6 \cos \gamma \xi \quad (7)$$

$$W(\xi) = A_1 \cosh \alpha \xi + A_2 \sinh \alpha \xi + A_3 \cos \beta \xi + A_4 \sin \beta \xi \quad (8)$$

$$\Theta(\xi) = A_1 \frac{k_\alpha}{L} \sinh \alpha \xi + A_2 \frac{k_\alpha}{L} \cosh \alpha \xi + A_3 \frac{k_\beta}{L} \sin \beta \xi - A_4 \frac{k_\beta}{L} \cos \beta \xi \quad (9)$$

where α , β , γ , k_α , and k_β are given by

$$\alpha = \sqrt{-\frac{C_1}{2} + \frac{\sqrt{C_1^2 + 4C_2}}{2}}; \beta = \sqrt{\frac{C_1}{2} + \frac{\sqrt{C_1^2 + 4C_2}}{2}}; \gamma = \sqrt{\frac{\omega^2 \rho AL^2}{EA}} \quad k_\alpha = \frac{b^2 s^2 + \alpha^2 \lambda^2}{\alpha}; k_\beta = \frac{b^2 s^2 - \beta^2 \lambda^2}{\beta} \quad (10)$$

with

$$C_1 = \frac{(a^2 - \mu^2 b^2) \{b^2 (r^2 + s^2) (a^2 - \mu^2 b^2) + a^2 p^2 - b^2 r^2 s^2 (a^2 - \mu^2 b^2)\}}{(1 - p^2 s^2) (a^2 - \mu^2 b^2)}; \quad C_2 = \frac{\{a^2 b^2 - b^4 r^2 s^2 (a^2 - \mu^2 b^2)\}}{(1 - p^2 s^2) (a^2 - \mu^2 b^2)} \quad (11)$$

$$a^2 = \frac{\omega^2 \rho AL^2}{EA}; \quad b^2 = \frac{\omega^2 \rho AL^4}{EI_e}; \quad p^2 = \frac{PL^2}{EI} \quad r^2 = \frac{EI_e}{EAL^2}; \quad s^2 = \frac{EI_e}{kAGL^2}; \quad \mu^2 = \frac{z_\alpha^2}{L^2}; \quad \lambda^2 = 1 - p^2 s^2 \quad (12)$$

Similarly, the expressions for the amplitudes of axial force (F), shear force (S) and bending moment (M) for harmonic oscillation can be obtained as

$$F(\xi) = -\frac{EA}{L} \left(\frac{dV}{d\xi} - \mu \frac{d\theta}{d\xi} \right) = -\frac{EA}{L} \gamma (A_5 \cos \gamma \xi - A_6 \sin \gamma \xi) \quad (13)$$

$$S(\xi) = \frac{EI_e}{L^3} (A_1 g_\alpha \sinh \alpha \xi + A_2 g_\alpha \cosh \alpha \xi + A_3 g_\beta \sin \beta \xi - A_4 g_\beta \cos \beta \xi) \quad (14)$$

$$M(\xi) = -\frac{EI}{L^2} (A_1 h_\alpha \cosh \alpha \xi + A_2 h_\alpha \sinh \alpha \xi + A_3 h_\beta \cos \beta \xi + A_4 h_\beta \sin \beta \xi - A_5 h_\gamma \cos \gamma \xi + A_6 h_\gamma \sin \gamma \xi) \quad (15)$$

where

$$g_\alpha = \frac{b^2}{\alpha}; \quad g_\beta = \frac{b^2}{\beta}; \quad h_\alpha = \alpha k_\alpha (1 - \mu^2 b^2 / a^2); \quad h_\beta = \beta k_\beta (1 - \mu^2 b^2 / a^2); \quad h_\gamma = \gamma \mu b^2 / a^2 \quad (16)$$

Now, Equations (7)-(9) and Equations (13)-(15) can be used to apply boundary conditions for displacements and rotations, as well as for forces and moments, respectively, to eliminate the constants A_1 - A_6 and arrive at the frequency equation which yields the natural frequencies of the axially loaded axial-bending coupled Timoshenko-Ehrenfest beam. The mode shapes can be recovered by assigning a chosen value of one the constants and determining the rest of the constants in terms of the chosen one.

3. Discussion of results and conclusions

To demonstrate the application of the developed theory, an axially loaded coupled axial-bending Timoshenko-Ehrenfest beam made of aluminium and with the inverted T cross-section shown Figure 2 which is that of [5] is now analysed for its free vibration characteristics. The dimensions used for the cross-section (see Figure 2) are $b = 40$ mm, $t = 4$ mm and the length of the beam L is taken as 1 m. The distance between the shear centre and the centroid of the cross-section is worked out to be $z_\alpha = 9.474$ mm. The material properties used in the analysis are the Young's modulus $E = 70$ GPa, the shear modulus $G = 26.92$ GPa and the density $\rho = 2700$ kg/m³. The shear correction factor (also known as the shape factor) k is taken to be 2/3. Using the above data, the stiffness and mass properties of the section are calculated as axial stiffness (EA) = 2.128×10^7 N, (ii) bending stiffness (EI_e) = 5135.57 Nm², (iii) shear stiffness (kAG) = 5.4564×10^6 N, (iv) mass per unit length (ρA) = 0.8208 kg/m and (v) the mass moment of inertia (rotatory) per unit length (ρI_e) = 0.001981 kgm.

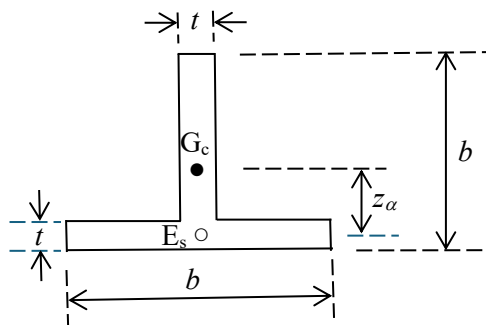


Figure 2. Cross-sectional details of an axially loaded coupled axial-bending Timoshenko-Ehrenfest beam, mass axis (centroid): G_c , elastic axis: E_s .

The critical buckling loads (P_{cr}) of the axial-bending coupled Timoshenko-Ehrenfest beam for clamped-Free (C-F), Pinned-Pinned (P-P) and clamped-clamped (C-C) boundary conditions were established at 7.9471 kN, 45.055kN and 124.44 kN, respectively using the theory of [6]. (Note that the P-P boundary condition prevents axial and bending motions at the ends, but not the bending rotation.) The first five natural frequencies of the beam for C-F, P-P and C-C boundary conditions were computed considering the axial load 0.0, $0.5P_{cr}$ and $-0.5P_{cr}$, respectively, and the results are shown in Table 1. These results were checked using the computer program BUNVIS-RG [7] which has the capability to connect eccentrically an axially loaded beam to nodes at the centroid of the cross-section to idealise an axially loaded axial-bending coupled beam, giving approximate, but sufficiently accurate results.

Table 1. Natural frequencies of an axially loaded axial-bending coupled Timoshenko-Ehrenfest beam for different boundary conditions.

Frequency Number (<i>i</i>)	Natural frequencies ω_i (rad/s)								
	C-F			P-P			C-C		
	Axial Load (P)			Axial Load (P)			Axial Load (P)		
	0.0	$0.5P_{cr}$	$-0.5P_{cr}$	0.0	$0.5P_{cr}$	$-0.5P_{cr}$	0.0	$0.5P_{cr}$	$-0.5P_{cr}$
1	220.036	158.654	264.873	736.381	520.752	901.802	1381.23	985.952	1678.63
2	1364.98	1306.85	1420.42	2431.11	2200.10	2641.98	3735.55	3243.68	4165.44
3	3761.76	3712.99	3809.90	5510.47	5288.36	5723.95	7147.55	6620.77	7636.82
4	7210.10	7163.85	7256.04	9214.82	8992.90	9430.97	11478.1	10923.3	12006.6
5	7998.11	7998.11	7998.11	14275.8	14046.7	14501.1	15996.2	15996.2	15996.2

The results shown in Table 1 indicate as expected that the effect of the compressive axial load ($P=0.5P_{cr}$) is to reduce the natural frequencies whereas the corresponding effect of a tensile load ($P=-0.5P_{cr}$) is to increase the natural frequencies. For instance, the presence of the axial load (P) altered the fundamental natural frequency ω_1 for the C-F boundary condition of the beam, by -27.9% for the compressive load ($0.5P_{cr}$) and 20.4% for the tensile load ($-0.5P_{cr}$), which are significant changes. It should be noted that the fifth natural frequency for the C-F and C-C boundary conditions is unaltered because it corresponds to a pure axial mode for which the axial load is not expected to have any major effect. The theory developed and the results presented demonstrate the importance of axial-bending coupling effects on the free vibration characteristics of axially loaded axial-bending coupled Timoshenko-Ehrenfest beams.

References

- [1] Lei, Z., Su, J., Hua, H. Longitudinal and transverse coupling dynamic properties of a Timoshenko beam with mass eccentricity. *International Journal Structural Stability and Dynamics*, Vol. 17 (07) (2017) Paper No. 1750077.
- [2] Ni, Z., Hua, H. Axial-bending coupled vibration analysis of an axially-loaded stepped multi-layered beam with arbitrary boundary conditions. *International Journal of Mechanical Sciences*, Vol. 138-139 (2018) pp. 187–198.
- [3] Tomović, A., Šalinić, S., Obradović, A., Grbović, A., Milovančević, M. Closed-form solution for the free axial-bending vibration problem of structures composed of rigid bodies and elastic beam segments. *Applied Mathematical Modelling*, Vol. 77 (2020) pp.1148–1167.
- [4] Banerjee, J.R., Ananthapuvirajah, A. Coupled axial-bending dynamic stiffness matrix for beam elements. *Computers and Structures* Vol. 215 (2019) pp. 1-9.
- [5] Banerjee, J.R., Ananthapuvirajah, A., Liu, X. and Sun, C. Coupled axial-bending dynamic stiffness matrix and its applications for a Timoshenko beam with mass and elastic axes eccentricity. *Thin-Walled Structures* Vol. 159 (2021) Paper No. 107197.
- [6] Banerjee, J.R. Coupled axial-flexural buckling of shear deformable columns using an exact stiffness matrix. *Computers and Structures*, Vol. 298 (2024) Paper No. 107349.
- [7] Anderson, M.S., Williams, F.W., Banerjee, J.R., Durling, B.J., Herstorm, C.L., Kennedy, D., Warnaar, D.B. User manual for BUNVIS-RG: An exact buckling and vibration program for lattice structures, with repetitive geometry and substructuring options, NASA Technical Memorandum 87669, (1986).

Vibrations of Rectangular Plates with Mixed Boundary Conditions

Aharon Deutsch*, Moshe Eisenberger[#]

* SOFiSTiK
Ness Ziona, Israel
tvruis@gmail.com

[#] Faculty of Civil and Environmental Engineering
Technion, Technion City, Haifa 32000, Israel
cvrmosh@technion.ac.il

Summary

The vibrational analysis of thin rectangular plates is a very important and studied topic in structural design. For rectangular plates there are 100 combinations of the classical types of boundary restraints along the four edges. These include simply supported (S), Clamped (C), Free (F), and Guided (G). For square plates the number is reduced to 55 possible cases. The benchmark results for the frequencies of rectangular plates were presented in a previous paper by the authors [1]. In the current work we extend the analysis to cases where along any edge there are two or more segments with different restraints leading to a much more complex problem. This problem was studied in many publications and here we mention just two by Narita [2] and Shu and Wang [3].

The free vibrations is governed by the following equation

$$D \left(\frac{\partial^4 w}{\partial x^4} + 2 \frac{\partial^4 w}{\partial x^2 \partial y^2} + \frac{\partial^4 w}{\partial y^4} \right) - \rho h \omega^2 w = 0 \quad (1)$$

where $w(x, y)$ is the out of plane deflections of the plate, $D = Eh^3/12(1 - \nu^2)$, is the flexural stiffness of the plate, ρ is the mass density of the material, h is the plate thickness, and ω is the free vibration frequency. The edge slope, bending moment, and shear force are given in [1]. The solution for this partial differential equation will be derived as the sum of two parts

$$w(x, y) = w_1(x, y) + w_2(x, y) = \sum_{m=0}^{\infty} \bar{X}_m Y_m + \sum_{n=0}^{\infty} X_n \bar{Y}_n \quad (2)$$

$$\bar{X}_m = \sin(\lambda_a x) \sin(m\pi/2) + \cos(\lambda_a x) \cos(m\pi/2) \quad (3)$$

$$\bar{Y}_n = \sin(\lambda_b y) \sin(n\pi/2) + \cos(\lambda_b y) \cos(n\pi/2) \quad (4)$$

$$\lambda_a = \frac{m\pi}{a}; \quad \lambda_b = \frac{n\pi}{b} \quad (5)$$

and substituting the assumed functions \bar{X}_m and \bar{Y}_n into Eq. 1 we obtain two fourth order ordinary differential equation for Y_m and X_n . The solutions for the two functions X_n and Y_m are hyperbolic functions

$$Y_m = A_m \cosh(\alpha_1 y) + B_m \cosh(\alpha_2 y) + C_m \sinh(\alpha_1 y) + D_m \sinh(\alpha_2 y) \quad (6)$$

$$X_n = E_n \cosh(\alpha_3 x) + F_n \cosh(\alpha_4 x) + G_n \sinh(\alpha_3 x) + H_n \sinh(\alpha_4 x) \quad (7)$$

with

$$\alpha_1 = \sqrt{\lambda_a^2 - \delta}; \quad \alpha_2 = \sqrt{\lambda_a^2 + \delta}; \quad \alpha_3 = \sqrt{\lambda_b^2 - \delta}; \quad \alpha_4 = \sqrt{\lambda_b^2 + \delta}; \quad \delta = \sqrt{\frac{\rho h \omega^2}{D}} \quad (8)$$

The solution is dependent on 8 unknown constants for the values of m and n in the summation in Eqs. (6,7). These are $A_m, B_m, C_m, D_m, E_n, F_n, G_n$, and H_n . The plate has 4 edges, and on each

of them we can prescribe 2 quantities, making for the 8 unknowns. For the current case we divide the plate into rectangular segments in such a way that on every edge the conditions are not changing. Then we apply the usual boundary condition where applicable, and we have a new set of continuation conditions along edges common to two segments. On these, the condition is that the displacement, slope, bending moment and the shear are equal. Utilizing the technique in [1] we can obtain a system of linear equations for the unknowns. When the determinant of the system is equal to 0 it indicates ω is a natural frequency.

Two examples are given as shown in Fig. 1. In the first case the plate is divided into two equal segments with one connecting edge in the middle. The second plate is divided into nine segments with few types of boundary and connecting conditions. The examples were analyzed using 30 terms in the summation in Eq. 2, and the results are very accurate. In Table 1 the results are compared to the values given in [2, 3]. The first six frequencies for this case are compared with a plate with simply supported edges all around, and the percentage increase in the frequencies is given in the last row. It can be observed that in this case the raise for the second and fifth frequencies is minor as compared to the other four frequencies. In Table 2 the results for the nine segment plate are compared to the results by Narita [2]. In this case the increase is much more significant with respect to all the frequencies. In this case a total of 50% of the edge length is clamped, as compared to only 12.5% in the first case. In Table 3 we show the modes of vibration and observe that the effect of the stiffening of the corners has little effect on the modes. It can be concluded that the extent and the location along the edges of the stiffer clamped sections has a major effect and it will be explored further in the future.

References

- [1] A. Deutsch, J. Tenenbaum, and M. Eisenberger. Benchmark vibration frequencies of square thin plates with all possible combinations of classical boundary conditions. *Int. Jour. Structural Stability and Dynamics*, 19:1950131, 2019.
- [2] Y. Narita. Application of a series-type method to vibration of orthotropic rectangular plates with mixed boundary conditions. *Journal of Sound and Vibration*, 77(3):345–355, 1981.
- [3] C. Shu and C.M. Wang. Treatment of mixed and nonuniform boundary conditions in gdq vibration analysis of rectangular plates. *Engineering Structures*, 21(2):125–134, 1999.

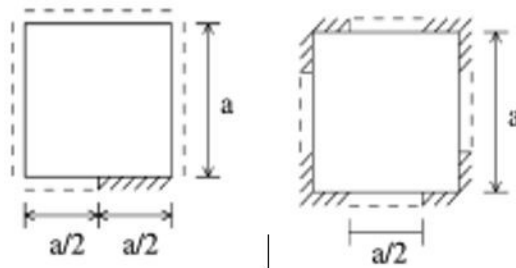


Figure 1: Two-segment and nine-segment plates

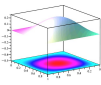
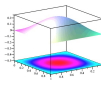
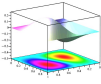
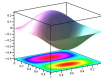
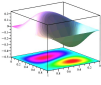
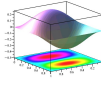
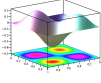
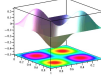
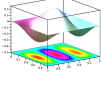
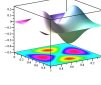
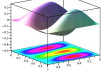
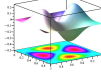
Table 1: Results for two segment plate - Fig. 1, case 1

	ω_1	ω_2	ω_3	ω_4	ω_5	ω_6
Narita [2]	22.63	50.04	55.95	82.34	99.71	107.6
Shu& Wang [3]	22.42	49.93	55.51	82.32	99.71	-
Current	22.4717	49.9165	55.6316	82.2725	99.6752	106.9284
SSSS Plate	19.7392	49.34802	49.34802	78.9568	98.6960	98.6960
% increase	13.8	1.15	12.7	4.20	0.992	8.34

Table 2: Results for nine segment plate - Fig. 1, case 2

	ω_1	ω_2	ω_3	ω_4	ω_5	ω_6
Narita [2]	26.18	58.70	58.70	98.58	102.0	114.9
Current	25.4554	57.7174	57.7174	97.2122	101.1986	101.1986
SSSS Plate	19.7392	49.34802	49.34802	78.9568	98.6960	98.6960
% increase	28.9	16.9	16.9	23.1	2.53	2.53

Table 3: Modes for the 9 segment plate

Frequency	Current Mode	SS Plate Mode
ω_1		
ω_2		
ω_3		
ω_4		
ω_5		
ω_6		

Variable-fidelity finite elements for nonlinear steady-state responses of structures

Matteo Filippi*, Erasmo Carrera*

Politecnico di Torino

* Department of Mechanical and Aerospace Engineering
Corso Duca degli Abruzzi 24, 10129, Torino, Italy
[matteo.filippi, erasmo.carrera]@polito.it

Summary

Nonlinear vibrations, including free and forced oscillations, are a critical study area in structural and mechanical engineering. Nonlinear systems can exhibit complex relationships between applied forces, vibration amplitudes, and frequencies. These phenomena may lead to amplitude-dependent responses, internal resonances, and bifurcation phenomena. Real-world operating conditions often cause structures to vibrate in nonlinear regimes, especially when the bodies are slender. These configurations are typically idealized as one-dimensional members, and understanding their nonlinear dynamic response is crucial for designing and analyzing various engineering structures, such as bridges, aircraft wings, and space components. This study investigates the steady-state response of beam-like structures characterized by large amplitude vibrations using variable-fidelity one-dimensional finite elements (FEs) to overcome the well-known limitations of analytical and semi-analytical approaches, which usually consider specific boundary conditions and reduce the number of equations. The nonlinear equation of motion to be solved is

$$\mathbf{M}\ddot{\mathbf{q}}(t) + \mathbf{K}_S(\mathbf{q})\mathbf{q}(t) = \mathbf{F}(t) \quad (1)$$

where \mathbf{M} , \mathbf{K}_S , \mathbf{F} , \mathbf{q} , and $\ddot{\mathbf{q}}$ are, respectively the mass matrix, the secant stiffness matrix, the vector of generalized forces, the unknown vector and its second time derivatives. The Carrera Unified Formulation (CUF) is used to derive the above FE operators [1]. Considering the system's response periodic with frequency ω and introducing the dimensionless time $\bar{t} = \omega t$, Equation 1 can be written as

$$\begin{aligned} \omega^2 \mathbf{M}\mathbf{q}'' + \mathbf{K}_s(\mathbf{q})\mathbf{q} &= \mathbf{F}(\bar{t}) \\ \mathbf{F}(\bar{t}) &= \sum_{n=1}^{Nf} (\mathbf{F}_c \cos(n\bar{t}) + \mathbf{F}_s \sin(n\bar{t})) \end{aligned} \quad (2)$$

where primes denote derivatives with respect to \bar{t} . The load is expressed as a sum of trigonometric functions with an arbitrary number of terms (Nf) to consider sub-harmonic, super-harmonic, and internal resonances. According to the Incremental Harmonic Method (IHM), the unknown state of vibration (\mathbf{q} and ω) is sought by incrementing a known solution (\mathbf{q}_0 and ω_0) of the quantities $\Delta\mathbf{q}$ and $\Delta\omega$

$$\mathbf{q} = \mathbf{q}_0 + \Delta\mathbf{q} \quad \omega = \omega_0 + \Delta\omega \quad (3)$$

The substitution of Equation 3 into Equation 2 and neglecting higher-order terms yields the following incremental equation

$$\begin{aligned} \omega_0^2 \mathbf{M}\Delta\mathbf{q}'' + \mathbf{K}_T(\mathbf{q}_0)\Delta\mathbf{q} &= \mathbf{R} - (2\omega_0 \mathbf{M}\mathbf{q}_0'')\Delta\omega \\ \mathbf{R} &= \mathbf{F}(\bar{t}) - (\omega_0^2 \mathbf{M}\mathbf{q}_0'' + \mathbf{K}_s(\mathbf{q}_0)\mathbf{q}_0) \end{aligned} \quad (4)$$

The term \mathbf{K}_T is the tangent stiffness matrix (see [2]), while \mathbf{R} is the residual (or correction) vector. An approximate solution of Equation 4 is obtained by applying Galerkin's procedure. The generic generalized coordinate (q_{r0}) and its increment (Δq_{r0}) are expanded in finite Fourier's series

$$\begin{aligned} q_{r0} &= \frac{1}{2}a_{r0} + \sum_{m=1}^{Nq} (a_{rm} \cos(m\bar{t}) + b_{rm} \sin(m\bar{t})) = \mathbf{H}_S \mathbf{A}_r \\ \Delta q_{r0} &= \frac{1}{2}\Delta a_{r0} + \sum_{m=1}^{Nq} (\Delta a_{rm} \cos(m\bar{t}) + \Delta b_{rm} \sin(m\bar{t})) = \mathbf{H}_S \Delta \mathbf{A}_r \end{aligned} \quad (5)$$

where \mathbf{H}_S is a row-vector collecting the trigonometric functions while \mathbf{A}_r and $\Delta \mathbf{A}_r$ are column-vectors of the unknown amplitudes and relative increments. Since Equations 5 represent approximate solutions, Equation 4 is not satisfied. Thus, the error is being minimized and the following equations in terms of increments are obtained

$$\bar{\mathbf{K}}_H \Delta \mathbf{A} = \bar{\mathbf{R}} - \bar{\mathbf{R}}_H \Delta \omega \quad (6)$$

Equation 6 is solved by starting from an acceptable guess solution, estimated with the cubic interpolation proposed in [3]. The guess attempt is modified until convergence parameters are below prescribed tolerances. The continuation method used to draw the equilibrium curves is based on the classical arc-length method. The procedure has been verified considering a hinged-hinged beam 150 mm long, 26 mm wide, and 0.514 mm thick subjected to a transversal concentrated load ($P_z = 0.15$ N) at the midspan. The structure was made of an isotropic material with Young's modulus $E = 69.7$ GPa, Poisson's ratio $\nu = 0.33$, and density $\rho = 2668.32$ kg m⁻³. Figure 1 shows the vibrational responses of the beam calculated at the loaded point. The mathematical

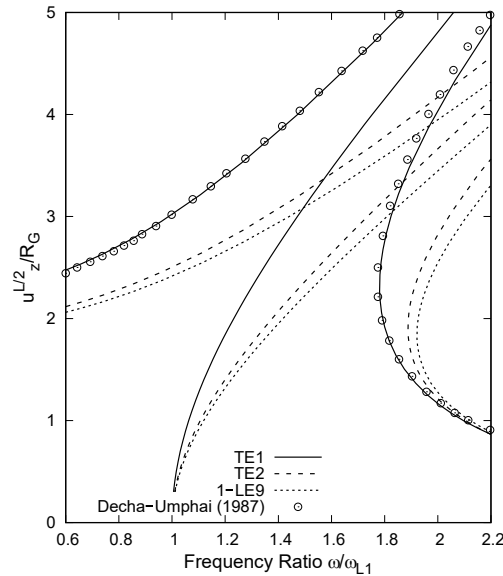


Figure 1: Nonlinear steady-state responses calculated at the midspan of the hinged-hinged beam subjected to a point load, $P_z = 0.15$ N.

model consisted of ten cubic Lagrangian finite elements along the beam axis while three different structural theories have been adopted to approximate the kinematic field: Taylor-based expansion of first and second order (TE1 and TE2) and a bi-quadratic Lagrange-based model (1-LE9). For comparison purposes, we reported the results presented in Ref. [4]. It can be observed that the TE1 solution closely agreed with the finite element results reported in [4] while the bi-quadratic theories predicted a more significant hardening effect. Nevertheless, this trend can also be observed in [5], where the harmonic balance method and the Galerkin approach were applied to investigate the influence of the initial curvature and axial displacement on the steady-state deflection of clamped-clamped beams.

References

- [1] Azzara, R.; Filippi, M.; Pagani, A.: Variable-kinematic finite beam elements for geometrically nonlinear dynamic analyses. *Mechanics of Advanced Materials and Structures*, Vol. 30, No. 20, pp. 4146-4154, 2023.
- [2] Pagani, A.; Carrera, E.: Unified formulation of geometrically nonlinear refined beam theories. *Mechanics of Advanced Materials and Structures*, Vol. 25, No. 1, pp. 15-31, 2018.
- [3] Cheung, Y.K.; Chen, S.H.; Lau, S.L.: Application of the incremental harmonic balance method to cubic non-linearity systems. *Journal of Sound and Vibration*, Vol. 140, No. 22, pp. 273-286, 1990.
- [4] Decha-Umphai, K: Finite Element Methodology for Nonlinear Free and Harmonic Forced Vibrations of Beam and Plate Structures. Ph.D. Thesis, Old Dominion University, doi:10.25777/22jn-wm37, 1987.
- [5] Yamaki, N.; Mori, A.: Non-linear vibrations of a clamped beam with initial deflection and initial axial displacement, part I: Theory. *Journal of Sound and Vibration*, Vol. 71, pp. 333-346, 1980.

The sliding beam formulation revisited: From the spaghetti problem to hot-rolled slabs

Alexander Humer^{*}, Ivo Steinbrecher[#]

^{*} Institute of Technical Mechanics
Johannes Kepler University Linz
Altenberger Str., 4040 Linz, Austria
alexander.humer@jku.at

[#]Institute for Mathematics and Computer-Based Simulation
University of the Bundeswehr Munich
Werner-Heisenberg-Weg 39, 85577 Neubiberg, Germany
ivo.steinbrecher@unibw.de

Summary

Sliding structures—such as beams that move through guides or deployable elements—have been studied for decades. Early applications include deployable antennas and tethered satellites, for instance. Problems of sliding beams became popularly known as the “spaghetti problem” [1], a term that reflects their most distinctive feature: similar to a noodle that is being sucked in, a structure slides in a preferred direction while its material domain changes over time as shown in Fig. 1 (left).

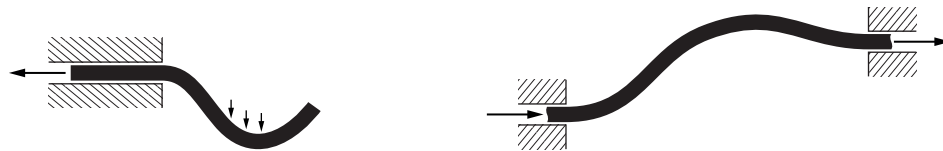


Figure 1: The “sliding spaghetti problem” of a beam being retrieved into a guide (left); axially moving continua characterized by a more or less continued sliding motion (right) [5].

In most modeling approaches, a coordinate transformation was used to map the time-dependent material domain to a fixed domain with respect to a stretched coordinate. Owing to such transformation, kinematic constraints and external loads can be prescribed at fixed points of the computational domain, which greatly facilitates the numerical modeling, see, e.g., [2] for a comparative study. Some time ago, we extended classical formulations to scenarios where the boundary motion is a function of the system’s state of deformation [3]. This approach marked a departure from earlier formulations, where the sliding motion had been imposed kinematically. In the proposed formulation, the relative motion of a structure and its supports emerged from the interaction between internal deformation, external forces, and kinematic constraints. As the boundary motion was no longer prescribed, the coordinate transformation introduced to accommodate for the variable material domain became state-dependent.

Sliding structures share key characteristics with axially moving continua—systems like conveyor belts or rolling sheets—where material flows through a fixed spatial domain, see, e.g., [4]. Our generalized formulation for sliding beams [5] bridges both types of problems by allowing for multiple variable material domain boundaries and domains, respectively, which enables the modeling

of a material flow through a control volume. Let the domain of interest $\mathcal{D} = \bigcup_{i=1}^n \mathcal{D}_i$ of some material body be decomposed into (sub-)domains $\mathcal{D}_i = [X_i^1(t), X_{i+1}^1(t)]$, which generally comprise a variable set of material points. By means of a piecewise-linear transformation, the (axial) material coordinate X^1 is mapped onto a stretched coordinate ξ^1 such that the transformed domain $\tilde{\mathcal{D}}_i$ is fixed with respect to ξ^1 :

$$\xi^1 = \frac{X_{i+1}^1(0) - X_i^1(0)}{X_{i+1}^1(t) - X_i^1(t)} (X^1 - X_i^1(t)) + X_i^1(0), \quad \xi^1 \in \tilde{\mathcal{D}}_i = [X_i^1(0), X_{i+1}^1(0)]. \quad (1)$$

The above relation assumes the boundaries of the stretched domains to coincide with the initial material boundaries, i.e., $\xi_i^1 = X_i^1(0)$. Any function f in the material coordinate X^1 is converted to a function \tilde{f} of the stretched coordinate ξ^1 , for which constraints and loads are fixed. Depending on the “physical” nature of the variable domains, appropriate constraints need to be provided to specify the evolution of the domain boundaries.

By including the variable domain boundaries of the individual non-material domains as additional unknowns, we re-establish the (anti-)symmetry properties of mass and convective terms introduced by the coordinate transformation. We base our formulation on Hamilton’s principle, where a variation in the domain boundaries naturally introduces the notion of configurational forces—a concept that has recently gained some attention and plays a central role in some of our own recent work, such as the “dancing rod” problem [6]. More specifically, the variation of the action integral S_i is composed from contributions of the individual variable domains,

$$\delta S = \sum_{i=1}^n \delta S_i = 0, \quad \delta S_i = \int_{t_0}^{t_1} (\delta T_i - \delta W_i^{\text{int}} + \delta W_i^{\text{ext}}) dt, \quad (2)$$

where we take the variation in both the generalized displacements $\tilde{\mathbf{U}}$ (comprising translation and rotation) and the domain boundaries X_i :

$$S_i = S_i(\tilde{\mathbf{U}}, \partial \tilde{\mathbf{U}} / \partial t, X_i^1, \dot{X}_i^1, X_{i+1}^1, \dot{X}_{i+1}^1), \quad \delta S_i = \delta_u S_i + \delta_l S_i. \quad (3)$$

The generalized sliding beam formulation allows us to efficiently solve problems of sliding beams and axially moving continua as illustrated in Fig. 2.

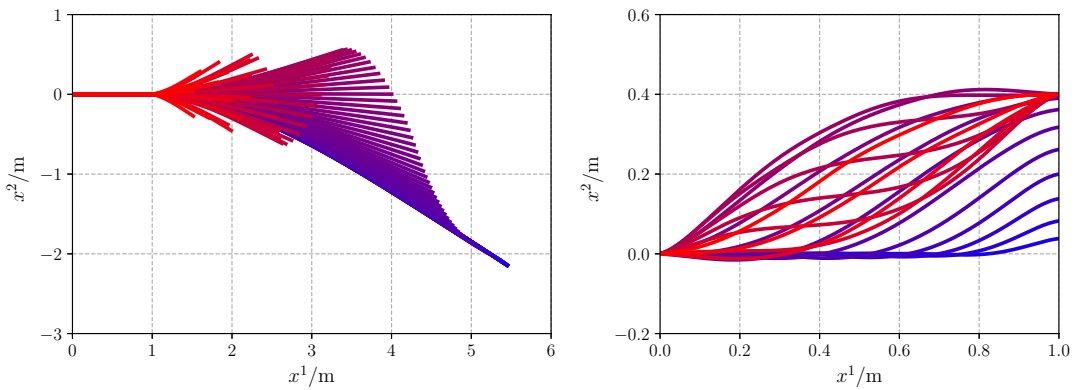


Figure 2: Snapshots of configurations of a sliding beam being retrieved into a rigid guide (left) and an axially moving beam with the right-hand support being lifted in the course of motion [5].

The extension of the sliding beam formulation to two dimensional continua is more or less straightforward. The domain boundaries $X_i^1 = X_i^1(X^2, t)$ additionally depend on the transverse coordinate

X^2 , which is accounted for by an extended transformation,

$$\xi^1(X^1, X^2, t) = \frac{l_i(0)}{l_i(X^2, t)} (X^1 - X_i^1(X^2, t)) + X_i^1(0), \quad \xi^1 \in \tilde{\mathcal{D}}_i = [X_i^1(0), X_{i+1}^1(0)], \quad (4)$$

where $l_i(X^2, t) = X_{i+1}^1(X^2, t) - X_i^1(X^2, t)$, see Fig. 3. The static example problem of a cantilever

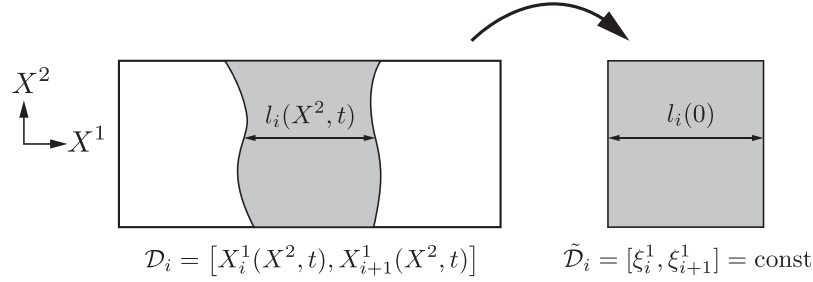


Figure 3: Generalization of the sliding beam formulation to two-dimensional continua.

subjected to a transverse shear load is meant to illustrate the mapping, see Fig. 4. The material body is composed from two non-material domains $\mathcal{D}_i = [X_i^1, X_{i+1}^1]$, $i = 1, 2$ (indicated in green and red). The nature of the domains is such that their interface is supposed to remain at a spatially fixed horizontal position, i.e., the position of the interface in the undeformed configuration. In other words, the left boundary of the first domain and the right boundary of the second domain are fixed with respect to the material points of the structure, i.e., $X_1^1 = 0$ and $X_3^1 = L$. The interface is spatially fixed, which implies

$$X_2^1(X^2) + u^1(X_2^1(X^2), X^2) = X_2^1(0) = \frac{L}{2}. \quad (5)$$

Applying the coordinate transformation (4) to the above relation, we obtain an algebraic relation that defines the position X_2^1 of the domain interface:

$$X_2^1(X^2) + \tilde{u}^1(\xi_2^1 = L/2, X^2) = \frac{L}{2}. \quad (6)$$

The deformed configuration (Fig. 4, right) shows the material lengths $l_i = l_i(X^2)$ currently located

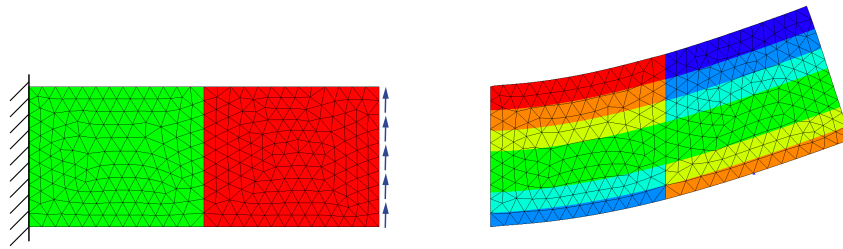


Figure 4: Generalization of the sliding beam formulation to two-dimensional continua.

in the respective domain as a function of the transverse coordinate.

Our ongoing research efforts focus on two distinct aspects: To apply the generalized sliding beam formulation in the industrial context of slab rolling, we combine the formulation with ideas proposed by Vetyukov et al. [7] in the framework of their mixed Eulerian-Lagrangian formulation: Inhomogeneities in the velocity profile of the material points at non-material domain boundaries

are accounted for by means of intrinsic strains that move along with the material point; so do internal variables related to plastic deformation. For this purpose, additional advection problems need to be solved to allow for the motion of material quantities relative to the stretched coordinate. Secondly, space-time finite-element formulations have recently seen increasing popularity. The intrinsic coupling of spatial and temporal variables renders sliding beams an ideal model problem for space-time approaches, which is confirmed by first results of our current research work.

References

- [1] Vu-Quoc, L.; Li, S.: Dynamics of sliding geometrically-exact beams: large angle maneuver and parametric resonance. *Computer Methods in Applied Mechanics and Engineering*, Vol. 120, No. 1-2, pp. 65–118, 1995.
- [2] Steinbrecher, I.; Humer, A.; Vu-Quoc, L.: On the numerical modeling of sliding beams: A comparison of different approaches. *Journal of Sound and Vibration*, Vol. 480, pp. 270–290, 2017.
- [3] Humer, A.: Dynamic modeling of beams with non-material, deformation-dependent boundary conditions. *Journal of Sound and Vibration*, Vol. 332, No. 3, pp. 622–641, 2013.
- [4] Scheidl, J.; Vetyukov, Y.: Review and perspectives in applied mechanics of axially moving flexible structures. *Acta Mechanica*, Vol. 234(4), pp. 1331–1364, 2023.
- [5] Humer, A.; Steinbrecher, I.; Vu-Quoc, L.: General sliding-beam formulation: A non-material description for analysis of sliding structures and axially moving beams. *Journal of Sound and Vibration*, Vol. 480, pp. 115341, 2020.
- [6] Vetyukov, Y.; Humer, A.; Steindl, A.: Nonlinear dynamics of a flexible rod partially sliding in a rigid sleeve under the action of gravity and configurational force. *Journal of the Mechanics and Physics of Solids*, Vol. 193, pp. 105854, 2024.
- [7] Vetyukov, Yu.; Gruber, P. G.; Krommer, M.; Gerstmayr, J.; Gafur, I.; Winter, G.: Mixed Eulerian–Lagrangian description in materials processing: deformation of a metal sheet in a rolling mill. *International Journal for Numerical Methods in Engineering*, Vol. 109, No. 10, pp. 1371–1390, 2017.

A study on the spacing of roving body placement for natural frequency-based crack detection

Xutao Sun*, Yusuke Mochida*, Sinniah Ilanko*, Rachael C. Tighe*, Brian R. Mace[#],

* School of Engineering,
University of Waikato,
Hamilton, New Zealand
briansun2018@hotmail.com
yusuke@waikato.ac.nz,
ilanko@waikato.ac.nz
rachael.tighe@waikato.ac.nz

[#] Acoustics and Vibration Research Centre,
Department of Mechanical Engineering,
University of Auckland,
Auckland, New Zealand
b.mace@auckland.ac.nz

Summary

Efforts to use natural frequency measurements to identify the presence of cracks in structures, as well as to locate them and assess their severity, remain an active subject of research [1-3]. The determination of natural frequencies for structures with cracks of known location and severity is relatively straightforward, with several methods—both exact and semi-analytical—commonly employed depending on the type of structure [4, 5]. However, determining the presence, location, and severity of cracks involves solving an inverse problem, which is considerably more challenging, as multiple combinations of crack number, location, and severity can lead to the same natural frequencies. While the use of measured frequencies from multiple modes can help, it still demands substantial computational effort. One promising approach leverages the characteristic that the natural frequencies of skeletal structures exhibit a steep change when the position of a roving auxiliary body is shifted across a crack [2]. This phenomenon arises from the discontinuity introduced by the crack's rotational flexibility and the rotary inertia of the attached body. In practical applications, the auxiliary body can only be attached over a finite area rather than at a point, resulting in a steep—but not abrupt—change in frequency.

Previous experimental work we conducted [1] demonstrated that the expected frequency change across a crack can be obscured by the inherent variation in natural frequency caused by the changing location of the roving mass itself. Specifically, our findings indicated that the observed frequency differences between adjacent positions of the roving body were not always due to the presence of a crack; instead, they could result from the mass-induced shift in the structure's dynamic response. For the beam tested and the roving body designed (Figure 1), it was a challenge to distinguish between frequency changes due to mass relocation and those due to the crack, for example as shown in Figure 2.

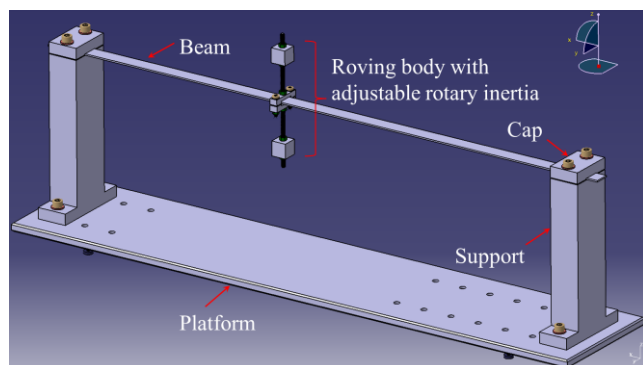


Figure 1. Experimental Setup in [1]

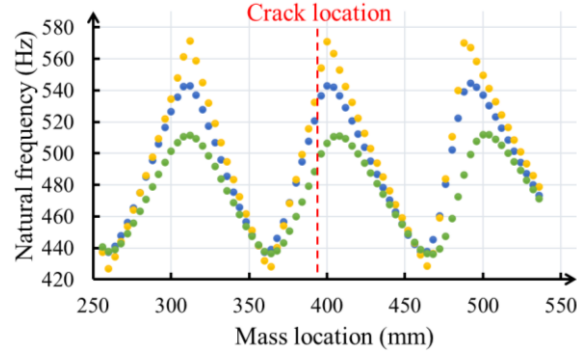


Figure 2. The 7th natural frequency versus mass location (20% crack. Green dots – experiment results using impact hammer test; blue dots – simulation results using ANSYS; yellow dots – analytical results using Dynamic Stiffness Method).

One aspect of our current work to address the above challenge is discussed here. That is to investigate how the spacing of roving body placement affects the measurability of frequency shifts due to crack as the body passes over a crack. Understanding this may help to find a way to determine a suitable spacing that is small enough to ensure that the effect of the frequency due to the mass relocation can be eliminated. The discussion is based on the experimental setup described in [1], wherein the same clamped-clamped cracked beam model and the same magnitude of mass and rotary inertia are used, and the crack depth remains 20% of the beam height. The results were generated using the Dynamic Stiffness Method (DSM).

The natural frequency change, denoted as Δf , resulting from shifting the mass across a crack, includes two components: the frequency change due to the mass relocation itself (Δf_{mass}) and the frequency change due to the crack as the mass passes it (Δf_{crack}). It is given by,

$$\Delta f = \Delta f_{mass} + \Delta f_{crack}. \quad (1)$$

Δf_{crack} is useful for crack detection but can be obscured by Δf_{mass} . Therefore, to extract Δf_{crack} , Δf_{mass} can be deducted from Δf .

In this study, Δf_{mass} is obtained by shifting the same auxiliary mass on an intact (uncracked) beam and calculating the frequency change between adjacent mass locations, while Δf is calculated under two different configurations. In the first configuration, the 20% crack is located at 0.394m from the left boundary (as in [1]) and the mass is incrementally shifted by Δx after each frequency calculation, as shown in Figure 3.

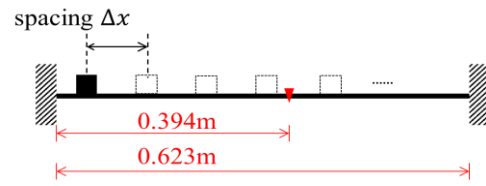


Figure 3. The first configuration for Δf calculation.

In the second configuration, the 20% crack is not located in a fixed position, instead, it is assumed that as the mass is shifted along the beam, it always passes over the crack in the subsequent placement, as illustrated in Figure 4.

Based on the first configuration, after subtracting Δf_{mass} from Δf , the results of Δf_{crack} versus mass location for the first four natural frequencies with spacings of 4mm, 10mm, and 20mm are shown in Figure 4. The results indicate that after removing the influence of Δf_{mass} , it is possible to locate the 20% crack using all three mass spacings, while in [1], it was challenging to pinpoint the crack location using 4mm spacing although the crack-induced frequency change was still measurable. However, it should be noted that the methodology in [1] relies solely on data obtained from the cracked beam, whereas the approach adopted here involves deducting Δf_{mass} from Δf , essentially introducing the response of the uncracked beam as baseline information, which may not be readily available in practice. However, the results here show that using a small spacing effectively suppresses fluctuations in Δf_{crack} curves due to the relocation of the mass.

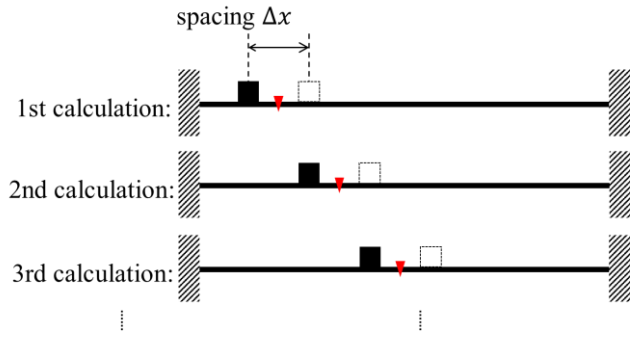


Figure 4. The second configuration for Δf calculation.

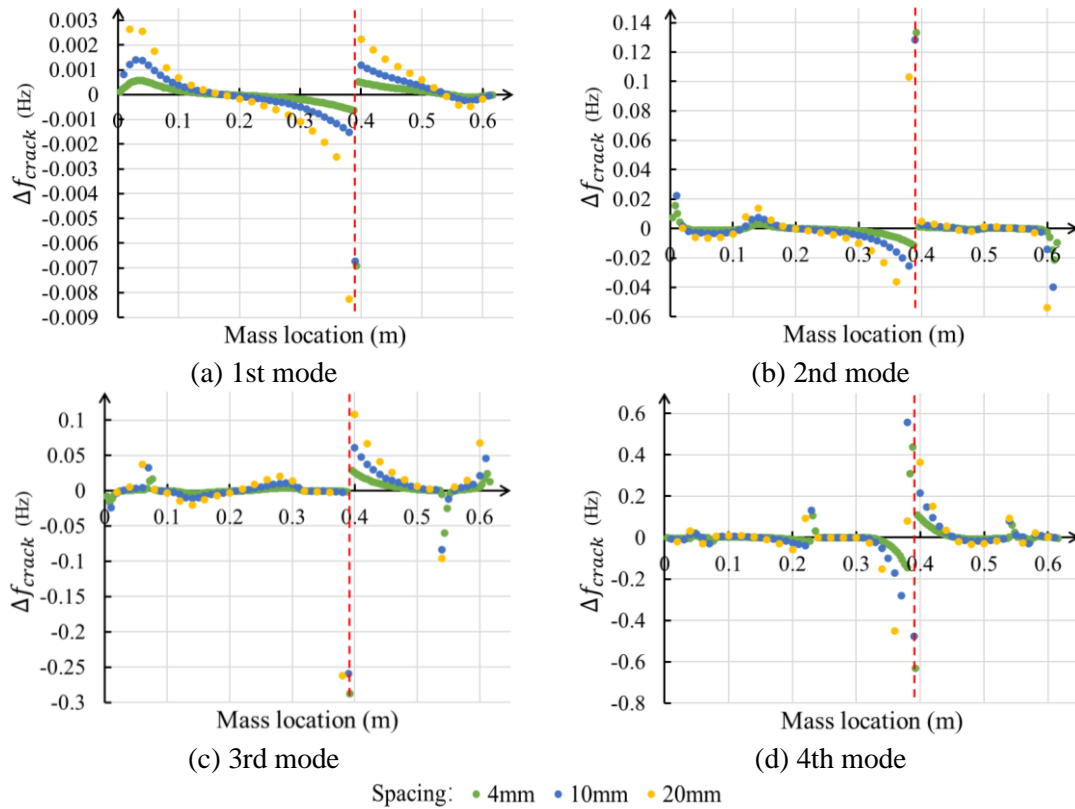


Figure 5. The results of Δf_{crack} using three different spacings based on the 1st configuration (the red dashed line indicates crack location).

Similarly, based on the second configuration, the results of Δf_{crack} versus mass location for the first four natural frequencies with spacings of 4mm, 10mm, and 20mm are shown in Figure 5. It can be observed that the influence of the crack on different modes varies with crack location,

while the effect of mass placement spacing is less pronounced than in the first configuration. The Δf_{crack} results exhibit anti-symmetry due to the symmetry of the structure, boundary conditions and layout of roving body positions. In different modes, Δf_{crack} approaches zero at different positions, possibly due to the modal curvature approaching zero near those locations, thereby effectively negating the influence of the rotational flexibility introduced by the crack. Thus, it is necessary to use more than two modes for crack detection as relying on a single mode may result in missed detection when the crack is located at positions where that mode is insensitive to its presence. These results show that the effect of the shift in the mass location is one of the factors that pose a challenge in identifying the location of crack through measured frequency shifts. It is acknowledged that other factors must also be considered in developing a reliable system to locate the cracks based on natural frequency measurements for practical applications.

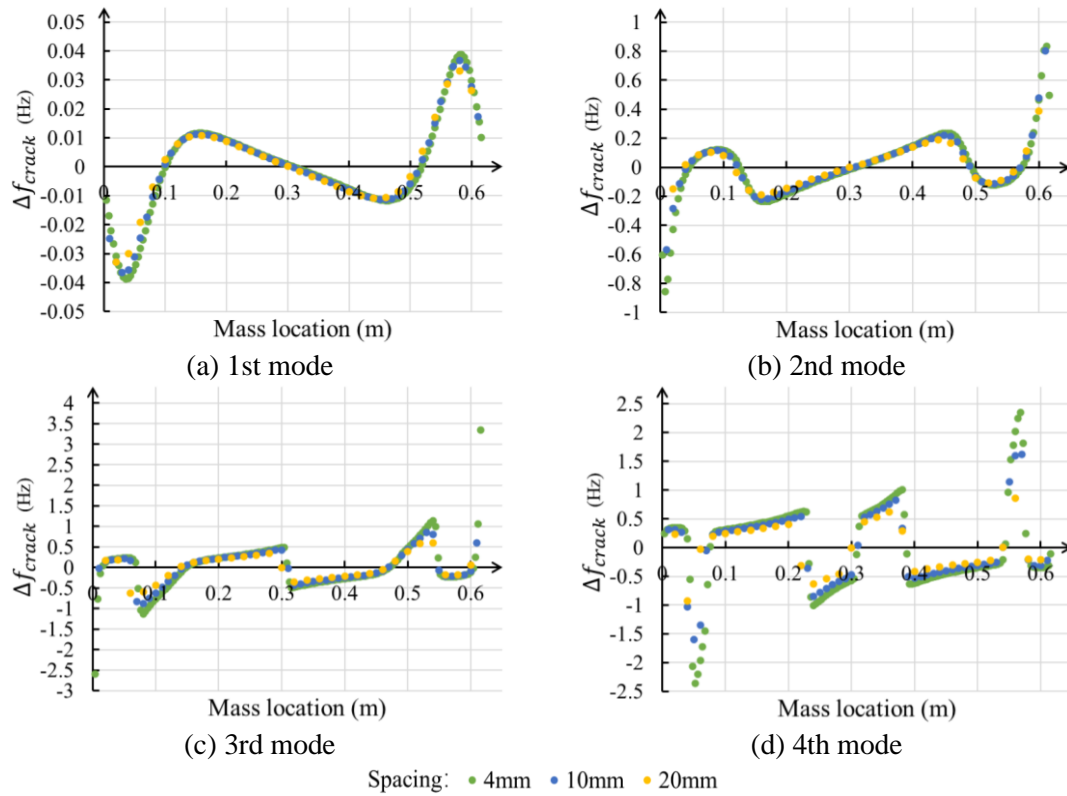


Figure 5. The results of Δf_{crack} using three different spacings based on the 2nd configuration.

References

- [1] Sun, X.; Ilanko, S.; Mochida, Y.; Tighe, R.C.; Mace, B.R.: Theoretical and Experimental Investigation of the Use of a Roving Mass with Rotary Inertia for Crack Detection in Beam-Like Structures. *Journal of Vibration Engineering & Technologies*, Vol. 13, No. 1, 105, 2025.
- [2] Cannizzaro, F.; De Los Rios, J.; Caddemi, S.; Calì, I.; Ilanko, S.: On the Use of a Roving Body with Rotary Inertia to Locate Cracks in Beams. *Journal of Sound and Vibration*, Vol. 425, pp. 275-300, 2018.
- [3] Labib, A.; Kennedy, D.; Featherston, C.A.: Crack Localisation in Frames Using Natural Frequency Degradations. *Computers & Structures*, Vol. 157, pp. 51-59, 2015.
- [4] Sun, X.: The Application of the Wittrick-Williams Algorithm for Free Vibration Analysis of Cracked Skeletal Structures. *Thin-Walled Structures*, Vol. 159, 107307, 2021.
- [5] Sun, X.; Ilanko, S.; Mochida, Y.; Tighe, R.C.: A Study on the Feasibility of Natural Frequency-Based Crack Detection. *Applied Sciences*, Vol. 14, No. 24, 11712, 2024.

Energy element method for vibration analysis of plates and solids with complex geometries

Zhao Jing^{1*}, Lei Duan², Siqi Wang¹

¹School of Aeronautics, National Key Laboratory of Aircraft Configuration Design, Northwestern Polytechnical University, Xi'an 710072, Shaanxi, China

²School of Civil Aviation, Northwestern Polytechnical University, Xi'an 710072, China.

jingzhao@nwpu.edu.cn, 2935469997@mail.nwpu.edu.cn, siqiwang@mail.nwpu.edu.cn

Summary

Numerical simulation of complex geometric structures using global admissible functions via the Ritz method was impossible in the past. Researchers have previously considered the problem insoluble due to the difficulty of constructing a general admissible function to approximate the deformation of structures with complex geometries and the difficulty of numerical integration on complex geometric domains. This fact has led to a large number of literatures examining the problems of two-dimensional (2D) and three-dimensional (3D) structures having regular geometries, e.g. rectangular, elliptical, circular, polygonal, spherical, cylindrical, and ellipsoidal etc. As pointed out by Reddy [1], the Ritz method is a true "meshless" method because it uses a global trial function for solving the problem, thus eschewing the necessity for meshes or nodes in the solution process. However, engineering problems are significantly more complex with irregular geometries, preventing the Ritz method from being applied, despite the fact that it is "meshless", efficient, and accurate.

Recently, literatures [2-5] have demonstrated that orthogonal polynomials, including Legendre polynomials and Chebyshev polynomials, are capable of predicting deformation of structures with complex geometries if high precision integration is possible on a complex geometric domain. Discrete Ritz methods [2-4] used the smallest rectangular domain to cover the plate domain in arbitrary geometries and generated a large number of Gauss points to perform numerical integration. With the Ritz R-function method [5], background rectangular meshes were generated with a constant number of Gauss points in each mesh, and dense meshes were used to approximate the geometric boundary of the plate. Despite the fact that both methods require a large number of Gauss points to perform numerical integration, the accuracy of integration cannot be determined mathematically for complex geometric domains. Furthermore, in the Ritz method [6], the development of universal formulas for numerical simulation of plates and solids with complex geometries using a global admissible function remains a challenge. Therefore, efficient numerical integration schemes and universal formulations are demanded to accurately simulate the deformation of plates and solids with complex geometries.

In order to solve the mechanical variational problems on complex geometric domains, a novel numerical method, energy element method, based on global admissible functions and high-precision global-local level mapping integration strategy, is proposed. By placing any geometric configuration structure into a standard geometric domain, combined with extended interval integration, and constructing variously-shaped energy integration elements (such as triangular [7], quadrilateral, circular, and elliptical energy elements, etc.) based on Gauss-Legendre quadrature and two-level mapping and inverse mapping in this geometric domain, high-

precision numerical integration and deformation simulation based on Boolean operations of energy elements on complex geometric domains are realized.

Since the energy functionals are constructed on a standard geometric domain, the modelling and solution procedures for any geometric configuration structure are completely standard, and the numerical simulation after the geometric configuration changes can be achieved through the Boolean operation of variously-shaped energy elements consist of Gaussian integration point sets, which bridges the gap between CAD geometry and CAE numerical model. The energy element method is used to solve the vibration problems of plates and solids with complex geometric configurations [3, 4, 7-10], and compared with analytical, numerical, and experimental results, the accuracy and efficiency of the energy element method are verified.

A simple example of the global-local level mapping integration strategy is introduced for a 2D problem, which is the vibration analysis of arbitrarily shaped polygonal plates. At the global level (see Fig. 1), the polygonal plate is embedded in a rectangular domain, and then the rectangular domain is mapped to a unit square domain. The polygonal plate is then divided into multiple triangular domains. At the local level (see Fig. 2), each triangular domain is mapped to a right-angled triangular domain and then to a unit square domain, from which triangular energy elements are constructed using Gauss-Legendre quadrature via inverse mapping. A flowchart is given in Fig. 3. By applying the global-local level mapping integration strategy to the vibration analysis of polygonal plates, the energy functionals in terms of global admissible functions can be established on the rectangular domain, and the integration of elements in the stiffness and mass matrices can be performed based on triangular energy elements. As a result, the energy functionals and computation procedures for arbitrarily shaped polygonal plates are standard, and will not be affected by variations in the polygonal plate's geometry. The vibrational behaviors of triangular, skew, trapezoidal, pentagonal, hexagonal, heptagonal, and octagonal plates are investigated, and compared with those reported in the literature [7]. Results demonstrate the generalization, reliability, accuracy of the proposed method. This method is universal for solving 2D mechanical variational problems on a complex geometric domain within Ritz formulation, and can be extended to 3D problems with complex geometries.

A general flowchart of the proposed energy element method for 2D and 3D mechanical variational problems is presented in Fig. 4. Modelling and solution procedures of the energy element method (EEM): Firstly, use a standard geometric domain covering the real geometric domain, and then map this rectangular/cuboidal domain into a unit square/cuboidal domain, which is the computation domain; The energy functional is constructed on this standard geometric domain, and will not alter with the variation of the geometry. Secondly, perform numerical integration within the real geometric domain of the standard geometric domain using variously-shaped energy elements based on Gauss-Legendre quadrature and their Boolean operation to simulate the geometry, this numerical integration strategy is performed for each element in the stiffness and mass matrices. Global admissible functions is used to simulate the deformation of the structure, and Ritz solution procedures are applied. Lastly, solving the vibrational eigenvalue problem to extract the frequencies and corresponding modes shapes.

References

- [1] Reddy JN, Srinivasa AR. Misattributions and misnomers in mechanics: Why they matter in the search for insight and precision of thought. Vietnam J Mech, 2020, 42(3): 283-291.
- [2] Jing Z, Duan L, Wang S. Buckling optimization of variable-stiffness composite plates with two circular holes using discrete Ritz method and potential flow. International Journal of Solids and Structures, 2024, 297: 112845.
- [3] Jing Z. Variable stiffness discrete Ritz method for free vibration analysis of plates in arbitrary geometries. Journal of Sound and Vibration, 2023, 553: 117662.
- [4] Jing Z, Duan L. Discrete Ritz method for buckling analysis of arbitrarily shaped plates with arbitrary cutouts. Thin-Walled Structures, 2023, 193: 111294.
- [5] Vescovini R. Ritz R-function method for the analysis of variable-stiffness plates. AIAA Journal, 2023, 61(6): 2689-2701.
- [6] Leissa AW. The historical bases of the Rayleigh and Ritz methods. Journal of Sound and Vibration, 2005, 287(4-5): 961-978.
- [7] Jing Z, Wang S. Vibration analysis of polygonal plates using triangular energy element via global-local level mapping. Journal of Sound and Vibration, 2025: 119138.
- [8] Jing Z, Duan L. Free vibration analysis of three-dimensional solids with arbitrary geometries using discrete Ritz method. Journal of Sound and Vibration, 2024, 571: 118132.
- [9] Jing Z. Energy Element Method for Three-Dimensional Vibration Analysis of Stiffened Plates with Complex Geometries. AIAA Journal, 2024, 62(11): 4189-4206.
- [10] Jing Z, Liu Y, Duan L, et al. Three-dimensional buckling analysis of stiffened plates with complex geometries using energy element method. International Journal of Solids and Structures, 2025, 306: 113105.

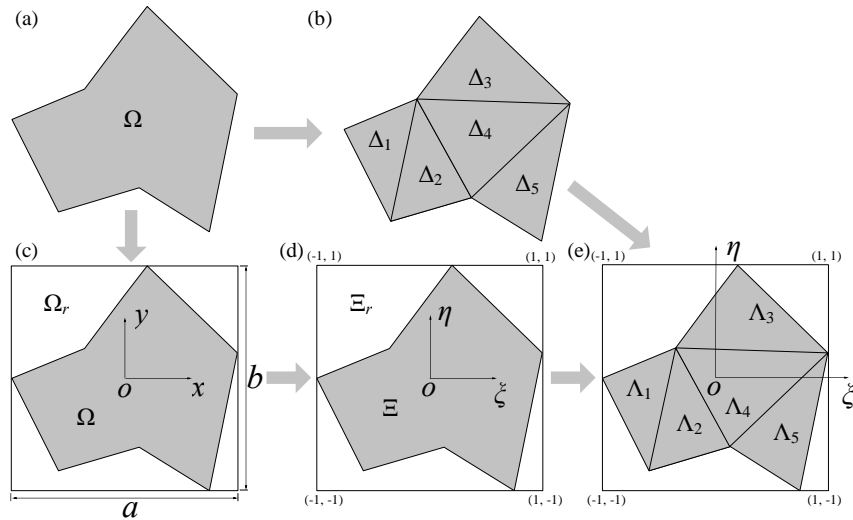


Figure 1. Global level mapping – construct the computational domain in a rectangular domain and the polygonal domain is divided into multiple triangular domains: (a) Original polygonal domain Ω ; (b) Polygonal domain Ω is divided into multiple triangular domain Δ_i ; (c) Using a rectangular domain Ω_r to cover the polygonal domain Ω ; (d) Mapping the rectangular domain Ω_r into a standard square domain Ξ_r defined in the range $[-1, 1]$; (e) The original triangular domains Δ_i are mapped to corresponding triangular domains Λ_i in the square domain Ξ_r .

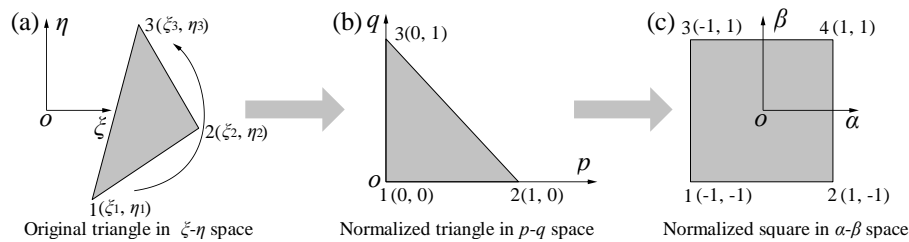
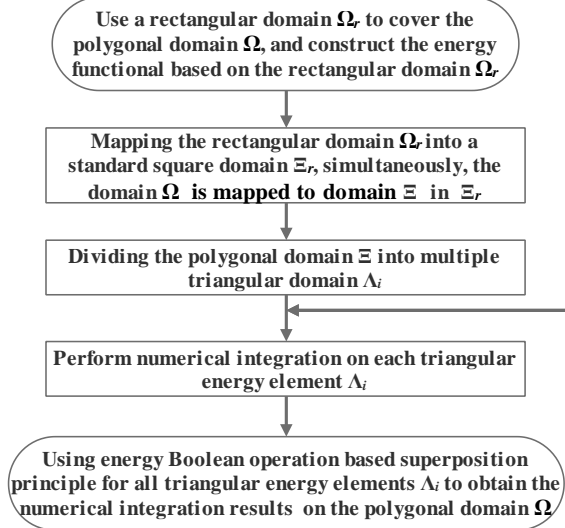


Figure 2. Local level mapping - arbitrary triangular domain transforms to a standard right-angled triangular domain, and then mapped it to a standard square domain: (a) triangular energy element i ; (b) normalized right-angled triangular domain; (c) normalized square domain. Gaussian integration points are generated in

the square (c), and mapped inversely to the triangular domain (a) to construct the triangular energy element, which characterizes the energy (strain energy or potential energy, etc.) of the triangular domain.

Global level energy computation in a rectangular domain



Local level energy computation in a triangular domain

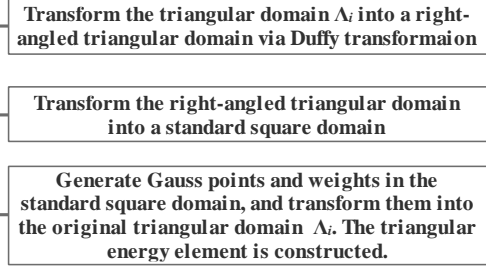


Figure 3 Flowchart of the global-local level mapping integration strategy

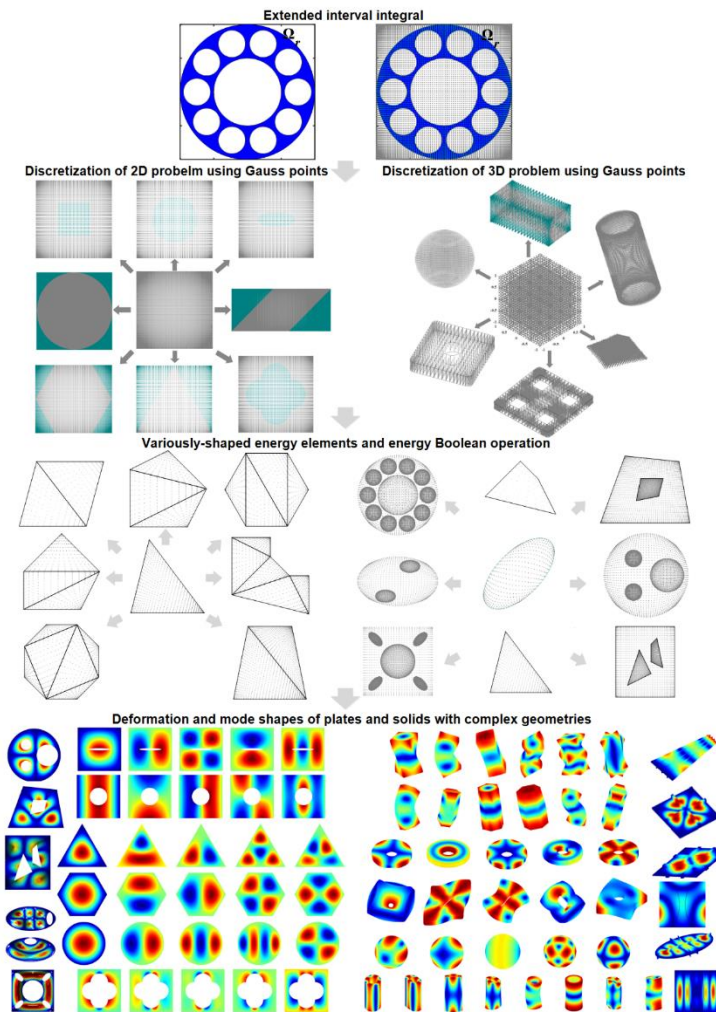


Figure 4. Modelling and solution procedures of the energy element method (EEM): Firstly, use a standard geometric domain covering the real geometric domain, and then map this rectangular/cuboidal domain into a unit square/cuboidal domain, which is the computation domain; The energy functional is constructed on this standard geometric domain, and will not alter with the variation of the geometry. Secondly, perform numerical integration within the real geometric domain of the standard geometric domain using variously-shaped energy elements based on Gauss-Legendre quadrature and their Boolean operation to simulate the geometry, this numerical integration strategy is performed for each element in the stiffness and mass matrices. Global admissible functions is used to simulate the deformation of the structure, and Ritz solution procedures are applied. Lastly, solving the vibrational eigenvalue problem to extract the frequencies and corresponding modes shapes.

Dynamic Analysis of Temperature-Sensitive Bi-Metallic Beams

**Moslem Molaie^{*}, Antonio Zippo^{*}, Francesco Pellicano^{*}, Emil Manoach[#], Simona Doneva[#],
Jerzy Warminski[†]**

^{*} Department of Engineering “Enzo Ferrari”,
University of Modena and Reggio Emilia,
Modena, Italy.
[moslem_molaie, antonio.zippo,
francesco.pellicano]@unimore.it

[#] Institute of Mechanics,
Bulgarian Academy of Sciences,
Sofia, Bulgaria.
[e.manoach, s.doneva]@imbm.bas.bg

[†] Department of Applied Mechanics,
Lublin University of Technology Lublin,
Lublin, Poland.
j.warminski@pollub.pl

Abstract

Beams are fundamental structural elements widely employed across various fields, ranging from micro/nanoscale systems to large-scale structures. Recent advancements in material science have driven the development of composite and multi-material structures to improve the mechanical performance. Among these, bi-metallic beams—comprising two metallic layers with distinct mechanical and thermal properties—are of particular interest due to their potential to exhibit tuneable dynamic responses. In this study, the dynamic behaviour of a bi-metallic beam composed of aluminium and copper layers, joined through an innovative welding technique, is investigated through experimental approach. A key focus is placed on understanding the influence of temperature on the system’s dynamic characteristics. Therefore, experimental tests are conducted within a controlled climate chamber using a shaking table to apply base excitations across a range of operational temperatures. Additionally, an experimental modal analysis is performed to characterize the beam's fundamental dynamic properties. The results provide critical insights into the temperature-dependent dynamic behaviour of bi-metallic structures, contributing to the design and optimization of advanced structural components for diverse engineering applications.

1. Introduction

Advances in technology have led to the development of composite structures with tailored mechanical properties by combining different materials in multilayered configurations. Understanding their behaviour is essential for ensuring structural safety. Pellicano et al. [1,2] studied the nonlinear dynamics of beams resting on a nonlinear spring with cubic stiffness and axially moving beams using a high dimension discrete model obtained by a Galerkin procedure. Tang et al. [3] examined how material gradation affects the buckling behaviour of functionally graded Euler–Bernoulli beams. This study experimentally investigates the dynamic behaviour of a bi-metallic beam made of aluminium and copper, focusing on how varying operational temperatures affect its response. Using controlled thermal conditions, the beam is mounted on an electrodynamic shaker and tested under base excitation to assess temperature-dependent dynamic characteristics.

2. Experimental Setup

The bi-metallic beam is made of two layers of metals: copper *C* 12500 (material 1 — upper layer) and aluminium alloy *Al* 1050 (material 2 — bottom layer), see Figure 1a. In this analysis clamped–clamped boundary conditions are considered, which allow to appreciate the effect of thermal loads. To implement clamped–clamped boundary conditions, the beam is fixed on an aluminum Vibration Table Adapter (VAT) through fastening the ends of the beam with two steel plates and tightening using M12 bolts, which can be seen in Figure 1b. The presence of VAT is necessary to connect the beam to the shaker.

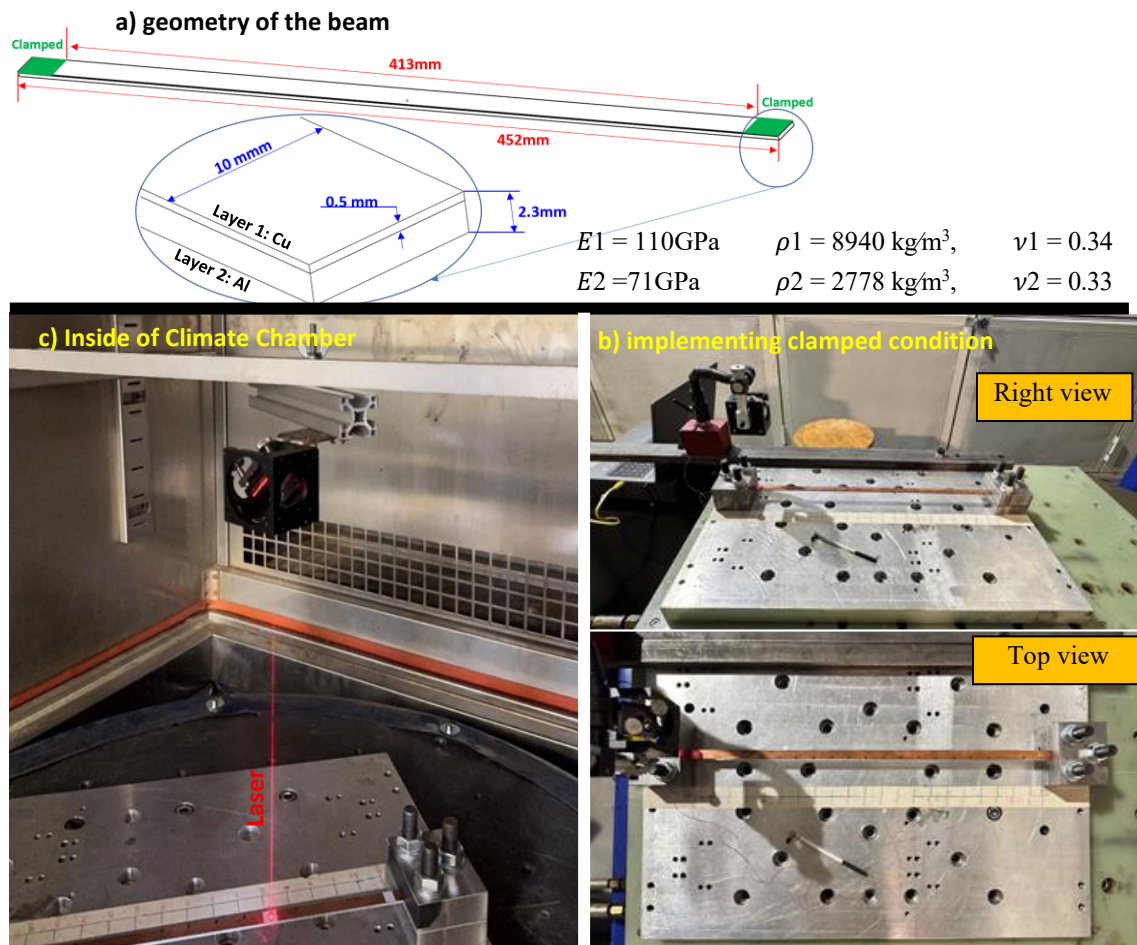


Figure 1. Geometry of the beam and implementing clamped condition

A Dongling ET-40-370 electrodynamic shaker (40 kN peak force, 100 g maximum acceleration, 500 kg maximum static payload, 1–2800 Hz frequency range) is used to apply seismic loading to the structure. The base motion directly excites the beam. The shaker is controlled by a Siemens LMS SCADAS system using TestLab software and is integrated with a climatic chamber, enabling tests under controlled thermohygrometric conditions. Beam displacement is measured using a Polytec OFV-505 laser vibrometer (± 25 m/s maximum velocity, 0.1 pm displacement resolution, 24 MHz frequency bandwidth). Due to the limited space inside the climatic chamber, the laser head cannot be positioned directly within it. Instead, a periscope system is employed to redirect the laser beam onto the side surface of the bi-metallic beam, as illustrated in Figure 1c. To monitor the displacement of the shaker base, a mono-axial accelerometer with a sensitivity of 108.11 mV/g is mounted on the shaker platform. The axial excitation is applied using an open-loop control strategy to prevent interference with potential nonlinear phenomena during testing. However, real-time closed-loop control is employed on the voltage signal sent to the shaker amplifier. A random excitation signal is used to stimulate the first three vibration modes of the beam, allowing the identification of all relevant modes within the 20–800 Hz frequency range. The standard frequency response function (FRF)-based method is adopted for experimental analysis. Tests are conducted at various temperatures ranging from 0 °C to 70 °C.

3. Experimental results

Tests are carried out at different temperatures and the modal properties variations are observed. Table 1 reports the first natural frequencies of the bi-metallic beam vs. temperature. The natural frequency initially decreases with temperature up to around 30°C, then increases steadily. The frequency variations can be addressed to the variation of the nominal beam length with the temperature, this variation is not allowed due to the presence of clamping, inducing internal compressive stresses (temperature higher than 25°C),

such variation is not trivial as the beam is made of two different metals. Moreover, the different expansions can induce additional bending deformations due to a nonsymmetric distribution of materials on the cross section. As can be seen from Table 1 and Figure 2, increasing the temperature leads to an increase in the damping ratio, and after temperature 35°C it has a downward trend with increasing the temperatures. Figure 3a illustrates the linear dynamic response of the beam under low-level excitation with a maximum acceleration of 0.02g. As the excitation amplitude increases to 0.4g, a clear hardening-type nonlinear behaviour emerges, as shown in Figure 3b. Indeed, the red line represents the upward results, where the system is excited starting from the lowest excitation frequency and gradually increasing to the highest. Conversely, the downward simulation—shown by the black line in Figure 3b—starts from the highest frequency and decreases step by step. It is worth mentioning that the tests are still ongoing.

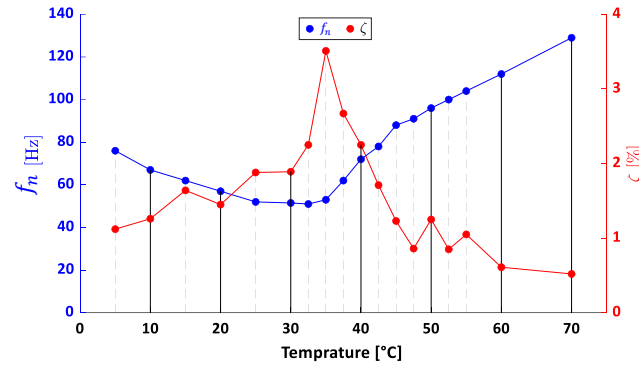


Figure 2. The variation of the beam damping ratio and natural frequency under different temperatures

Table 1. Natural frequency under different temperatures									
Temp. [°C]	5	10	15	20	25	30	32.5	35	37.5
f_n [Hz]	76	67	62	57	52	51.5	51	53	62
ζ [%]	1.12	1.26	1.64	1.45	1.88	1.89	2.25	3.51	2.67
Temp. [°C]	40	42.5	45	47.5	50	52.5	55	60	70
f_n [Hz]	72	78	88	91	96	100	104	112	129
ζ [%]	2.25	1.71	1.23	0.86	1.25	0.85	1.05	0.61	0.52

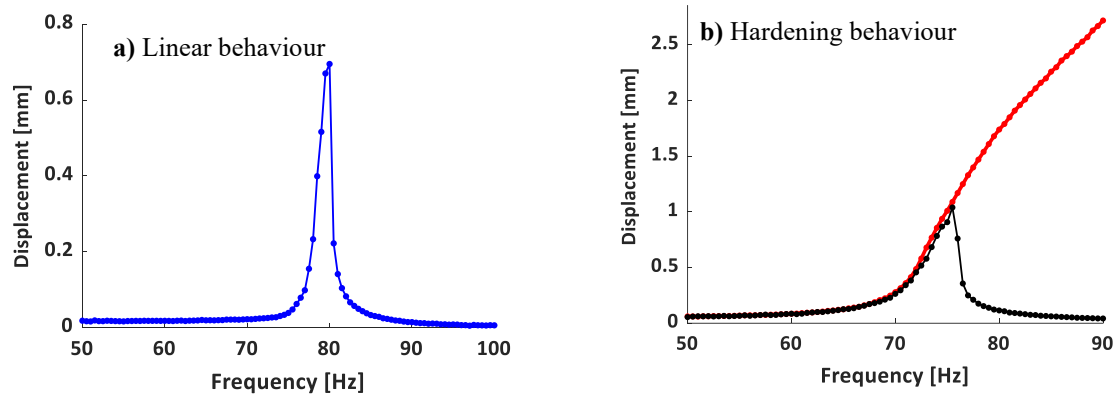


Figure 3. Dynamic response of the beam at $T=10^{\circ}\text{C}$ under two different level of energy: a) Low level energy, b) High level energy: — upward, - downward

References:

- [1]. Pellicano, F., Mastroddi, F. Nonlinear Dynamics of a Beam on Elastic Foundation, *Nonlinear Dynamics*, 14, 335355 (1997). <https://doi.org/10.1023/A:1008297721253>.
- [2]. Pellicano, F., Vestroni, F. Nonlinear Dynamics and Bifurcations of an Axially Moving Beam.” *ASME. J. Vib. Acoust.*; 122(1): 21–30,2000. <https://doi.org/10.1115/1.568433>.
- [3]. Tang Y., Zhong S., Yang T., Ding Q., *Interaction between thermal field and two-dimensional functionally graded materials: A structural mechanical example*, *Int. J. Appl. Mech.* 11 (10) (2019). <http://dx.doi.org/10.1142/S1758825119500996>.

Dynamic Modelling of Rigid-Flexible Coupled Beams with Flexoelectric Actuation

FAN Mu^{*}, ZHANG Jie[#], TZOU Hornsen[†]

College of Aerospace Engineering,
Nanjing University of Aeronautics and Astronautics,
Nanjing, 210010, China

*mfanz@nuaa.edu.cn; #nuaa_zhangjie@nuaa.edu.cn; † hstzou@nuaa.edu.cn.

Summary

This study introduces a dynamic model and flexoelectric vibration control method for rigid-flexible systems with single-sided flexible appendages. The system consists of a central rigid hub and flexible cantilever beams capable of single-axis rotation, with flexoelectric elements attached. Using Hamilton's principle, the equations of motion are derived, incorporating flexoelectric effects, centrifugal stiffening, and rigid-flexible coupling. Numerical simulations validate the accuracy and effectiveness of the proposed model and control approach.

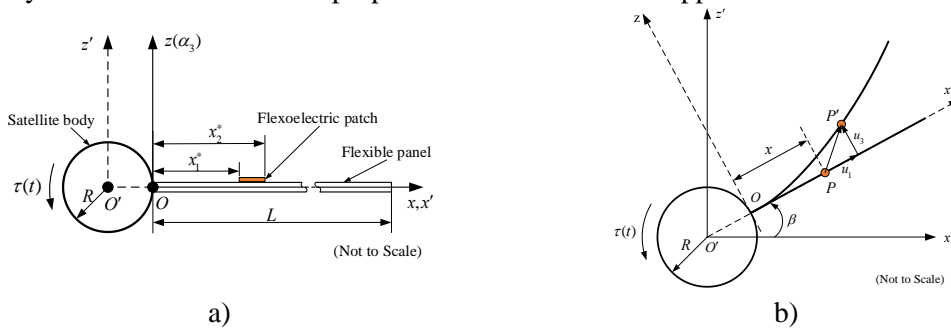


Fig. 1 The physical problem, a) Model of spacecraft with flexible appendages with the bonded flexoelectric patch; b) Kinematics of the rigid body motion and panel deformation

The geometric structure of current study is shown in Fig.1a), the system comprises an ideally central rigid body and one-sided flexible appendage, which can be simplified to a central rigid body - flexible beam model. The deformation of the flexible structure is shown in Fig.1b). To derive the dynamic model of the rigid-flexible system, the motion of the beam is restricted to the horizontal $x-z$ plane, and the gravitational force is ignored. The longitudinal and transverse displacements of the beam are denoted as u_1 and u_3 , respectively. In the natural state, any point P on the neutral axis x of the beam moves to point P' after the beam deforms.

To derive the dynamic model of the rigid-flexible coupled system, the modeling process follows Hamilton's principle, considering the kinetic and potential energy contributions from the rigid hub, the flexible beam, and the flexoelectric patch. The flexible appendage is modeled as an Euler-Bernoulli beam, with only transverse bending deformation considered[1,2]. The flexoelectric actuator is assumed to be perfectly bonded to the beam and exhibits uniaxial polarization. Using modal expansion method for the beam's transverse displacement and incorporating the effects of centrifugal stiffening and flexoelectric coupling through energy functional derivation[3,4], the equations of motion are systematically formulated. The final coupled system dynamics are obtained by assembling the resulting kinetic energy, potential energy and external work terms into a unified expression:

$$J\ddot{\beta} + \ddot{\beta}\{q\}^T [M]\{q\} + 2\dot{\beta}\{q\}^T [M]\{q\} + [\tilde{U}]\{\ddot{q}\} = \tau \quad (1)$$

$$[\tilde{U}]^T \{\ddot{\beta}\} + [M]\{\ddot{q}\} + ([K] - \dot{\beta}^2 [M])\{q\} = -[B]\{V\} + \frac{1}{2}[\chi]\{V\} - \frac{1}{2}[f]\{V\} \quad (2)$$

$$[C]\{V\} = [B]^T \{q\} + \frac{1}{2}[f]^T \{q\} - \frac{1}{2}[\chi]^T \{q\} \quad (3)$$

where, J is moment of inertia, β is the attitude angle, $[M]$ is mass matrix, $[\tilde{U}]$ is coupling matrix, $[K]$ is stiffness matrix, and $\{q\}$ is the vector of elastic generalized coordinates.

If the elastic displacement is small compared with the rigid body rotation, the second-order coupling effect can be ignored in the equation of motion of the above system, which is then simplified to

$$J\ddot{\beta} + [\tilde{U}]\{\ddot{q}\} = \tau \quad (4)$$

$$[\tilde{U}]^T \{\ddot{\beta}\} + [M]\{\ddot{q}\} + [K]\{q\} = -[B_a][G_a]\{V_a\} + \frac{1}{2}[\chi_a][G_a]\{V_a\} - \frac{1}{2}[f_a][G_a]\{V_a\} \quad (5)$$

$$\{V_s\} = [G_s][C_s^{-1}][B]^T \{q\} + \frac{1}{2}[G_s][C_s^{-1}][f]^T \{q\} - \frac{1}{2}[G_s][C_s^{-1}][\chi]^T \{q\} \quad (6)$$

where a and s in the subscript represent the actuator and sensor respectively. $[B]$ and $[C]$ matrices can be broken down into sensor and actuator parts corresponding to the sensor and actuator voltages, $\{V_s\}$ and $\{V_a\}$. $[G_a]$ and $[G_s]$ represent the actuator and sensor amplifier gains respectively.

According to the normalization and orthogonal properties of the mode shape, there are the following transformations

$$[N]^T [M][N] = [I], [N]^T [K][N] = [\Lambda] \quad (7)$$

where $[N]$ is a matrix with columns consisting of orthonormal eigenvectors, $[\Lambda] = \text{diag}\{\omega_i^2\}$ is an eigenvalue matrix, and $[I]$ is the identity matrix. Inserting the coordinate transformation $\{q\} = [N]\{\eta\}$, at the same time, the modal damping term $C_d \dot{\eta}$ is introduced. The modal damping matrix $[C_d]$ can be expressed as $[C_d] = \text{diag}[2\zeta_k \omega_k]$, ($k = 1, 2, \dots, n$), in which ζ_k is the damping ratio and ω_k is the modal vibration frequency.

Equations (4), (5), and (6) can be rewritten in terms of modal coordinates and as

$$J\ddot{\beta} + [F]^T \{\ddot{\eta}\} = \tau \quad (8)$$

$$\{\ddot{\eta}\} + [C_d]\{\dot{\eta}\} + [\Lambda]\{\eta\} + [F]\ddot{\beta} = -[N]^T [B_a][G_a]\{V_a\} - \frac{1}{2}[N]^T ([f_a] - [\chi_a])[G_a]\{V_a\} \quad (9)$$

$$\{V_s\} = [G_s][C_s^{-1}][B]^T [N]\{\eta\} + \frac{1}{2}[G_s][C_s^{-1}]([f]^T - [\chi]^T) [N]\{\eta\} \quad (10)$$

where $[F]^T = [\tilde{U}][N]$. It can be seen from the above derivation process that the motion equation of the flexible spacecraft, the vibration equation of the flexible structure, and the flexoelectric equation of the flexoelectric element are coupled. With the derived dynamic model, case studies can be carried out to explore the effects of vibration on the flexible appendage during the system's attitude motion, as well as the influence of vibration generated by the flexible appendage due to flexoelectricity on the attitude angle of the rigid body.

Firstly, the results obtained from this work were compared with that in literature[5]. During the simulation process, the rigid body is required to execute an attitude maneuver of 60° to fulfill

a specific task. As depicted in Fig. 2, both the model parameters utilized in this study and those employed in the comparative literature yield a system-stable convergence time of approximately 25 seconds. This duration represents the time required for the system's attitude to adjust to the target attitude angle.

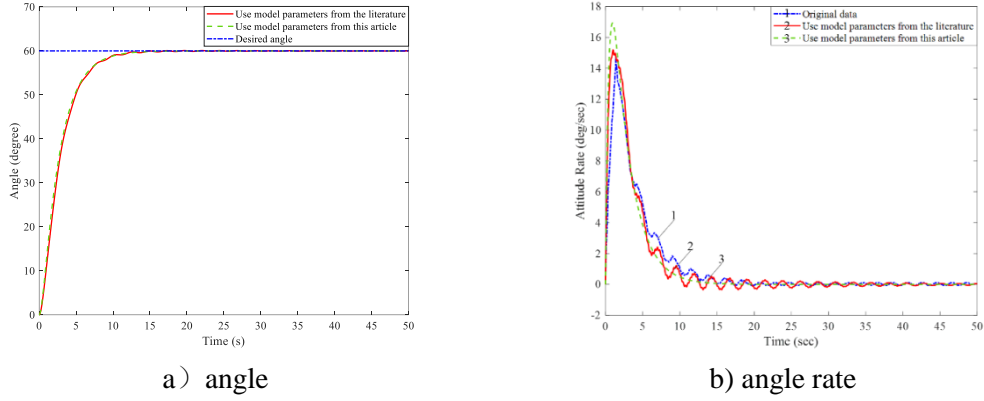


Fig.2 Attitude maneuver simulation curve.

Secondly, under open-loop control conditions, we also studied the control effects of different control voltages (0, 10, 50, 100 V) on the system, as shown in Fig. 3.

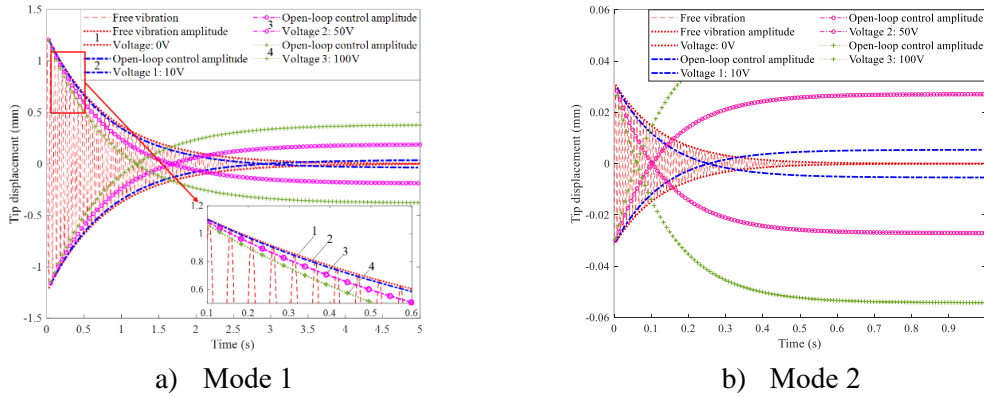


Fig. 3 Control efficiency of open-loop control of mode 1 and mode 2 vibration

The comparison of Fig. 4 illustrates the relationship between the system's posture rotation and the vibration of the flexible appendage under the continuous and constant external control torque exerted on the central rigid body.

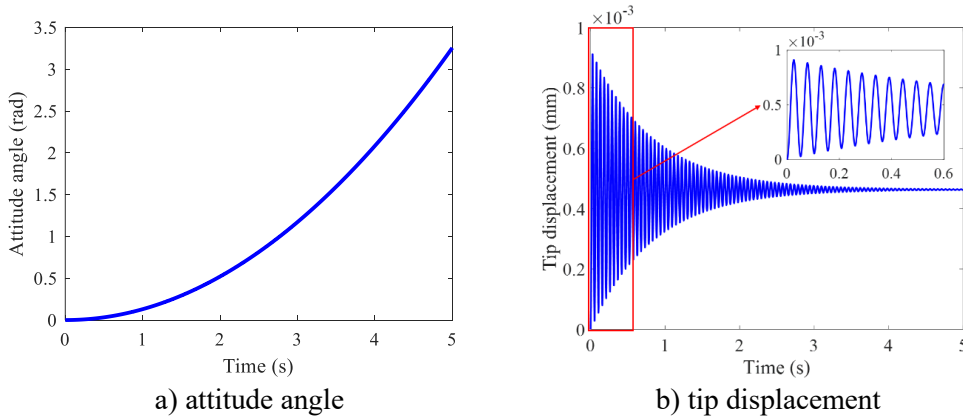


Fig. 4 The effects of different control torques on attitude angle and tip displacement ($V=0$ V, $\tau=1.0$ N·m).

To investigate whether the vibration of the flexible appendage, influenced by flexoelectricity, impacts the posture motion of the central rigid body, we conducted the following simulation calculations. Excluding other external excitation forces and control torques, we applied control voltages of 10V, 50V, and 100V solely to the flexoelectric actuator and observed the variations in the tip displacement and attitude angle of the flexible appendage.

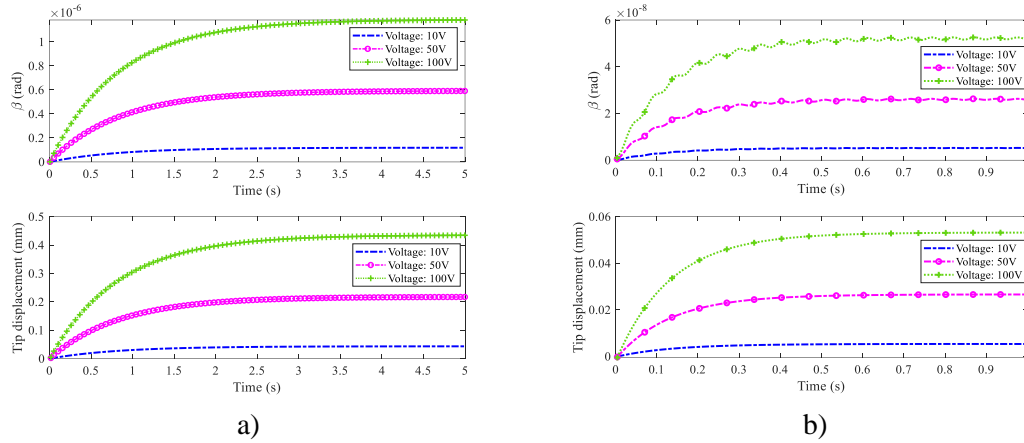


Fig. 5 Effect of tip displacement on rigid body attitude angle under different flexoelectric control voltages, a) Mode 1, b) Mode 2.

In Fig. 5, the rigid body's attitude angle and tip displacement vary under different control voltages (10V, 50V, 100V) for flexible appendage modes 1 and 2. As voltage increases, both the attitude angle and tip displacement increase, indicating a direct correlation between control voltage and system response. These results confirm that flexoelectric-induced vibrations in flexible appendages affect the central rigid body's motion, demonstrating rigid-flexible coupling. Future research endeavors will extend this work to address the complexities of multi-body systems, nonlinear dynamics, and environmental disturbances. Experimental validations will be pursued to corroborate theoretical and numerical findings, providing insights into practical implementation challenges and limitations inherent to flexoelectricity in flexible spacecraft engineering.

References

- [1] Yang, J. B., Jiang, L. J., and Chen, D. C. "Dynamic modelling and control of a rotating Euler–Bernoulli beam," *Journal of Sound and Vibration*, Vol. 274, No. 3, 2004, pp. 863-875.
- [2] Sales, T. P., Rade, D. A., and de Souza, L. C. G. "Passive vibration control of flexible spacecraft using shunted piezoelectric transducers," *Aerospace Science and Technology*, Vol. 29, No. 1, 2013, pp. 403-412.
- [3] Shen, S., and Hu, S. "A theory of flexoelectricity with surface effect for elastic dielectrics," *Journal of the Mechanics and Physics of Solids*, Vol. 58, No. 5, 2010, pp. 665-677.
- [4] Toupin, R. A. "The Elastic Dielectric," *Journal of Rational Mechanics and Analysis* Vol. 5, No. 6, 1956, pp. 849-915.
- [5] Hu, Q. "Active vibration control of flexible spacecraft during attitude maneuver." Harbin Institute of Technology, 2006.

Use of Non-integer Boundary Index for Vibration of Elastically Supported Continuous Systems

Y. Narita

Hokkaido University (Professor Emeritus)

N-13 W-8, 060-8628 Sapporo, Japan

ynarita1951@gmail.com

Introduction

When continuous systems (beam, plate, shell) are supported by translational and rotational springs, there are basically two analytical approaches. The first one is to solve the governing equation of motion by satisfying the boundary conditions involving relations of shear force and moment with reactions of the springs, but general solutions are unavailable in many problems of the continuous systems. More general way is the second approach to use the energy functional of strain and kinetic energies stored in the continuous system and to add the energies of elastic springs. In this latter case, so-called energy methods such as Ritz method and others are applicable. These energy methods have advantages in wide applicability, but the spring stiffness should be infinite when one considers continuous frequency increase, for example, from simply supported edge to the clamped edge. In practice, the infinitely large stiffness is replaced by a very large (non-dimensional) stiffness of 10^5 or 10^6 , and theoretically speaking such ambiguity is inevitable. Also use of very large stiffness values often causes numerical difficulty, as explained later, in the computation.

The present author has analyzed vibration problems of plates and shells [1-8] by using polynomial displacement functions multiplied by the term of satisfying kinematical boundary conditions, and such modification is easily possible by use of “integer boundary index” in the function. With this, the displacement functions become easily manipulatable to satisfy the kinematical boundary conditions. In a simple case of beam bending vibration, for example, $w(x)=x^m(x-a)^{bc}$ is used, i.e., to realize no constraint $w(x)=x^m$ at $x=a$ for free edge, simple support $w(x)=x^m(x-a)$ and at the clamped edge, $w(x)=x^m(x-a)^2$. Such additional power term $bc=0, 1, 2$ (non-negative integer) used to be called “boundary index”.

In the present paper, the restraint of the index being *integer* is removed. By extending the index to be in real number, an assumption is proposed to realize accordingly the physical condition between free and simple support with real index between $bc=0$ and 1, and similarly to realize the physical condition between simple support and clamp with the real number index between $bc=1$ and 2. This extension is quite new and original in the theoretical aspect.

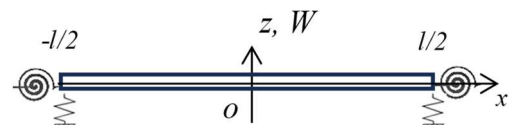


Fig. 1. Test example: Uniform beam with translational and rotational springs.

Test example: bending vibration of a beam constrained by springs at both ends

The idea of using non-integer boundary index can be applied to plates and shells. For testing here the validity of idea, one of the easiest example is introduced, i.e., a uniform beam elastically supported at both ends, as shown in Fig.1. An energy functional is given by

$$L = T - U = \frac{1}{2} \int_{-l/2}^{l/2} \rho A \left(\frac{\partial w}{\partial t} \right)^2 dx - \frac{1}{2} \int_{-l/2}^{l/2} EI \left(\frac{\partial^2 w}{\partial x^2} \right)^2 dx \quad (1)$$

where w is lateral deflection, ρ is density, A is area of cross-section, E is Young's modulus and I is the second moment of cross-section. After assuming a free vibration solution $w(x,t)=W(x)\sin \omega t$ and applying principle of virtual work, one gets

$$0 = \delta(T_{max} - U_{max}) = - \left[\delta \left(\frac{dW}{dx} \right) \times EI \left(\frac{d^2 W}{dx^2} \right) \right]_{-l/2}^{l/2} + \left[\delta W \times EI \left(\frac{d^3 W}{dx^3} \right) \right]_{-l/2}^{l/2} - \int_{-l/2}^{l/2} \delta W \left\{ EI \frac{d^4 W}{dx^4} - \rho A \omega^2 W \right\} dx \quad (2)$$

As well known, this process results in a governing equation and two sets of boundary condition (specifically in this case, kinematical boundary conditions) to satisfy Eq.(2) being zero.

Ritz method by using elastic energies of springs (conventional approach)

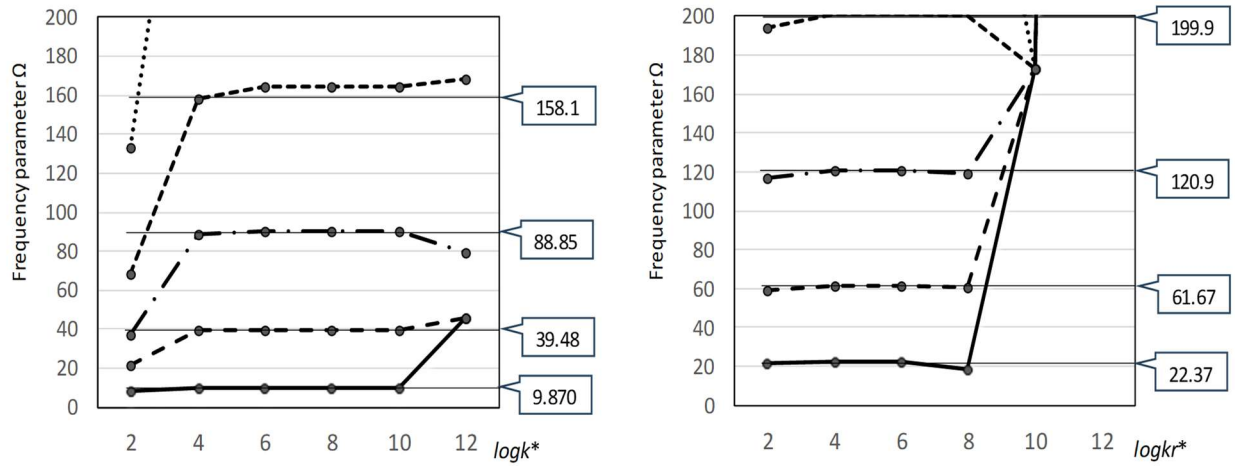
When one analyzes vibration of beam, one must introduce amplitude function so that two kinematical boundary conditions on w and dw/dx are satisfied. Such amplitude function includes unknown coefficients, and minimization is carried out with respect to the coefficients. In the conventional approach, the energies stored in the translational and rotational springs are also considered in the functional in Eq.(1) as

$$U = \frac{1}{2} \int_{-l/2}^{l/2} EI \left(\frac{\partial^2 W}{\partial x^2} \right)^2 dx + \frac{1}{2} k_{t,1} \left\{ W \left(-\frac{l}{2} \right) \right\}^2 + \frac{1}{2} k_{t,2} \left\{ W \left(\frac{l}{2} \right) \right\}^2 + \frac{1}{2} k_{r,1} \left\{ \frac{dW(-l/2)}{dx} \right\}^2 + \frac{1}{2} k_{r,2} \left\{ \frac{dW(l/2)}{dx} \right\}^2 \quad (3)$$

and after introducing dimensionless coordinate ($\xi=2x/l$), the amplitude has been proposed as

$$W(\xi) = \sum_{m=0}^{M-1} A_m \xi^m (\xi+1)^{bc1} (\xi-1)^{bc2} \quad (4)$$

where A_m are unknown coefficients, $bc1$ and $bc2$ are the boundary index at left-hand and right-hand ends, respectively. When the left-hand edge is free, one sets $bc1=0$, and for simple support and clamp, $bc1=1$ and $bc1=2$ are inserted, respectively, to satisfy the kinematical boundary condition. When the left-hand end is constrained by translational spring (i.e., between free and simple support), the spring stiffness against translation $k_{t,1}$ is increased with keeping $bc1=0$. Similarly, the constraint between simple support and clamp is made possible by setting $bc1=1$ and increasing the rotational stiffness $k_{r,1}$ from zero to infinity. Thorough numerical results for the plate examples are summarized [7,8] and comparison with relevant literature by other authors is made including recent papers [9,10].



(a) Free beam with increasing translational stiffness (b) Simply supported beam with increasing rotational stiffness

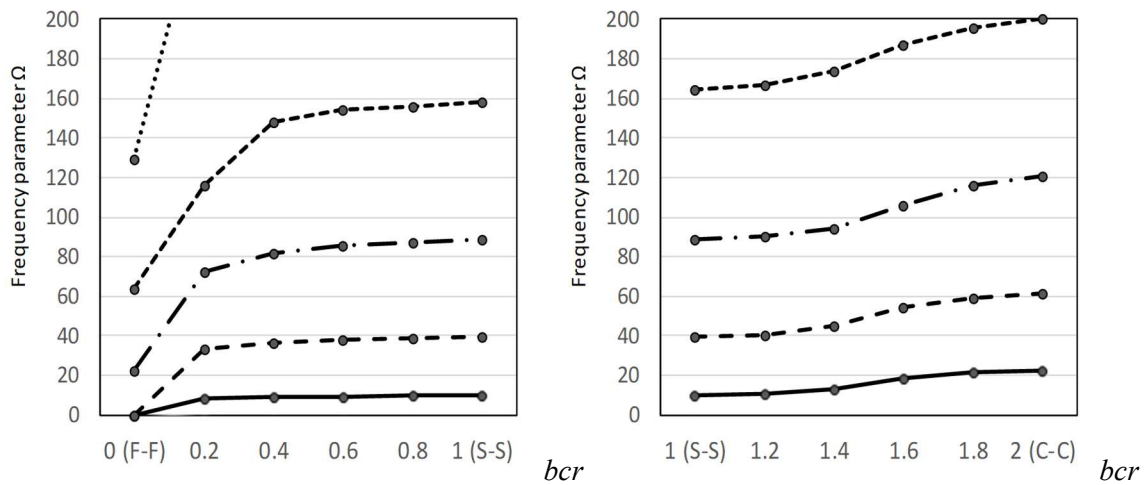
Fig.2 Frequency variations of beams both ends supported by the springs (conventional approach).

Ritz method by using non-integer boundary index (new approach)

Non-integer index $rbc1$ and $rbc2$ (real number is used here), where “ r ” is added to bc to distinct “the real number index” from the conventional integer one. In this approach, amplitude is modified as

$$W(\xi) = \sum_{m=0}^{M-1} A_m \xi^m (\xi+1)^{rbc1} (\xi-1)^{rbc2} \quad (5)$$

Equations (4) and (5) may appear the same equation, but the energy of springs is replaced by new kinematical constraints by real index at the edges. Therefore, functional (1) is used instead of (3) because the effect of the spring energy is included in the amplitude function directly. When $rbc1$ and $rbc2$ happen to take integer, the new approach is the same as the conventional approach because integer is a subset of real number.



(a) Frequency variations between F-F and S-S beams (b) Frequency variations between S-S and C-C beams

Fig.3 Frequency variations versus (a) $0 < bcr < 1$ and (b) $1 < bcr < 2$ (new approach).

Numerical examples

Figure 2 presents frequency variations of beams constrained with the dimensionless translational stiffness $k^*=kl^3/EI$ and rotational stiffness $k_r^*=kl^2/EI$ in the conventional approach. In (a), frequency parameters are plotted against the translational stiffness k^* and the exact frequency values of simply supported beam are written in the box. The frequencies increase and become identical with the exact values for $k^*=10^6$ - 10^8 but then for further increase of the stiffness, numerical problem occurs. Also in (b), where the rotational stiffness k_r^* is increased, numerical problem occurs for more than $k_r^*=10^8$. From these results, it is clear in the past (conventional method) that the dimensionless stiffness around $k^*=k_r^*=10^4$ or 10^5 has been used for convenience to claim the infinite stiffness $k^*=k_r^*=\infty$.

In Eq. (4), it is possible to expand the amplitude into *finite* binomial expansion due to integer index (power) and to evaluate integrals exactly, but in Eq.(5) one has to expand it into *infinite* binomial expansion. One has to truncate the expansion with finite number of terms. It turned out in the numerical experiment that the convergence is observed with 20 or 30 terms. Figure 3(a) presents variation of frequency parameters $\Omega=\omega l^2(\rho/EI)^{1/2}$ from a F-F beam to a S-S beam with changing non-integer boundary index for $0<rbc<1$. It is observed here that the rapid increase of Ω takes place for $0<rbc<0.4$. In Fig.2(b), it depicts that the frequency parameters increase moderately for $1<rbc<2$ between the frequencies of simply supported beam and clamped beam. In both figures (a) and (b), the frequency variations show very natural and moderate increase, and agreement between new and conventional approach is found in one-to-one relation.

References

- (1) Narita Y., "Combinations for the Free-vibration Behaviors of Anisotropic Rectangular Plates under General Edge Conditions", *Trans. ASME Journal Applied Mechanics*, Vol.67, (2000), pp.568-573.
- (2) Narita Y. and Robinson P., "Maximizing the Fundamental Frequency of Laminated Cylindrical Panels Using Layerwise Optimization", *International Journal of Mechanical Sciences*, Vol.48, (2006), pp.1516-1524.
- (3) Narita D. and Narita Y., "Vibration Analysis of Shallow Shells with General Surfaces Expressed by Cubic Polynomial Function", *Journal of System Design and Dynamics*, Vol.2 (2008), no.1, pp.105-116.
- (4) Narita D. and Narita Y., "Accurate Results for Free Vibration of Doubly Curved Shallow Shells of Rectangular Planform (Part.1)", *EPI International Journal of Engineering*, Vol.4, no.1 (2021), pp.29-36.
- (5) Narita Y., "Accurate Results for Free Vibration of Doubly Curved Shallow Shells of Rectangular Planform (Part.2 Thickness effect)", *EPI International Journal of Engineering*, Vol.4, no.2 (2021), pp.204-211.
- (6) Narita Y. and Innami M., "Identifying All Combinations of Boundary Conditions for In-plane Vibration of Isotropic and Anisotropic Rectangular plates", *Thin-Walled Structures*, Vol.164, (2021), 107320.
- (7) Narita Y., "Vibration Analysis of Free Rectangular Plates Constrained by Translational Edge Springs", *EPI International Journal of Engineering*, Vol.6, no.1, (2022), pp. 9-17.
- (8) Narita Y., "Vibration Analysis of Simply Supported Rectangular Plates Constrained by Rotational Edge Springs", *EPI International Journal of Engineering*, Vol.7, no.2, (2024), pp.58-67.
- (9) Li WL, Zhang X., Du J and Liu Z, "An Exact Series Solution for the Transverse Vibration of Rectangular Plates with General Elastic Boundary Supports", *J. Sound Vibr.*, 321 (2009), 254-269.
- (10) Eftekhari SA, Jafari AA, "Accurate Variational Approach for the Free Vibration of Variable Thickness Thin and Thick Plates with Edges Elastically Restrained against Translation and Rotation", *Int. J. Mech. Sci.*, 68 (2013), pp.35-46.

Linearized vibration analysis of fibre-reinforced multilayered soft materials by high order 2D finite elements

A. Pagani^{*}, P. Chiaia[#] E. Carrera[†]

^{*} Department of Mechanical and Aerospace Engineering
Politecnico di Torino

Corso Duca degli Abruzzi 24, 10129, Italy
alfonso.pagani@polito.it

[#] Department of Mechanical and Aerospace Engineering
Politecnico di Torino

Corso Duca degli Abruzzi 24, 10129, Italy
piero.chiaia@polito.it

[†] Department of Mechanical and Aerospace Engineering
Politecnico di Torino

Corso Duca degli Abruzzi 24, 10129, Italy
erasmo.carrera@polito.it

Summary

Hyperelastic soft materials are widely spread in engineering applications that mimic biological systems thanks to their capacity to undergo fully elastic deformations. These materials are extensively used in designing artificial organs, vascular grafts, and soft robotic actuators, where replicating the mechanical behavior of tissues is essential. Many biological tissues, such as skin, tendons, and arteries, are fiber-reinforced laminated structures with anisotropic properties due to their layered composition [1]. Accurately analyzing these structures requires advanced mathematical and numerical models that capture the full three-dimensional stress field at large strain and the relative influence between fibers and the surrounding matrix across layers. Due to their enhanced nonlinear behavior, accurate models are required to study the structural response under dynamic conditions. The Finite Element Method (FEM) is a valuable tool in this context, providing a versatile framework to simulate the dynamic and modal responses of such complex structures.

In the present work, high-order unified 2D plate model models for hyperelasticity and vibrations around non-trivial equilibrium states are presented in the well-established Carrera Unified Formulation (CUF). In this pure displacement-based FE model, the displacement field is expressed by a recursive polynomial expansion of kinematic models and arbitrary thickness expansion functions:

$$\mathbf{u}(x, y, z) = F_\tau(z) N_i(x, y) \mathbf{q}_{\tau i} \quad \tau = 1, 2, \dots, M; \quad i = 1, 2, \dots, N_n \quad (1)$$

where $F_\tau(z)$ is the set of expansion functions representing the theory of structure approximation adopted, $N_i(x, y)$ is the set of 2D Lagrange polynomials adopted in the FEM discretization of the reference surface, $\mathbf{q}_{\tau i}$ are the final generalized displacement components, M is a function of the structural theory adopted, and N_n is the total number of finite nodes adopted in the single element discretization. In the present framework, the weak-form governing equations are written in terms of Fundamental Nuclei (FN) [2], the elementary fundamental blocks of the present model, that allow the definition of FE matrices independently of the mathematical model adopted. Recently, high-order CUF models have been extended for the vibration analysis of a pre-stressed isotropic beam [3] and the static analysis of fibre-reinforced structures [4, 5].

The nonlinear governing equation for the static and linearized vibration problems (or undamped vibration problems) are carried out through the Principle of Virtual Displacements (PVD):

$$\delta \mathcal{L}_{int} + \delta \mathcal{L}_{ine} = \delta \mathcal{L}_{ext} \quad (2)$$

where $\delta \mathcal{L}_{int}$ is the virtual variation of the internal work, $\delta \mathcal{L}_{ine}$ and $\delta \mathcal{L}_{ext}$ are the virtual variation of the work done by inertia and external forces, respectively. Adopting the same index notation for the full Green-Lagrange strain tensor, the FN of FE matrices stem from the equilibrium equations [3], written as:

$$\delta \mathbf{u}_{sj}^T \mathbf{F}_{int}^{sj} + \delta \mathbf{u}_{sj}^T \mathbf{M}^{tsij} \ddot{\mathbf{u}}_{ti} = \delta \mathbf{u}_{sj}^T \mathbf{F}_{ext}^{sj} \quad (3)$$

The FN of internal forces \mathbf{F}_{int}^{sj} , external forces \mathbf{F}_{ext}^{sj} and mass matrix \mathbf{M}^{tsij} are independent of the kinematic model adopted and the theory of structure approximation considered; thus, Eq. (3) is the final governing equation in a hierarchical form, where the global FE matrices are obtained exploiting the summation over the recursive indices expansion. For a quasi-static nonlinear analysis, the numerical iterative scheme employed is a Newton-Raphson iterative scheme coupled with the arc-length constraint [6]. Linearizing the equilibrium equation Eq. (3), the global incremental equation is then obtained:

$$\mathbf{K}_T \Delta \mathbf{u} + \mathbf{M} \Delta \ddot{\mathbf{u}} = -\boldsymbol{\varphi}_{res}(\mathbf{u}_0, \ddot{\mathbf{u}}_0, \mathbf{f}_0) + \mathbf{I} \Delta \lambda \mathbf{f}^{rif} \quad (4)$$

The derivation of the FN of the tangent stiffness matrix can be found in [3]. Afterward, in the neighborhood of a non-trivial equilibrium state, the linearized undamped vibration analysis is defined by the linear eigenvalue problem adopting the tangent stiffness matrix:

$$(\mathbf{K}_T - \omega^2 \mathbf{M}) \boldsymbol{\Phi} = 0 \quad (5)$$

After computing the tangent stiffness matrix at equilibrium, the linear eigenvalue problem is solved to obtain natural frequencies and mode shapes around the non-trivial equilibrium state. This allows one to investigate how the pre-stressed conditions affect the modal structural properties.

In this last paragraph, the numerical results obtained for a multilayered plate made of fibre-reinforced biological tissue (iliac adventitial strips) considered in Gasser *et al.* [7] are presented. The strain energy function model adopted is then:

$$\Psi = \frac{K}{2} \left(\frac{J^2 - 1}{2} - \log J \right) + \frac{c}{2} (\bar{I}_1 - 3) + \sum_{j=4,6} \frac{k_1}{2k_2} \left[e^{k_2(k\bar{I}_1 + (1-3k)\bar{I}_j - 1)^2} - 1 \right] \quad (6)$$

where c is the initial shear modulus of the Neo-Hookean model adopted for the isotropic ground matrix, k_1 and k_2 are material constants calibrated from experimental data, K is the material bulk modulus, and k is the fiber dispersion parameter [7]. The square plate is made of two equal thicknesses $h_l = 1$ mm layers, while the lateral side of the plate is fixed to $L = 100$ mm. The geometrical features are depicted in Fig. 1(a). The material constants are described in [7] considering an aortic iliac material, for which $c = 7.6400$ kPa, $k_1 = 996.6000$ kPa, $k_2 = 524.6000$ and $K = 3.8147$ MPa, considering then a typical density value of $\rho = 1300$ kg/m³. The clamped-clamped plate of fibrous soft tissues is considered with fibers oriented in the $x-y$ plane with opening angles $\gamma_1 = 30^\circ$ and $\gamma_2 = 45^\circ$, as shown in Fig. 1(b). The first analysis considered is the global static nonlinear analysis, in which a single quadratic piece-wise Lagrange LE2 expansion model for each layer and a convergent 30×30 Q9 discretization of the reference mid-surface have been considered [4].

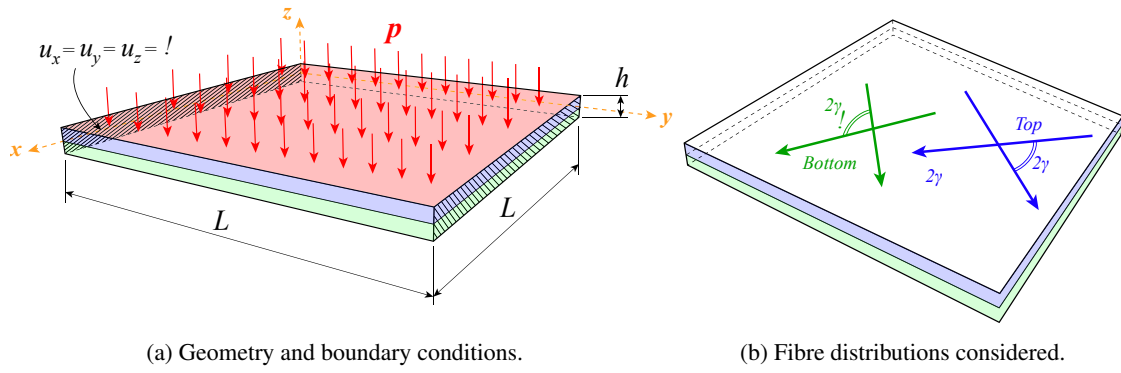


Figure 1: Multilayered biological cantilever plate: geometrical and material features considered.

The results obtained with high-order 2D CUF models are compared with a reference solution obtained with ABAQUS commercial software, comparing the proposed equilibrium paths with the load-displacement results obtained by fully 3D solutions. The ABAQUS models adopt 5000 C8D20R (20-node brick elements with reduced integrations). The proposed results obtained by 2D CUF models show a good agreement with the reference 3D solution. Thereafter, the free vibration analysis around the trivial equilibrium state is performed, assessing the performance and accuracy of the present model and analyzing the influence of the fibre dispersion parameter k on the modal behavior. Table 1 shows the convergence analysis performed considering the dispersed fibre distribution case, for which $k = 0.226$, analyzing the influence of the mid-surface discretization and theory of structure approximation regarding the first five natural frequencies. The numerical results obtained via 2D CUF models are again compared against a 3D reference solution obtained by ABAQUS commercial software, reporting the relative percentage difference in brackets. The same comparison is proposed in Table 2 regarding the case of perfectly aligned fibre ($k = 0$) case. A stiffer behavior of the structure is observed in the perfectly aligned fibre case, as also expected by the global equilibrium path shown in Fig. 2, concluding then that a softer behavior of the structure is observed when dispersed fibre is considered, both in terms of static and modal response. The constitutive behavior from a micro-mechanical level strongly influences the global dynamical features of these materials. The capabilities of the present model to analyze the static and modal behavior of biological tissues are intended to be applied for further research analysis in the field of dynamical properties of biological tissue, pulsatile and harmonic mechanical response under cyclic load, fatigue, and hysteresis.

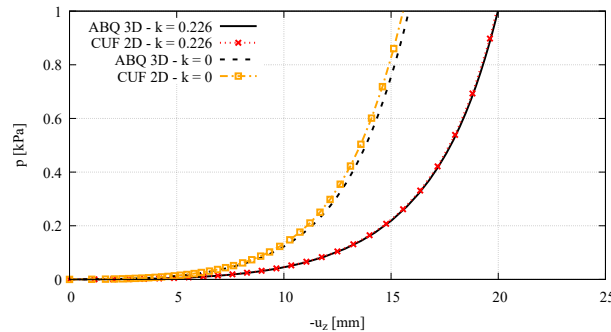


Figure 2: Biological doubly cantilever plate: equilibrium paths both for dispersed fibre ($k = 0.226$) and perfectly aligned fibre ($k = 0$) cases. Comparison between high order 2D CUF models and 3D ABAQUS reference solution.

Mode	Parabolic LE-2 (three nodes)			Cubic LE-3 (four nodes)			ABQ 3D
	10x10	20x20	30x30	10x10	20x20	30x30	C8D20
1	2.065 ^(12.53%)	1.905 ^(3.78%)	1.867 ^(1.72%)	2.063 ^(12.42%)	1.903 ^(3.71%)	1.865 ^(1.65%)	1.835
2	3.288 ^(7.82%)	3.120 ^(2.32%)	3.081 ^(1.03%)	3.284 ^(7.69%)	3.117 ^(2.22%)	3.078 ^(0.93%)	3.049
3	5.738 ^(14.39%)	5.214 ^(3.95%)	5.103 ^(1.73%)	5.727 ^(14.19%)	5.208 ^(3.83%)	5.097 ^(1.61%)	5.016
4	6.374 ^(4.33%)	6.189 ^(1.30%)	6.144 ^(0.56%)	6.365 ^(4.18%)	6.181 ^(1.16%)	6.136 ^(0.43%)	6.110
5	7.363 ^(9.96%)	6.877 ^(2.70%)	6.774 ^(1.17%)	7.348 ^(9.74%)	6.866 ^(2.55%)	6.764 ^(1.02%)	6.696
DOFs	3969	25215	55815	9261	35301	78141	84915

Table 1: Biological doubly cantilever plate: free vibration analysis around the trivial equilibrium state, dispersed fibre ($k = 0.226$) case. Natural frequencies in [Hz].

Mode	Parabolic LE-2 (three nodes)			Cubic LE-3 (four nodes)			ABQ 3D
	10x10	20x20	30x30	10x10	20x20	30x30	C8D20
1	4.193 ^(6.86%)	4.028 ^(2.64%)	3.980 ^(1.43%)	4.182 ^(6.56%)	4.016 ^(2.34%)	3.968 ^(1.13%)	3.924
2	7.329 ^(2.40%)	7.228 ^(0.99%)	7.202 ^(0.62%)	7.305 ^(2.07%)	7.205 ^(0.67%)	7.178 ^(0.29%)	7.157
3	10.817 ^(6.48%)	10.397 ^(2.34%)	10.286 ^(1.25%)	10.765 ^(5.97%)	10.346 ^(1.84%)	10.235 ^(0.75%)	10.159
4	13.812 ^(0.85%)	13.764 ^(0.50%)	13.753 ^(0.42%)	13.757 ^(0.45%)	13.708 ^(0.09%)	13.697 ^(0.01%)	13.695
5	14.375 ^(3.25%)	14.092 ^(1.21%)	14.025 ^(0.73%)	14.300 ^(2.71%)	14.017 ^(0.68%)	13.950 ^(0.19%)	13.923
DOFs	3969	25215	55815	9261	35301	78141	84915

Table 2: Biological doubly cantilever plate: free vibration analysis around the trivial equilibrium state, perfectly aligned fibre ($k = 0$) case. Natural frequencies in [Hz].

References

- [1] Holzapfel, G.A.; Humphrey, J.D.; Ogden, R.W.: “Biomechanics of soft biological tissues and organs, mechanobiology, homeostasis and modelling”. In: *Journal of The Royal Society Interface* 22.222 (2025, DOI: 10.1098/rsif.2024.0361).
- [2] Carrera, E.; Cinefra, M.; Zappino, E.; Petrolo, M.: *Finite Element Analysis of Structures Through Unified Formulation*. Wiley, 2014.
- [3] Pagani, A.; Chiaia, P.; Carrera, E.: “Vibration of solid and thin-walled slender structures made of soft materials by high-order beam finite elements”. In: *International Journal of Non-Linear Mechanics* 160 (), p. 104634.
- [4] Chiaia, P.; Pagani, A.; Cinefra, M.; Carrera, E.: “Analysis of transversely isotropic compressible and nearly-incompressible soft material structures by high order unified finite elements”. In: *Mechanics of Advanced Materials and Structures* 31.27 (), pp. 9451–9467.
- [5] Chiaia, P.; Pagani, A.; Carrera, E.: “Large strain and 3D stress analysis of laminated fiber-reinforced soft material structures with high order beam finite elements”. In: *Computers & Structures* 313 (2025), p. 107735.
- [6] Pagani, A.; Carrera, E.: “Unified formulation of geometrically nonlinear refined beam theories”. In: *Mechanics of Advanced Materials and Structures* 25.1 (2016), pp. 15–31.
- [7] Gasser, T.C.; Ogden, R.W.; Holzapfel, G.A.: “Hyperelastic modelling of arterial layers with distributed collagen fibre orientations”. In: *Journal of The Royal Society Interface* 3.6 (), pp. 15–35.

Shells under Random excitation: unusual phenomena

Francesco Pellicano^{*}, Antonio Zippo^{*}

^{*} Dept. of Engineering Enzo Ferrari, Centre Intermech MoRe
University of Modena and Reggio Emilia
V. P. Vivarelli 10 Modena, 41125, Italy
francesco.pellicano@unimore.it, antonio.zippo@unimore.it

Summary

Thin-walled structures are fundamental in various branches of structural engineering due to their high strength-to-weight ratio. For instance, in the aerospace industry, shells and plates are widely used in the structural components of aircraft fuselages and wings. Similarly, in the energy production sector, pipes and heat exchangers—often exposed to significant temperature gradients—are typically composed of thin-walled materials. Although plates and shells may appear structurally simple, their dynamic behavior is often highly complex in particular when subjected to random excitation.

Random phenomena are prevalent across many scientific fields, including Engineering, Physics, Geophysics, and Medicine. These non-deterministic occurrences often arise from the natural variability inherent in physical processes. In Engineering [1,2,3], random vibrations can result from unpredictable external forces such as wind, seismic events, or ocean waves. Buildings may experience vibrations due to wind gusts or nearby traffic, while machines and engines exhibit randomness from manufacturing imperfections, wear, and component tolerances. In electronics and communications, acoustic noise or electromagnetic interference can induce mechanical vibrations in sensitive devices. Physics addresses randomness on both microscopic and macroscopic levels [4]. Quantum mechanics is fundamentally probabilistic, while thermodynamics and statistical mechanics also rely on the concept of randomness to describe complex systems. In Geophysics, random processes underlie phenomena such as seismic activity, volcanic eruptions, and weather patterns [5]. Earthquakes, for example, are driven by sudden, unpredictable shifts in tectonic plates. While long-term patterns may be studied, the precise timing and intensity of an earthquake remain uncertain. Medicine also deals with randomness, especially in biological systems, disease dynamics, and treatment responses [6]. Neurons, for instance, do not respond to stimuli in a strictly deterministic way. Their electrical activity fluctuates due to factors like ion channel noise, synaptic variability, and intrinsic membrane properties. These variations influence when and how frequently action potentials occur, even under constant stimuli. As a result, neural behavior is often modeled using stochastic approaches to capture this variability. In all these fields, embracing randomness is essential for understanding, predicting, and managing complex systems governed by uncertain dynamics.

In the present work we report a wide experimental analysis of a polymeric shell subjected to a purely random excitation, characterized by a limited frequency band (almost monochromatic noise), which show the evidence that Extreme Events can take place also in structural systems. The system under investigation is a circular cylindrical shell, excited seismically from the base along its longitudinal axis. Such excitation gives direct forcing to axisymmetric modes and autoparametric excitation to the shell-like modes. Under extreme conditions, i.e. high forcing energy levels, the response to the random excitation exhibits unexpected Spikes, irregular both in amplitude and in temporal distribution. Such spikes present strong similitude with the phenomena observed in neuronal models, electronic circuits, laser waves and rough waves; therefore, models based on van der Pol, FitzHugh–Nagumo, Morris–Lecar, Langevin are extremely important for

interpreting the experimental evidence. The analysis of extreme events detected during the experiments revealed an oscillatory nature of spikes, with a spectral content coincident with the natural frequencies of the system, and a decay that appears to be similar to a transient response of the free oscillations of the structure. For this reason we call the events “ghost hammering”; indeed, it seems that an invisible impact excites the shell and generates the transient response.

In the paper the experimental setup and the main characteristics of the system under investigation are described. A section is dedicated to the standard linear modal analysis that is fundamental for interpreting the subsequent section focused on the stochastic resonance and the main features of the extreme events.

Figure 1a shows the experimental setup, a circular cylindrical shell clamped at the base on a shaker, which imposes a vertical motion; the top of the shell is closed with a rigid disk, where three tri-axial accelerometers are mounted to measure the vertical, tangential and radial acceleration. In Figure 1b the Laser measurement point is visible, a red spot; this allows to measure the radial vibration of the shell without perturbing the system. The physical properties and the dimensions of the shell and the upper disk are reported in Table 1. The shell material is PET (Polyethylene terephthalate) that has been selected due to the good flexibility, resilience to long heavy vibration test, and sensitivity to thermal conditions. The specimen is located inside a climate chamber to control the temperature during the tests.

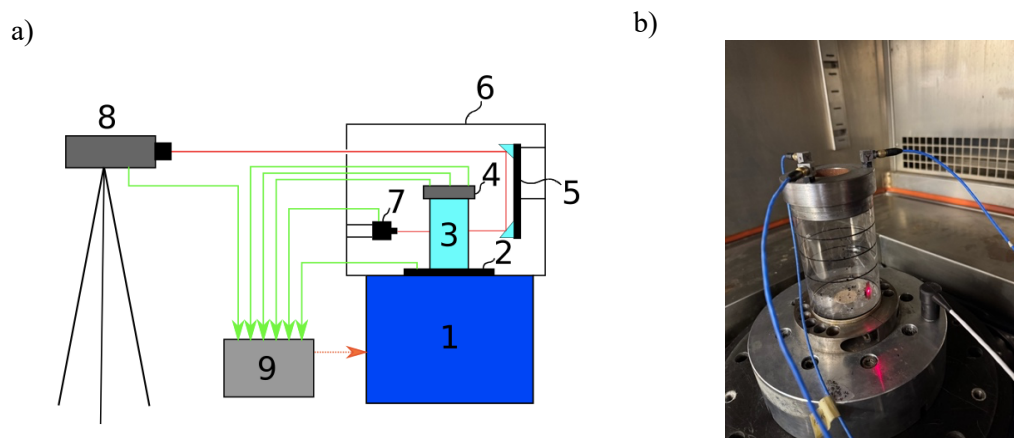


Figure 1. Test rig and detail of the measurement points

Table 1. Specimen geometric dimensions and material properties.

Shell		
Material	PET	
Density	ρ_s	1366 kg/m ³
Young modulus	E	$3.2 \cdot 10^9$ Pa
Length	L	0.135 m
External radius	R_e	0.040 m
Thickness	h	$0.38 \cdot 10^{-3}$ m
Top disk		
Material	Steel	
Mass	m_D	1.34 kg

The system is excited from the base in the vertical direction, using a narrow band random signal; see Figs. 2a,b, the bandwidth is 230-700Hz. This band is selected for two reasons: i) a wider band was impossible due to limitations of the shaker power; ii) the frequency of the first axisymmetric mode at 0°C is 270Hz, allowing the excitation of the vertical top disk vibration. The amplification of the top disk is clearly visible from the three vertical accelerometric measurements, which show

a random spectrum, Fig 2c, having the character of a monochromatic noise centred at the resonance; the time history shows a standard random character. The lateral vibration (Figures 2e,f), i.e. the shell vibration, is indirectly excited by: i) Poisson effect (very marginal); ii) autoparametric resonance. The latter indicates a high energy transfer to higher modes; such phenomenon was already observed in ref. [3]; however, here the time history shows an unexpected character, even though an almost uniform random forcing is given, the response is made by a sequence of spikes. The phenomenon has never been observed in structural systems but is known in literature as “Stochastic Resonance” or “Extreme Events”. A wide literature on such phenomena is present in studies of neuronal behaviour; typically, it is due to bi-stability of the system.

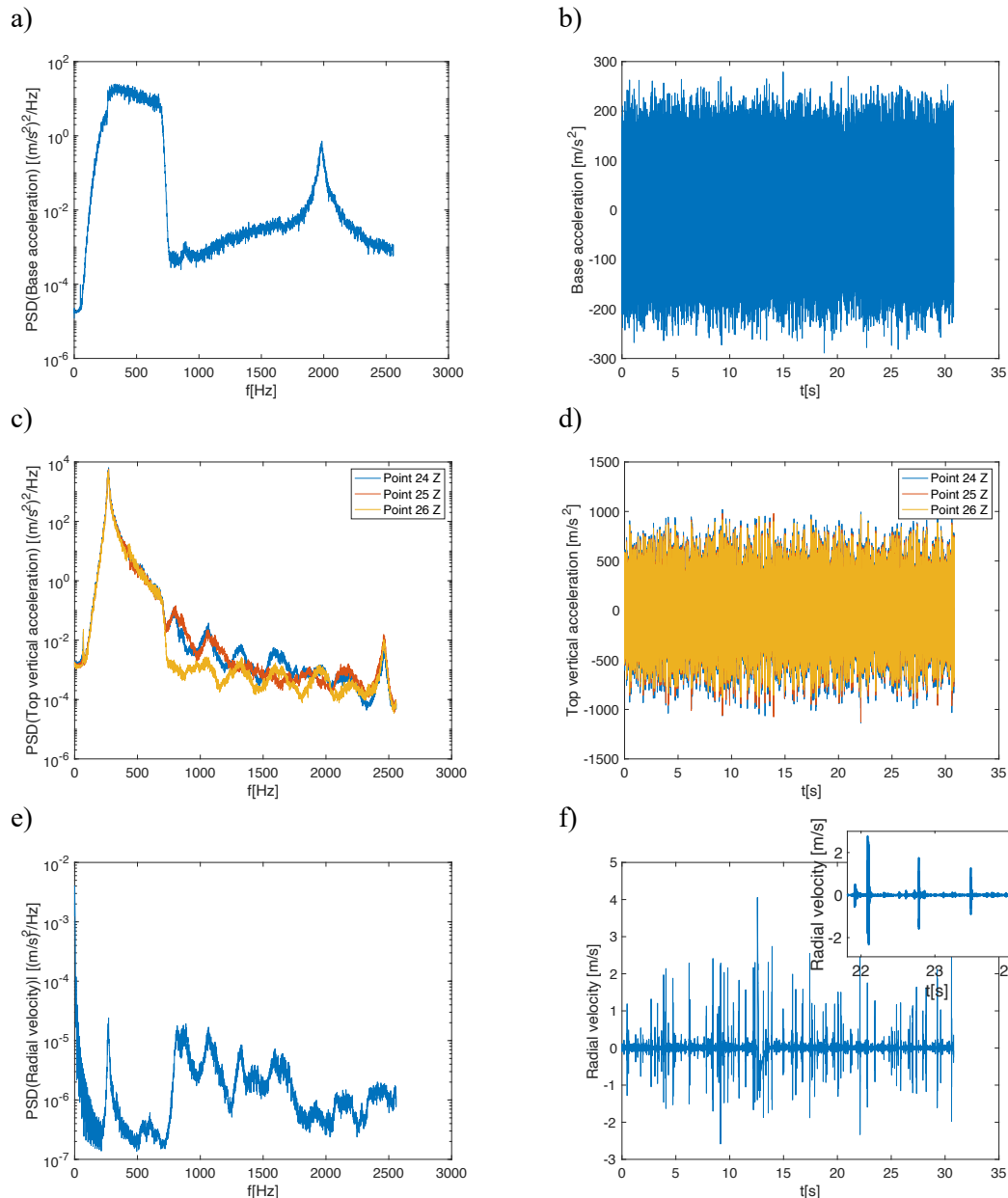


Figure 2. Response to random forcing, 0°C: a) base spectrum, b) base time response, c) top vertical spectrum, d) top vertical time response, e) lateral spectrum, f) lateral time response and zoom.

Here, the reason of the onset of events is due to a random induction of parametric instabilities due to the forcing of the first axisymmetric mode, which responds with a monochromatic noise and induces a stochastic Mathieu-like instability of the shell modes at higher frequencies.

Acknowledgement: COMETA G6176

References

- [1] Caughey, T.K., Nonlinear Theory of Random Vibrations, *Advances in Applied Mechanics* Vol. 11, Elsevier, 1971; 209-253. [https://doi.org/10.1016/S0065-2156\(08\)70343-0](https://doi.org/10.1016/S0065-2156(08)70343-0).
- [2] Roberts J. B. and Spanos P. D.. Random vibration and statistical linearization. John Wiley & Sons, 1999.
- [3] Zippo A., Iariccio G., Pellicano F. (2021) Synchronicity Phenomena in Circular Cylindrical Shells Under Random Excitation. *Advanced Structured Materials*, 157, pp. 127 – 157 DOI: 10.1007/978-3-030-75890-5_8
- [4] Zhang R., Meng L., Yuan G. X., Wang H., Collective dynamics of coupled oscillators with damping fluctuation in small-world complex networks. *Chinese Journal of Physics*. 2024; 92: 1628-1640, <https://doi.org/10.1016/j.cjph.2024.11.026>.
- [5] Bonatto C., Feyereisen M., Barland S., Giudici M., Masoller C., Rios Leite J. R., Tredicce J. R. Deterministic Optical Rogue Waves. *Physical Review Letters*. 2011; 107: 053901.
- [6] Fitzhugh R., Impulses and Physiological States in Theoretical Models of Nerve Membrane. *Biophysical Journal*. 1961; 1; 445-466.

Dynamics of a moving bandsaw blade in a narrow lubricated gap subjected to parametric excitation in axial direction

Jakob Scheidl^{*}, Alois Steindl^{*}

^{*} Institute of Mechanics and Mechatronics,
TU Wien
Getreidemarkt 9, 1060 Wien, Austria
jakob.scheidl@tuwien.ac.at, alois.steindl@tuwien.ac.at

1 Introduction and problem statement

Bandsaw blades in metal cutting operations are subjected to different excitation sources, which may increase wear, affect the accuracy of the cut or even induce violent resonant vibrations as in regenerative chattering [1, 2]. Although lubrication is always used to avoid overheating and decrease wear of the blade in practice, it is rarely taken into account in mechanical simulation models. The present contribution aims to partially bridge this gap by considering a comparatively simple planar fluid structure interaction problem featuring an axially moving Euler-Bernoulli beam (the blade) that is moving through a narrow fully lubricated gap (the sawing kerf), see Figure 1. The

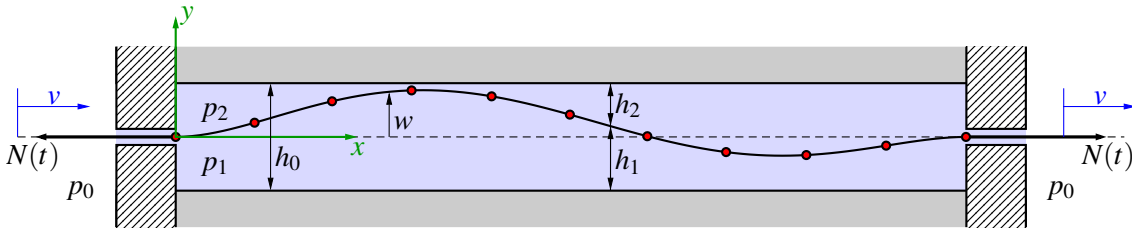


Figure 1: Fluid structure interaction problem of an axially moving beam in a lubricated narrow gap; geometric imperfections of the drive system may induce a parametric excitation due to a periodic variation of the pre-tension force N .

purely mechanical model relies on the significant simplifying assumption that the fluid-problem is governed by Reynold's lubrication theory, i.e. Newtonian fluid, negligible fluid inertia, no pressure gradient in thickness direction and uniaxial flow [3]. For this theory to hold, the lubrication film must be intact at all times and the gap width must be small in comparison to its length but large in comparison to the roughness of the kerf. Naturally, these prerequisites may be difficult to guarantee in actual cutting operations.

The primary goal of the research is an estimation of the load bearing and damping properties of a fully established lubrication film. We first conclude on these properties by performing the modal analysis of the system about the undisturbed straight reference motion; the large pre-tension N_0 of the blade is taken into account by means of classic second order beam theory. Secondly, the impact of the lubrication film on the dynamics of the blade is examined in a study on the parametric excitation in terms of a periodic variation of the pre-tension force $N(t)$, see [4, 5] for the corresponding methodology. Semi-analytical models and non-material finite element formulations are developed to perform the respective numerical computations.

1.1 Governing equations and methodology

The variational problem of the structural part follows from Hamilton's principle:

$$\int_{t_1}^{t_2} (\delta T^\Sigma - \delta U^\Sigma + \delta A_p^\Sigma) dt = 0. \quad (1)$$

It contains variations of the total kinetic energy T^Σ , the elastic strain energy U^Σ as well as the virtual work of fluid pressure forces δA_p^Σ . The energy contributions are determined by means of an integration over the active material volume currently residing in the open control domain $x \in [0, \ell]$:

$$T^\Sigma = \frac{1}{2} \int_\ell (\dot{w}^2 \rho) ds, \quad U^\Sigma = \frac{1}{2} \int_\ell (aw''^2 + N(t)w'^2) ds. \quad (2)$$

Rotatory inertia is disregarded, ρ denotes the mass per unit reference length and a the bending stiffness. The additional contribution to the strain energy accounts for von Kármán coupling of the axial pre-tension with the bending deflection w . Owing to the axial motion with constant material transport rate v , the conventional Lagrangian description in terms of the material coordinate s is replaced with a Eulerian one in terms of x by means of:

$$s = x - vt. \quad (3)$$

It follows that derivatives with respect to s and x are interchangeable and total time derivatives of a field in Eulerian parametrisation may be split into local and convective parts. In particular, the transverse particle velocity expands to:

$$\dot{w} = \partial_t w + vw', \quad (4)$$

where ∂_t is introduced to denote time derivatives at fixed points in space (at $x = \text{const.}$).

As depicted in Figure 1, the deflection and inclination of the blade are constrained by linear guides at the inlet and outlet, which also mark the boundary positions of the lubrication gap for the sake of simplicity. The pressure distributions p_1 and p_2 in either gap are governed by the Reynold's equation of lubrication theory, whose solutions are stationary values of the following quasistatic potential:

$$\Pi^\Sigma[p_\alpha] = \int_\ell \left(\frac{h_\alpha^3 p_\alpha^2}{2\eta} + 6vh'_\alpha p_\alpha + 12p_\alpha \partial_t h_\alpha \right) dx, \quad (5)$$

where η denotes dynamic viscosity of the Newtonian fluid and $\alpha \in \{1, 2\}$ is used to distinguish the lower and upper gap, respectively. Environmental pressure p_0 determines the values of the pressure fields at the boundaries of the control domain. The gap thickness depends on the nominal thickness of the kerf h_0 and the transverse displacement at the given point:

$$h_1 = \frac{h_0}{2} + w, \quad h_2 = \frac{h_0}{2} - w, \quad (6)$$

which induces the fluid-structure interaction.

The finite element description utilizes a cubic Hermitian interpolation of the primary fields $\{w, p\}$ and originates from the above stated coupled variational problem, while the semi-analytical models are derived from the corresponding strong form. A Eulerian parametrisation of the primary fields in the spatial coordinate x is natural for the fluid problem and yields a particularly efficient description for the axially moving blade, see [6, 7].

Two sources of nonlinearity are present in the given problem, namely: the coupling of primary variables in (5) and the follower-force action of the fluid on the structure in terms of a second order expansion of the virtual work δA_p^Σ . Naturally, these higher order effects do not enter the first order system that governs the small vibration problem as obtained from a linearisation about the straight reference motion. Let $\{\mathbf{q}, \mathbf{p}\}$ denote the vectors of generalised variables for the primary fields w and p_α , respectively. Then, the direct solution of the correspondingly linearised fluid problem facilitates substitution of \mathbf{p} , which leads to a reduced problem for the structural variables \mathbf{q} , given by the following linear gyroscopic system:

$$\mathbf{M} \cdot \ddot{\mathbf{q}} + (\mathbf{C} + \mathbf{G}) \cdot \dot{\mathbf{q}} + (\mathbf{K} + \mathbf{N}) \cdot \mathbf{q} = 0. \quad (7)$$

The fluid pressure distribution contributes to the damping \mathbf{C} , stiffness \mathbf{K} and circulatoric \mathbf{N} matrices, but has no impact on the mass \mathbf{M} and gyroscopic \mathbf{G} matrices. The parametric excitation in terms of a time-dependent action of the pre-tension force $N(t)$ leads to a periodic variation of the stiffness matrix. We perform a modal analysis of the homogeneous pre-tensioned problem, proceed with the analysis of the parametrically excited system and gradually extend the investigation by incorporation of the aforementioned sources of nonlinearity.

References

- [1] Tilen Thaler, Primož Potočnik, Ivan Bric, and Edvard Govekar. Chatter detection in band sawing based on discriminant analysis of sound features. *Applied Acoustics*, 77:114–121, 2014.
- [2] L. Lengoc and H. McCallion. Wide bandsaw blade under cutting conditions: Part iii: Stability of a plate moving in its plane while subjected to non-conservative cutting forces. *Journal of Sound and Vibration*, 186(1):163–179, 1995.
- [3] B.J. Hamrock, S.R. Schmid, and B.O. Jacobson. *Fundamentals of Fluid Film Lubrication*. CRC Press, 2nd edition, 2004.
- [4] Alois Steindl, Roman Buchta, Michael Ruttman, and Yury Vetyukov. Numerical investigations of large amplitude oscillations of planar parametrically excited beams. In Holm Altenbach, Hans Irschik, and Alexey V. Porubov, editors, *Progress in Continuum Mechanics*, pages 411–428. Springer Nature Switzerland, Cham, 2023.
- [5] Ivana Kovacic, Richard Rand, and Si Mohamed Sah. Mathieu’s equation and its generalizations: Overview of stability charts and their features. *Applied Mechanics Reviews*, 70(2), 2018.
- [6] Jakob Scheidl and Yury Vetyukov. Review and perspectives in applied mechanics of axially moving flexible structures. *Acta Mechanica*, 234(4):1331–1364, Apr 2023.
- [7] Yury Vetyukov. Non-material finite element modelling of large vibrations of axially moving strings and beams. *Journal of Sound and Vibration*, 414:299–317, 2018.

Structural Damage Identification Leveraging High-Frequency Interrogation and Inverse Dynamic Analysis

Jiong Tang

School of Mechanical, Aerospace, and Manufacturing Engineering
University of Connecticut
Storrs, CT 06269, USA
jiong.tang@uconn.edu

Summary

The advent of various transducer materials/devices and the rapid progress in microelectronics have resulted in the fast development of embedded structural health monitoring (SHM) systems. Currently there are two main classes of methods in SHM utilizing structural dynamic responses: the vibration-based and the wave propagation-based. The vibration-based methods utilize the change of global natural frequencies/modes as inputs. However, for this approach to be effective, the wavelength of the response measurement should be smaller than the characteristic length of the damage. Obviously, the vibration-based methods have low detection sensitivity. Alternatively, high-frequency ultrasonic wave-based methods have been studied, which use the change of transient wave propagations to infer damage occurrence. Although this class of methods lead to high detection sensitivity due to the high-frequency nature, it is difficult to use the transient responses to identify the damage accurately and especially to quantify the severity.

The piezoelectric transducers possess two-way electro-mechanical coupling, which has triggered the recent interest in developing a third type of embedded SHM methods, the piezoelectric impedance-based methods. In such an approach, the piezoelectric transducer is driven by a sinusoidal voltage sweep, and the electrical response (i.e., the resulted current) is measured to extract the impedance/admittance information. The change of piezoelectric impedance/admittance signature with respect to that under the undamaged baseline state can be used as the damage indicator. The piezoelectric impedance/admittance can be extracted in high-frequency range (e.g., higher than 30 kHz), leading to much higher detection sensitivity. Here we report how to utilize piezoelectric impedance/admittance measurement as active interrogation to identify both the location and severity of damage in a structure.

When a piezoelectric transducer is integrated to a host structure, the coupled structure-transducer interaction is characterized by the following finite element based equations [1],

$$\mathbf{M}\ddot{\mathbf{q}} + \mathbf{C}\dot{\mathbf{q}} + \mathbf{K}\mathbf{q} + \mathbf{K}_{12}\mathbf{Q} = \mathbf{0} \quad (1a)$$

$$R\dot{\mathbf{Q}} + k_c\mathbf{Q} + \mathbf{K}_{12}^T\mathbf{q} = V_{in} \quad (1b)$$

where \mathbf{q} is the displacement vector, k_c is the reciprocal of the piezoelectric capacitance; \mathbf{K}_{12} is the electromechanical coupling vector, and \mathbf{K} , \mathbf{C} , and \mathbf{M} are the stiffness, damping, and mass matrices, respectively. In this research, we use piezoelectric admittance which is the reciprocal of impedance as information carrier for damage identification. We apply frequency-sweeping harmonic voltage excitation, denoted as V_{in} . \mathbf{Q} is the electrical charge, and R is the resistance in the measurement circuitry. Here we measure the voltage drop across the resistor, which is denoted as V_{out} , and subsequently obtain the current as $\dot{\mathbf{Q}} = V_{out} / R$. We let the excitation frequency be denoted as ω , and use overbar hereafter to indicate magnitude of the corresponding response variable. Under such an active interrogation, the piezoelectric admittance of the healthy structure can be derived, based on Equations (1a) and (1b) as

$$y_h(\omega) = \frac{\dot{\bar{Q}}}{\bar{V}_{in}} = \frac{j\omega\bar{Q}}{\bar{V}_{in}} = \frac{j\omega}{j\omega R + k_c - \mathbf{K}_{12}^T (\mathbf{K} + j\omega\mathbf{C} - \omega^2\mathbf{M})^{-1} \mathbf{K}_{12}} \quad (2)$$

where j is the imaginary unit. In a finite element model for damage identification, the structure is generally divided into n segments. As such, the stiffness matrix with structural damage occurrence, \mathbf{K}_d , can then be expressed as $\mathbf{K}_d = \sum_{i=1}^n \mathbf{K}_h^i (1 - \alpha_i)$, in which \mathbf{K}_h^i is stiffness matrix of the i th segment under the healthy status. $\alpha_i \in [0, 1]$ is the damage index indicating the possible stiffness loss percentage of the i th segment, which is to be identified. The piezoelectric admittance corresponding to the damaged structure can thus be written as

$$y_d(\omega) = \frac{j\omega}{j\omega R + k_c - \mathbf{K}_{12}^T (\mathbf{K}_d + j\omega\mathbf{C} - \omega^2\mathbf{M})^{-1} \mathbf{K}_{12}} \quad (3)$$

Based on the assumption of damage being small in size, we apply the Taylor series expansion to the expression of the change of admittance and ignore the higher-order terms. In damage identification practice, we conduct frequency sweeping in the frequency-range of interest, and acquire a series of admittance changes $\Delta y(\omega_1), \dots, \Delta y(\omega_m)$, under m different excitation frequencies $\omega_1, \dots, \omega_m$. We introduce the following notations of excitation frequency vector, admittance change vector, and damage index vector,

$$\boldsymbol{\omega} = [\omega_1, \dots, \omega_m]^T \quad (4a)$$

$$\Delta \mathbf{y}(\boldsymbol{\omega}) = [\Delta y(\omega_1), \dots, \Delta y(\omega_m)]^T \quad (4b)$$

$$\boldsymbol{\alpha} = [\alpha_1, \dots, \alpha_n]^T \quad (4c)$$

Based on Equations (2) and (3), we can then obtain the following relation [2],

$$\Delta \mathbf{y} = \begin{bmatrix} \Delta y(\omega_1) \\ \vdots \\ \Delta y(\omega_m) \end{bmatrix} = \mathbf{T}_{m \times n} \boldsymbol{\alpha}_{n \times 1} \quad (5)$$

where \mathbf{T} is the finite element-based sensitivity matrix that links the admittance change vector with the damage index vector.

It is worth emphasizing that, while the damage index vector $\boldsymbol{\alpha}$ and the admittance change vector is related directly as shown in Equation (5), this equation for solving for the damage index vector is oftentimes under-determined. Structural damage manifests itself only in the vicinity of the resonant peaks in the admittance measurements, which means the information for damage inference is generally limited. Although one can increase the number of sweeping frequency points of admittance measurement, there is no guarantee that the additional measurement would lead to linearly independent information in Equation (5). In other words, simply increasing the number of measurement points does not necessarily increase the row rank of the sensitivity matrix \mathbf{T} . Aiming at tackling this issue, in this research we cast the inverse identification into a multi-objective optimization formulation. One objective is obvious, i.e., we need to minimize the difference between the measured admittance change, $\Delta \mathbf{y}$, and the model prediction in damage parametric space, $\mathbf{T}\boldsymbol{\alpha}$. In practical situation, damage usually occurs within a small region of the structure, especially when the damage is at its beginning stage with small size. Therefore, we introduce another objective function that the damage index vector $\boldsymbol{\alpha}$ is sparse with small l_0 norm. The optimization problem then takes the following form with two objective functions,

$$\text{Find: } \boldsymbol{\alpha} \in \mathbf{E}^n, \alpha_i \leq \alpha_i \leq \alpha_u, i = 1, \dots, n \quad (6a)$$

$$\text{Minimize: } f_1 = \|\Delta \mathbf{y} - \mathbf{T} \mathbf{a}\|_2 \text{ and } f_2 = \|\mathbf{a}\|_0 \quad (6b)$$

where $\|\cdot\|_2$ and $\|\cdot\|_0$ denote, respectively, the l_2 norm and the l_0 norm. It is important to note that a multi-objective optimization problem generally produces multiple solutions. This may fit well the under-determined nature of damage identification. The multiple solutions can be used as foundation for decision making in operations and maintenance (O&M), e.g., to continue operation, to dispatch further sensing mechanisms, or to pause for immediate repair.

Our goal is to develop an effective algorithm to solve the above multi-objective optimization for a solution set that is small and diverse. In recent years, significant attention has been paid to integrating metaheuristics into stochastic optimization algorithms. Here we specifically choose the multi-objective particle swarm optimization (MOPSO) as the basic approach, owing to its fast convergence and the capability of obtaining a set of trade-off solutions in a single run [3]. This offers the opportunity to significantly improve the solution quality and diversity for damage identification inverse analysis with sparsity. Particle swarm optimization employs a single search strategy to quickly converge to an optimal local region. In the absence of external interference, particles may become trapped in a valley with poor solution quality. On the other hand, while reinforcement learning [4] allows for the selection of desired actions, the absence of a fitness function in these methods makes it difficult to determine how quickly the agent (i.e., particle) can control the system's state to achieve a set of goal states. To address this, we combine the features of reinforcement learning and the MOPSO process. This combination allows for action selection by incorporating the Q-Table [4] into the fitness assessment of the MOPSO. As a result, agents can find the optimal path and learn the environment more efficiently with less complexity. Throughout the solution process, we embed a sparse population generation technique into the MOPSO, which enables the initialization and guidance of the solution sparsity.

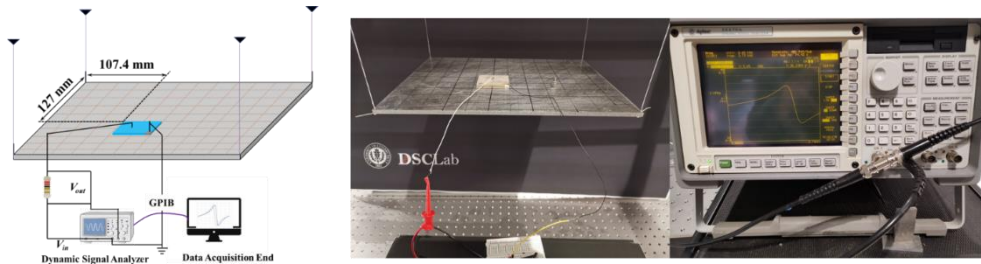


Figure 1. Case study setup

The experimental setup is shown in Figure 1. Without loss of generality, we acquire the admittance change information around two frequencies, 3,194.95 Hz (the 28th natural frequency) and 3,705.8 Hz (the 31st natural frequency). The first frequency range for admittance measurement is from 3,150 Hz to 3,230 Hz and the second is from 3,650 Hz to 3,730 Hz. Each range has 401 frequency sweeping points. In order to facilitate precise identification of damage location/severity, we divide the plate structure into 120 segments, i.e., $n = 120$ in Equations (4c) and (5). Two cases are examined. For Case 1, the true damage is positioned at the 97th segment with a local severity of 12.5%. For Case 2, damage is present at segments 59 and 97, exhibiting stiffness reductions of 9.8% and 12.5% respectively. The identification results for the two cases are presented in Figures 2 and 3. In these figures, the horizontal axis indicates the segment number or the damage location.

Four distinct observations can be obtained. First, within the setting of multi-objective optimization, for both cases we have obtained a set of multiple solutions for the under-determined problem. Second, the sizes of the solution sets are generally small, which align with our goal of

having a small solution set. Third, in both cases each individual solution/prediction exhibits good sparsity, with the maximum number of identified damage locations being four, which is indeed a very small number compared with the potential 120 damage locations, indicating the effectiveness of our identification process. Forth, for Case 1, solution (a) matches well with the true damage scenario, and for Case 2, solution (b) matches well with the true damage scenario. Therefore, we can conclude that the proposed technique can successfully identify the damage location and severity. In actual practice, once we obtain mutiple (e.g., 4) solutions for eaither case, we may dispatch further inspection to elucidate the actual situation, or decide O&M actions.

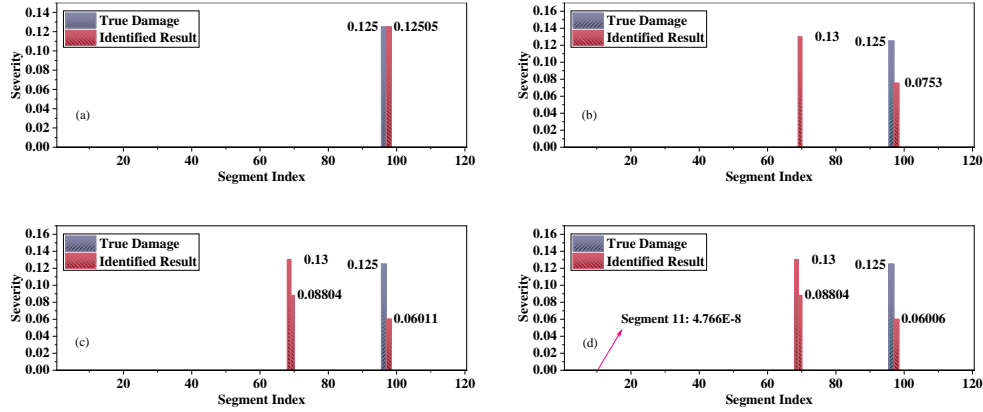


Figure 2 Case 1 identification result: solution (a) matches with true damage scenario

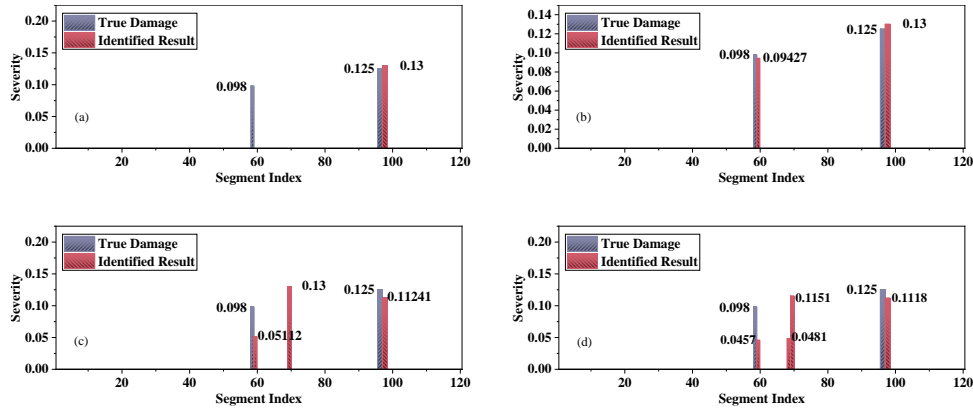


Figure 3 Case 2 identification result: solution (b) matches with true damage scenario

References

- [1] Wang, K.W., and Tang, J., Adaptive Structural System with Piezoelectric Transducer Circuitry, Springer, 2008.
- [2] Shuai, Q., Zhou, K., Zhou, S., and Tang, J., "Fault identification using piezoelectric impedance measurement and model-based intelligent inference with pre-screening," Smart Materials and Structures, V26(4), 045007, 2017.
- [3] Minh, H.L., Khatir, S., Wahab, M.A. and Cuong-Le, T., "An enhancing particle swarm optimization algorithm (EHVPSO) for damage identification in 3D transmission tower," Engineering Structures, 242, 112412, 2021.
- [4] Zhang, Y., Zhou, K., and Tang, J., "Harnessing collaborative learning automata to guide multi-objective optimization based inverse analysis for structural damage identification," Applied Soft Computing, V160, 111697, 2024.

Distributed Control of Multi-function Structronic Shell Systems with Piezo/Flexo-electric, Electro/Photo-strictive, LaSMP Actuators

Hornsen (HS) TZOU*, Mu FAN#, Dan WANG†, Yan DENG†

State Key Laboratory of Mechanics and Control of Aerospace Structures;
Interdisciplinary Research Institute of Aeronautics and Astronautics,
College of Aerospace Engineering,
Nanjing University of Aeronautics and Astronautics,
Nanjing, 210016, China
hstzou@nuaa.edu.cn*;

#mfanz@nuaa.edu.cn; †wangd12@nuaa.edu.cn; †ydeng@nuaa.edu.cn

Summary

Synergistic integration of modern "smart" materials (Table 1), structures, machines, sensors, actuators, and control electronics can transform conventional passive structures and machines to active, multi-functional and adaptive "smart" structronic (structure+electronic) systems with inherent self-sensing, diagnosis, control, heal/repair capabilities, etc [1,2]. Table 1 summarizes conventional smart materials, including piezo-/flexo-/pyro-electric, shape-memory, electro-/magneto-/photo-strictive, polyelectrolyte, electro-/magneto-rheological, superconducting, electro-luminescence, magneto-optical, etc. materials. Starting with an overview of smart materials, smart structures and advanced distributed parameter systems (DPSs) (e.g., nozzles, rockets, blades, mirrors, reflectors, antennas, solar panels/collectors, etc.), this report focuses on 1) multi-field coupling and photo-magneto-thermoelectromechanical responses of distributed photo-magneto-piezoelectric-thermoelastic structronic shell systems and 2) distributed sensing, energy generation and control of structronic shell systems.

Table 1. List of smart materials.

Piezo/pyro-electric (PZT, PVDF...)	Shape memory materials (...)	Electro-/Magneto- strictive matls.
Flexoelectric	LaSMP	
Polyelectrolyte gels (pH muscles)	Photostrictive materials, LCD	Electro-/Magneto- rheological Fluids
Superconductors, electrostatic matl.	Optical fibers, Electro- luminescence particles...	Magneto-optical, electromagnets, magnetoelastic...

The first topic focuses on distributed actuation and control using various smart materials. Actuation forces and moments defined by piezo-/flexo-electric, electro-/magneto-/photo-strictive, light-actuated shape-memory polymer (LaSMP) actuators are discussed, Figures 1-4 [1,3-8].

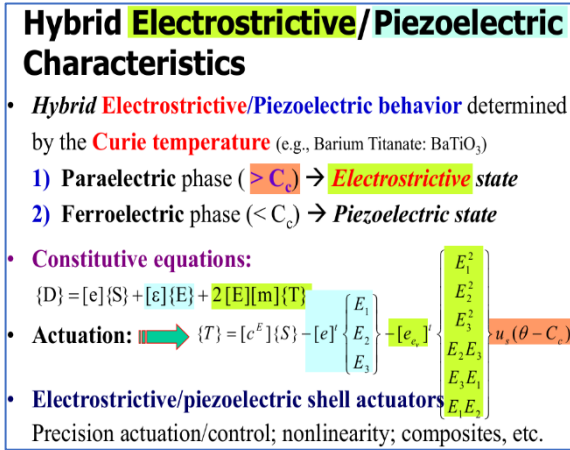


Figure 1. Hybrid piezoelectric/electrostriction.

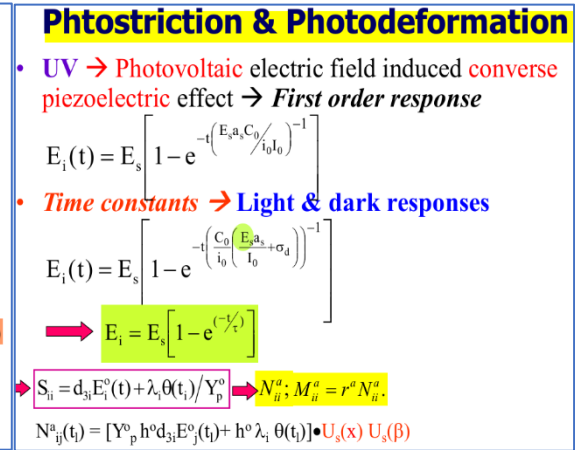


Figure 2. Photostrictive actuation.

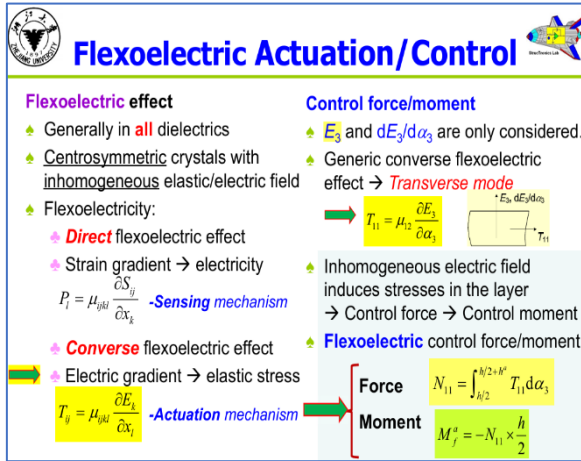


Figure 3. Flexoelectric stresses and actuation.

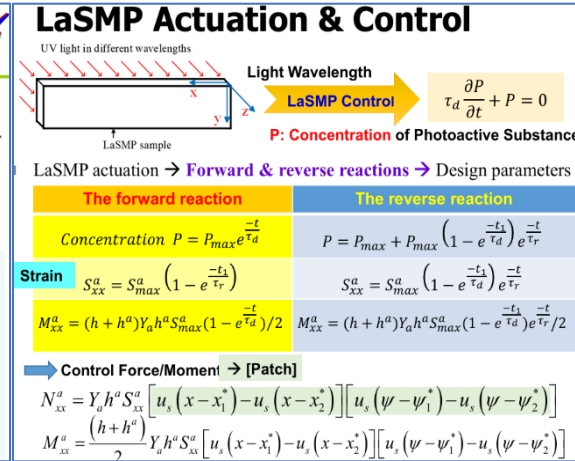


Figure 4. LaSMP induced control actions.

Figure 1 illustrates the governing actuation $\{T\}$ relationship of a hybrid electrostrictive/piezoelectric actuator with control voltage inputs E_i [3,4]; Figure 2 shows the photostrictive actuation force/moment N_{ij}^a/M_{ij}^a behaviours when subjected to ultraviolet (UV) lights [5]. Figure 3 presents the flexoelectric actuation forces/moments induced by electric field gradients $\partial E_i / \partial \alpha_i$ [6] and Figure 4, furthermore, presents the control forces/moments N_{ij}^a/M_{ij}^a of an LaSMP actuator when subjected to UV lights [7,8].

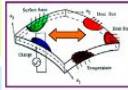
Imposing Hamilton's principle and incorporating all mechanical, electric, photo, etc. energies, one can derive shell's dynamic equations in three principle directions α_1 , α_2 and α_3 (Figure 5) and boundary conditions [1], where N_{ij} and M_{ij} are membrane forces and bending moments (including both elastic, actuator and temperature induced components respectively denoted by superscripts m, c and θ), A_1 and A_2 are Lamé parameters, R_1 and R_2 are radii of curvature, F_i ($i=1,2,3$) are the input mechanical forces, u_i ($i=1,2,3$) are the displacements on the neutral surface. In practical applications, two design principles, i.e., the segmentation technique and the shaping technique, are proposed.

$$\delta \int_{t_0}^{t_1} \left\{ \int_V \left(\frac{1}{2} \rho \dot{U}_j \dot{U}_j \right) dV - \left[\int_V (H(S_i, E_i, \Theta) + \mathfrak{T}\Theta) dV - \int_S (t_j U_j - Q_j \Phi) dS \right] \right\} dt = 0$$

- Opto-piezo-thermoelastic shell or control equations: $\alpha_1, \alpha_2, \alpha_3$

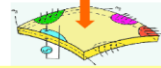
$$-\frac{\partial(N_{11}A_2)}{\partial\alpha_1} + N_{22}\frac{\partial A_2}{\partial\alpha_1} - \frac{\partial(N_{21}A_1)}{\partial\alpha_2} - N_{12}\frac{\partial A_1}{\partial\alpha_2} - \frac{1}{R_1}\left[\frac{\partial(M_{11}A_2)}{\partial\alpha_1} - M_{22}\frac{\partial A_2}{\partial\alpha_1} + \frac{\partial(M_{21}A_1)}{\partial\alpha_2} + M_{12}\frac{\partial A_1}{\partial\alpha_2}\right] + A_1A_2\text{ph\"u} = A_1A_2F_1$$

$$-\frac{\partial(N_{22}A_1)}{\partial\alpha_2}+N_{11}\frac{\partial A_1}{\partial\alpha_2}-\frac{\partial(N_{12}A_2)}{\partial\alpha_1}-N_{21}\frac{\partial A_2}{\partial\alpha_1}-\frac{1}{R_2}\left[\frac{\partial(M_{22}A_1)}{\partial\alpha_2}\right. \\ \left.-M_{11}\frac{\partial A_1}{\partial\alpha}+\frac{\partial(M_{12}A_2)}{\partial\alpha}+M_{21}\frac{\partial A_2}{\partial\alpha}\right]+A_1A_2\rho\ddot{u}_2=A_1A_2F_2$$



- **Transverse equation u_3 :**

$$\begin{aligned}
& -\frac{\partial}{\partial \alpha_1} \left[\frac{1}{A_1} \left(\frac{\partial (M_{11}A_2)}{\partial \alpha_1} - M_{22} \frac{\partial A_2}{\partial \alpha_1} + \frac{\partial (M_{21}A_1)}{\partial \alpha_2} + M_{12} \frac{\partial A_1}{\partial \alpha_2} \right) \right] \\
& -\frac{\partial}{\partial \alpha_2} \left[\frac{1}{A_2} \left(\frac{\partial (M_{22}A_1)}{\partial \alpha_2} - M_{11} \frac{\partial A_1}{\partial \alpha_2} + \frac{\partial (M_{12}A_2)}{\partial \alpha_1} + M_{21} \frac{\partial A_2}{\partial \alpha_1} \right) \right] \\
& + A_1A_2 \left(\frac{N_{11}}{R_1} + \frac{N_{22}}{R_2} \right) + (A_1A_2\rho\hbar\dot{\alpha}_3) = A_1A_2F_3
\end{aligned}$$



- * Force / Moment : Elastic, electric, and thermal effects

$$N_{ij} / M_{ij} = N_{ij}^m / M_{ij}^m + N_{ij}^e / M_{ij}^e + N_{ij}^{\theta} / M_{ij}^{\theta}$$

- **Nonlinearity:** von Karman nonlinearity - u_3

$$- \left\{ \left[\frac{\partial(N_{11} A_2/A_1)}{\partial \alpha_1} + \frac{\partial N_{12}}{\partial \alpha_2} \right] \frac{\partial u_3}{\partial \alpha_1} + \left[\frac{\partial(N_{22} A_1/A_2)}{\partial \alpha_2} + \frac{\partial N_{12}}{\partial \alpha_1} \right] \frac{\partial u_3}{\partial \alpha_2} \right. \\ \left. + 2N_{12} \frac{\partial^2 u_3}{\partial \alpha_1 \partial \alpha_2} + N_{11} \frac{A_2}{A} \frac{\partial^2 u_3}{\partial \alpha_1^2} + N_{22} \frac{A_1}{A} \frac{\partial^2 u_3}{\partial \alpha_2^2} \right\}$$

Figure 5. Hamilton's principle, three dynamic equations & von Karman nonlinearity of shells.

Simplifications of the generic double-curvature shell equations, Figure 5, to other shell/non-shell engineering structures, e.g., parabolic, toroidal, spherical, conical, cylindrical shells, rings, circular/rectangular plates, beams, etc. with two radii of curvatures R_1 and R_2 and two Lamé parameters A_1 and A_2 of selected shell/non-shell structures are demonstrated, Figure 6 [1].

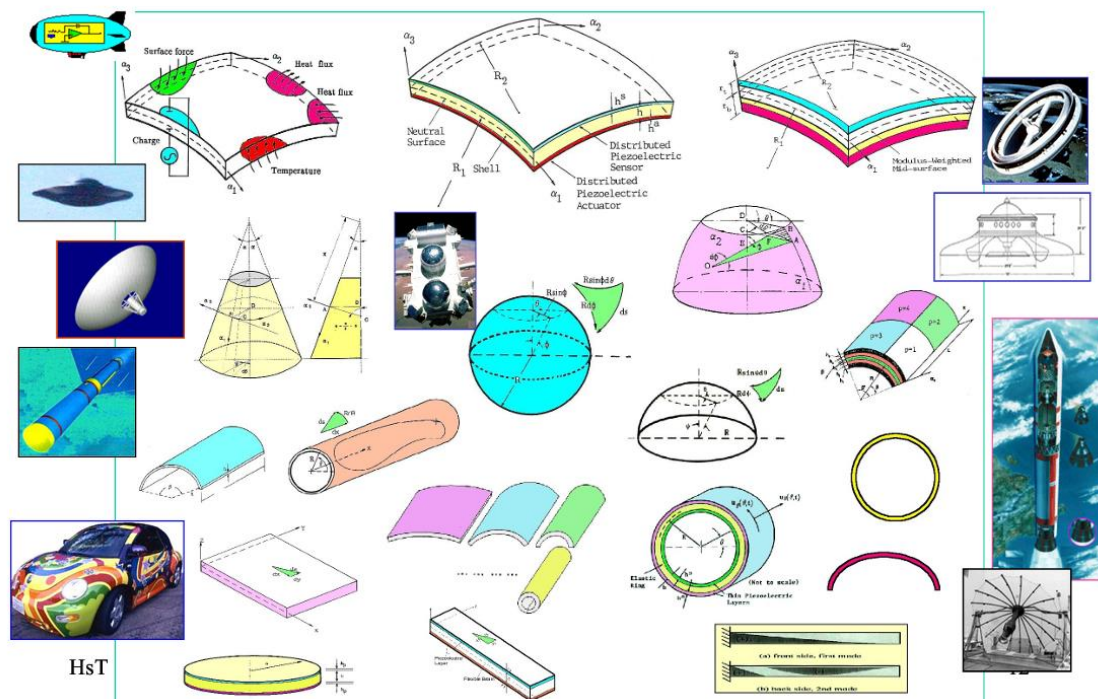


Figure 6. Generic double-curvature structronic shells and their derivative geometries.

The second topic focuses on distributed sensing, energy conversion and control of structroinc shells, i.e., elastic shells coupled with distributed sensing and control layers, including piezo-/flexo-electric, LaSMP, electro-/photo-strictive, etc. materials. Microscopic distributed energies, membrane control forces and control moments are evaluated. Practical applications to other shell/non-shell structures (Figure 6) are also discussed.

Acknowledgement

This work was supported by the National Natural Science Foundation of China (NOs. 12272175, 12102182, 12472346 and 11872206), and the State Key Laboratory of Mechanics and Control of Aerospace Structures (Nanjing University of Aeronautics and astronautics) (Grant No. MCMS-E-0521G01). Previous supports from AFOSR, ARO, NASA and NSF in USA are also gratefully acknowledged.

References

- [1] Tzou, H.S.: Piezoelectric Shells (Sensing, Energy Harvesting and Distributed Control), 2nd Edition (ISBN 978 94-024-1256-7), Springer Nature Publishers, 2019.
- [2] Tzou, H.S.; Lee, H.-J. and Arnold, S.M.: Smart Materials, Precision Sensors/Actuators, Smart Structures and Structronic Systems. *Mechanics of Advanced Materials and Structures*, Vol.11, pp.367-393, 2004.
- [3] Tzou, H.S.; Chai, W.K.; Arnold, S.M.: Structronics and Actuation of Hybrid Electrostrictive/piezoelectric Thin Shells. *ASME Journal of Vibration and Acoustics*. Vol.128, pp.79-87, Feb.2006.
- [4] Chai, W.K.; Tzou, H.S.; Arnold, S.M.; Lee, H.J.: Magnetostrictive Micro-actuators and Modal Sensitivities of Thin Cylindrical Magnetoelastic Shells. *ASME Transactions, Journal of Pressure Vessel Technology*, Vol.130, pp.011206-011206-5, Feb.2008.
- [5] Jiang, J.; Yue, H.H.; Den, Z.Q.; Tzou, H.S.: Cylindrical Shell Control with Center- and Corner-Placed Photostrictive Skew-Quad Actuator Systems. *ASME Journal of Vibration and Acoustics*, Vol.134, Issue 2: 024503-024505, 2013.
- [6] Tzou, H. S.; Deng, B; Li, H.: Flexoelectric Actuation and Vibration Control of Ring Shells. *ASME Journal of Vibration and Acoustics*, Vol.139, No.3, pp.031014, doi:10.1115/1.4036097, April, 2017.
- [7] Wang, D. ; Fan, M.; Su, Z.; Tzou, H.S.: Vibration Control of Hemispherical Shells with Light-Activated Shape Memory Polymers. *AIAA Journal*, Vol.58, No.3, pp.1369-1376, doi:10.2514/1.J058948, October, 2020
- [8] Li, H.Y. ; Wang, D. ; Tzou,H.S. : Experimental Study of Frequency Control of LaSMP Laminated Beams. *ASME Journal of Vibration and Acoustics*, Vol.144, No.5, pp.051012, doi:10.1115/1.4054436, October, 2022.

Asymptotic justification of the energy approach for estimating changes of natural frequencies of elastic structures due to damage

Yury Vetyukov

Institute of Mechanics and Mechatronics
TU Wien
Getreidemarkt 9, 1230 Vienna, Austria
yury.vetyukov@tuwien.ac.at

Introduction

Changes in an elastic structure, such as additional compliance due to local damage (cracks) or variation of inertial properties, influence the spectrum of natural frequencies. This allows to infer the severity and location of the damage by measuring the evolution of the natural frequencies, which is relevant for the goals of structural health monitoring and requires efficient prediction methods [1, 2]. The energy approach [3] estimates the small frequency shifts when the vibration modes of the unperturbed (original) structure are available, which greatly simplifies the solution of problems of structural optimization and damage identification. The asymptotic proof of the relations of the energy approach is easy in case of simple changes in mass distribution or stiffness [4]. Another explanation, presented in [5], features the asymptotic study of the continuum problem of elasticity for a 3D body with perturbations in the geometry, thus modeling a crack as a cutout. Things get more sophisticated in structural mechanics, when the damaged structure possesses richer kinematics than the original one, i.e. when the perturbed vibration modes become incompatible with the constraints of the original structure. Thus, it is common to model cracks in beams or plates by local hinges with rotational springs, which essentially introduces new degrees of freedom [6, 7]. Another example is the correction of the vibration frequency due to shear flexibility compared to a Bernoulli-Euler beam or Kirchhoff plate model. Elastic supports also fall into this category.

This conference talk provides a novel proof of the energy approach using methods of structural and analytical mechanics. With an asymptotic procedure at the abstract level of a discretized model, we capture the full variety of linearly elastic structures such as rods, plates, and shells. We show for the first time that the simple relations of the energy approach lose their validity in the situation of multiple (repeating) natural frequencies and must be replaced by a specially constructed eigenvalue problem of reduced dimensionality. Furthermore, we investigate the practically relevant vibrations of a plate with a crack of arbitrary shape, modeled as a rotational spring. Small frequency changes are evaluated at a post-processing stage based on the vibration modes of the unperturbed plate.

While the mathematical details of the formal proof of the energy approach for structures with damage will be demonstrated in the conference talk, in the following we illustrate the theoretical conclusions by simple "toy models". These models demonstrate the asymptotic accuracy of the linearized relations for frequency increments.

Energy approach for a beam with added mass

The energy approach states the following expression for the increment of a natural frequency of an elastic structure because of added elastic and inertial elements:

$$\omega_1 = \frac{\omega_0}{2T_0} (U_1 - T_1). \quad (1)$$

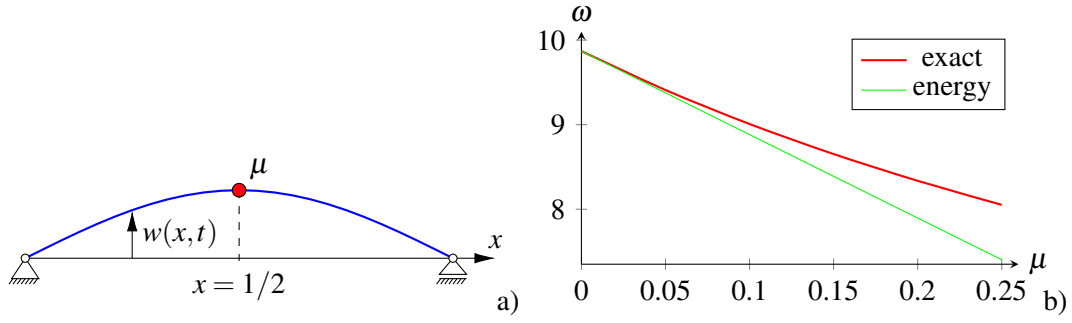


Figure 1: Natural vibration of a beam with concentrated mass in the middle (a), frequency response as of the exact eigenvalue problem Eq. (2) and the energy approach Eq. (6) (b)

Here ω_0 is a frequency of the unperturbed (original) structure and T_0 is the maximum value of its kinetic energy over the vibration period with the respective vibration mode. The maximum strain energy of the added elastic elements U_1 and the maximum kinetic energy of the added inertial elements T_1 are as well computed for the unperturbed vibration mode. A formal proof on the level of a discretized model as well as using the relations of the theory of elasticity is provided e.g. in [4]. We illustrate the theoretical considerations by a simple example of vibrations of a simply supported Bernoulli-Euler beam with a concentrated mass in the middle, see Fig. 1a. Non-dimensionalizing, seeking the deflection in the form $w(x, t) = W(x) \sin \omega t$ and considering symmetric vibration modes only, for the amplitude W we obtain the homogeneous boundary value problem (BVP) in the left half of the domain $0 \leq x \leq 1/2$:

$$\begin{aligned} W^{IV} &= \omega^2 W, & W(0) &= 0, & W''(0) &= 0, \\ W'(1/2) &= 0, & 2W'''(1/2) + \omega^2 \mu W(1/2) &= 0. \end{aligned} \quad (2)$$

The first two boundary conditions express vanishing deflection and bending moment in the hinge at $x = 0$ and the third one is the symmetry condition in the middle. The last (fourth) boundary condition features the ratio of the added mass to the mass of the beam μ . Indeed, the beam acts on the mass with the force $Q = -w'''$ from the left and from the right, resulting into the acceleration $\ddot{w} = -2Q/\mu$. From the harmonic oscillation law follows, however, $\ddot{w} = -\omega^2 w$, which results into the last boundary condition for the amplitude W .

The BVP Eq. (2) allows for a non-trivial solution $W \neq 0$ when the parameter ω belongs to the frequency spectrum. To solve this eigenvalue problem, we insert the fundamental solution of the differential equation into the boundary conditions. Equating the determinant of the system of algebraic equations for four integration constants to zero, we obtain the lengthy characteristic equation for ω . Solving the equation numerically, we obtain the exact frequency in dependence on μ as depicted in Fig. 1b.

Now we apply the energy approach Eq. (1) and notice that $U_1 = 0$ (no change in stiffness). With the first frequency and vibration mode of the unperturbed beam

$$\omega_0 = \pi^2, \quad W_0(x) = \sin \pi x \quad (3)$$

we compute the maximum of the kinetic energy of the beam

$$T_0 = \omega_0^2 \int_0^1 \frac{1}{2} W_0^2 dx = \frac{\pi^4}{4} \quad (4)$$

and of the mass

$$T_1 = \omega_0^2 \frac{1}{2} \mu W_0^2(1/2) = \frac{\mu \pi^4}{2} \quad (5)$$

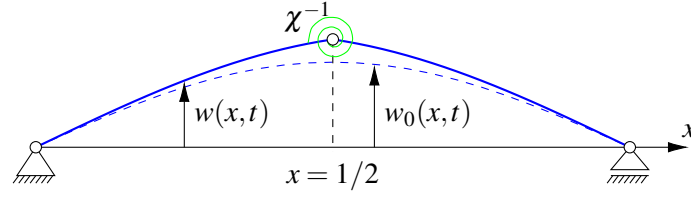


Figure 2: Natural vibration of a damaged beam with rotational spring $w(x, t)$ (solid line) and of a "healthy" beam $w_0(x, t)$ (dashed)

and find the linearized frequency correction:

$$\Rightarrow \omega_1 = -\frac{\pi^2 \mu \pi^4 / 2}{2\pi^4 / 4} = -\pi^2 \mu. \quad (6)$$

The comparison in Fig. 1b confirms the first order accuracy of the energy approach for this case.

Additional flexibility associated with released kinematic constraints

Experience shows that the energy approach successfully provides frequency changes because of cracks, modeled by introducing a hinge and a rotational spring. This might be a single spring in case of a beam or it can be distributed along a line on the surface of a vibrating plate, see [3]. The only theoretical justification to date is given in [5] and features an asymptotic study of the continuum problem of elasticity with a small change of the volume of the body. A rigorous justification on the level of structural mechanics is possible by considering a discretized model of the perturbed problem featuring its richer kinematics: the discontinuities are included in the kinematic description involving the set of the generalized coordinates. For a finite element model this means decoupling the rotational degrees of freedom in the nodes on the crack, thus allowing for a slope discontinuity and keeping the deflections C^0 continuous. Furthermore, one might consider other kinematic constraints of the original structure replaced by elastic elements in the perturbed one: adding shear deformability to a Bernoulli-Euler beam, taking flexibility of the support conditions into account, etc. The asymptotic procedure on the level of a discretized model results into an expression for the frequency reduction

$$\omega_1 = -\frac{\omega_0 U_1}{2T_0}. \quad (7)$$

Not only the negative sign differs Eq. (7) from Eq. (1) with $T_1 = 0$. More essentially, U_1 is no longer related to kinematic variables, but rather computed as the complementary strain energy of the added elastic elements available in terms of the reaction forces and internal force factors in the vibration mode of the unperturbed "healthy" structure.

As an illustration we consider a simply supported beam with a crack in the middle, modeled by a hinge and a rotational spring with the stiffness χ^{-1} , see Fig. 2. The amplitude $W(x)$ follows from the BVP Eq. (2) with the last two boundary conditions in the middle $x = 1/2$ replaced by the conditions of the absence of the transverse shear force in the middle of the beam $Q(1/2) = -W'''(1/2) = 0$ (symmetry) and the balance of the bending moment $W''(1/2)$ and the moment in the spring, whose angular deformation equals $2W'(1/2)$:

$$W'''(1/2) = 0, \quad W''(1/2) + 2\chi^{-1}W'(1/2) = 0. \quad (8)$$

The unperturbed solution Eq. (3) follows at vanishing compliance $\chi \rightarrow 0$. The complementary energy of the rotational spring equals

$$U_1 = \frac{M_0^2}{2\chi^{-1}} = \frac{\chi W_0''^2(1/2)}{2} = \frac{\chi \pi^4}{2}, \quad (9)$$

here $M_0 = W_0''(1/2)$ stands for the amplitude of the bending moment in the middle of the undamaged beam. The unperturbed kinetic energy retains the expression Eq. (4), and the frequency correction follows with Eq. (7) to

$$\omega_1 = -\pi^2 \frac{\chi \pi^4 / 2}{2\pi^4 / 4} = -\pi^2 \chi. \quad (10)$$

Noticeably, this equals the expression in Eq. (6) when the mass parameter μ is replaced by the compliance χ . Moreover, it can be shown that the characteristic equation for the new BVP is mathematically equivalent to the characteristic equation of the BVP Eq. (2) with $\mu = \chi$ – as it was already demonstrated for axial vibrations in [8]. This means that the exact frequency response in the problem with additional compliance is also identical to the one depicted in Fig. 1b.

References

- [1] Salawu, O.S.: Detection of Structural Damage through Changes in Frequency: A Review. *Engineering Structures*, Vol. 19, No. 9, pp. 718–723, 1997.
- [2] Labib, A.; Kennedy, D.; Featherston, C.: Free Vibration Analysis of Beams and Frames with Multiple Cracks for Damage Detection. *Journal of Sound and Vibration*, Vol. 333, pp. 4991–5003, 2014.
- [3] Masoudian, F.; Satpute, A.A.; Kennedy, D.; Featherston, C.A.; Ilanko, S.: Natural Frequencies of Cracked Rectangular Plates: An Energy Approach. *ISVCS 2023 – Proceedings of 13th International Symposium on Vibrations of Continuous Systems*, pp. 33–35, 2023.
- [4] Eliseev, V.: *Mechanics of Deformable Solid Bodies* (in Russian). St. Petersburg State Polytechnical University Publishing House, St. Petersburg, 2006.
- [5] Gudmundson, P.: Eigenfrequency Changes of Structures Due to Cracks, Notches or Other Geometrical Changes. *Journal of the Mechanics and Physics of Solids*, Vol. 30, pp. 339–353, 1982.
- [6] Avramov, K.; Raimberdiyev, T.: Modal Asymptotic Analysis of Subharmonic and Quasi-Periodic Flexural Vibrations of Beams with Cracks. *Nonlinear Dynamics*, Vol. 88, pp. 1213–1228, 2017.
- [7] Cannizzaro, F.; De Los Rios, J.; Caddemi, S.; Calì, I.; Ilanko, S.: On the Use of a Roving Body with Rotary Inertia to Locate Cracks in Beams. *Journal of Sound and Vibration*, Vol. 425, pp. 275–300, 2018.
- [8] Ranjbaran, A.; Shokrzadeh, A. R.; Khosravi, S.: A New Finite Element Analysis of Free Axial Vibration of Cracked Bars. *International Journal for Numerical Methods in Biomedical Engineering*, Vol. 27(10), pp.1611–1621, 2011.

Exact computation of lower bound eigenvalues of vibrating beams

Andrew Watson^{*}, David Kennedy[#] and W. Paul Howson[†]

* Dept. of Aero and Auto Engineering
Loughborough University
Loughborough, LE11 3TU, UK
a.watson@lboro.ac.uk

Independent Consultant
Penarth, CF64 5TZ, UK
kennedydcf64@aol.com

† Independent Consultant
Gwanwyn, Craig Penlline, CF71 7RT, UK
w.p.howson@gmail.com

Introduction

The body of this paper considers a clamped free Bernoulli-Euler beam from which the natural frequencies corresponding to in-plane flexure can be determined easily. A discrete lateral negative stiffness support is applied to the cantilever at its free end. The effect of the spring support is to reduce the first eigenvalue to below zero. This paper shows that by redefining the problem as a vibrating beam on a distributed elastic foundation, providing rotational restraint, ensures the first eigenvalue becomes positive. For the problem considered the elastic foundation is equivalent to tensile loading. The modified problem leads to the first eigenvalue being positive. However the first eigenvalue of the original problem can also be computed with certainty by solving the original governing differential equation with no elastic foundation which will have an initial negative eigenvalue. Negative eigenvalues typically signal instability in structural systems — such as buckling or divergence — and arise in practical scenarios ranging from slender aerospace components under axial load to MEMS devices incorporating negative-stiffness elements for enhanced sensitivity. These modes are also intentionally exploited in compliant mechanisms and metamaterials designed for vibration isolation or energy absorption. Mathematically, such eigenvalues correspond to bound states in quantum graphs, where they reflect localized or unstable modes in a network of differential operators. This spectral analogy allows tools from quantum graph theory to inform the analysis of engineered structures with non-standard supports, reinforcing the interdisciplinary relevance of the methods developed in this paper.

Theory

Consider first the exact, fourth order differential equation governing the harmonic motion of an axially loaded Bernoulli-Euler beam of length, L , that is supported on a two parameter, distributed foundation, whose transverse and rotational restraining stiffnesses per unit length are k_y and k_θ , respectively. The resulting equation is well known, can be deduced easily from Howson and Watson [1] and can be written in the following non-dimensional form

$$[D^4 + \sigma^{*2}D^2 - b^{*2}]V = 0 \quad (1)$$

where $D = d/d\xi$, $\xi = x/L$ is the non-dimensional length parameter and V is the amplitude of the transverse displacement

$$\sigma^{*2} = \sigma^2 - k_\theta^* \quad b^{*2} = b^2 - k_y^* \quad (2)$$

$$\sigma^2 = PL^2/EI \quad k_\theta^* = k_\theta L^2/EI \quad b^2 = \rho AL^4 \omega^2/EI \quad k_y^* = k_y L^4/EI \quad (3)$$

ρ and E are the density and Young's modulus of the member material respectively, A and I are the area and second moment of area of the cross-section, ω is the radian frequency of vibration and P is the static axial load in the member, which is positive for compression, zero, or negative for tension. In this paper no axial loading is applied and no lateral elastic foundation is present hence $\sigma^2 = 0$ and $k_y = 0$. In the absence of axial loading and lateral stiffness ($\sigma^2 = 0$, $k_y = 0$), the composite parameter σ^{*2} becomes purely negative due to the presence of rotational stiffness — effectively modelling a tensile effect. More generally equations (2) and (3) establish the non-dimensional member parameters σ^2 and b^2 , which uniquely define the member effects of static axial load and frequency, respectively [2, 3], together with σ^{*2} and b^{*2} which define their interaction with the non-dimensional foundation parameters.

Vibrating beam on a distributed elastic foundation

Examining the form of equations(1) and (2) shows that the σ^{*2} term includes both axial load and the rotational elastic foundation parameters. In essence what this means is that an axial tensile load is equivalent to a rotational elastic stiffness foundation. Thus the exact dynamic stiffness matrix for a freely vibrating beam on an elastic foundation can be written using the well known expressions for an axially loaded beam, as follows.

$$\mathbf{K}_{\text{mem}}^* = \frac{EI}{L} \begin{pmatrix} \gamma & \nu & -\varepsilon & \delta \\ \nu & \alpha & -\delta & \beta \\ -\varepsilon & -\delta & \gamma & -\nu \\ \delta & \beta & -\nu & \alpha \end{pmatrix} \quad (4)$$

The individual terms of the matrix in Eq. (4) are given as

$$\alpha = \frac{(p^2 + q^2)(p \cosh p \sin q - q \cos q \sinh p)}{D} \quad (5a)$$

$$\beta = \frac{(p^2 + q^2)(q \sinh p - p \sin q)}{D} \quad (5b)$$

$$\delta = \frac{(p^2 + q^2)pq(\cosh p - \cos q)}{D} \quad (5c)$$

$$\nu = \frac{pq[(2pq \sinh p \sin q - (p^2 - q^2)(\cosh p \cos q - 1)]}{D} \quad (5d)$$

$$\varepsilon = \frac{(p^2 + q^2)pq(p \sinh p + q \sin q)}{D} \quad (5e)$$

$$p^2 = -\frac{\sigma^{*2}}{2} + \sqrt{\frac{\sigma^{*4}}{4} + \lambda} \quad (5f)$$

$$q^2 = \frac{\sigma^{*2}}{2} + \sqrt{\frac{\sigma^{*2}}{4} + \lambda} \quad (5g)$$

$$\lambda = \left(\frac{\rho A \omega^2}{EI} \right) L^4 \quad (5h)$$

The exact results presented in this paper are independently checked using a well tested computer program [4]. The independent check is an analytical result using one element for the beam. It should be noted, that for results computed in this paper with an elastic foundation $-\sigma^{*2}$, the numerical value of stiffness in equations (5f) and (5g) is large enough so that the first eigenvalue is positive. An alternative method is to solve the problem using no elastic foundation which results in imaginary frequencies i.e negative eigenvalues. Results using this approach are shown in Table (1) below.

Example: Cantilever with a negative stiffness spring support at the free end

Once the stiffness matrix for the member has been obtained it is possible to look at the case of the cantilever. For this case the left hand node all degrees of freedom are constrained hence with row and column elimination the system stiffness matrix is a reduced form of the member equation Eq. (4) and is expressed as a 2x2 matrix:

$$\mathbf{K}_{CF} = \frac{EI}{L} \begin{pmatrix} \gamma & -\nu \\ -\nu & \alpha \end{pmatrix} \quad (6)$$

where K_{CF} is the system matrix for a cantilever. By introducing a discrete rotational spring of stiffness h at node 2, we modify the (2,2) term of the reduced stiffness matrix. This is equivalent to a shift in the spectrum, particularly impactful for the first mode.

$$\mathbf{K}_{CF}^* = \frac{EI}{L} \begin{pmatrix} \gamma & -\nu \\ -\nu & \alpha + h \end{pmatrix} \quad (7)$$

In the absence of an elastic foundation i.e. $k_\theta = 0$ the first eigenvalue can be negative if the value of h is sufficiently large and negative. Computation of these eigenvalues can be difficult until it is realised that the spectrum for the cantilever supported on a spring with a negative stiffness can be shifted to the right i.e. increased by the addition of a distributed elastic foundation. It is seen that all eigenvalues are increased. Therefore provided the magnitude of the stiffness of the elastic foundation is sufficient to result in the first eigenvalue being a positive value, this first eigenvalue (and higher eigenvalues) can then be computed of the modified problem with the elastic foundation.

The determinant of Eq. (7) is given as

$$|\mathbf{K}_{CF}^*| = (\gamma)(\alpha + h) - \nu^2 \quad (8)$$

The first eigenvalue λ_1 that causes this determinant to be zero must be a positive number, i.e. be above zero when the beam is vibrating freely on an elastic foundation as illustrated in Table (1).

Table 1: First three eigenvalues for a cantilever beam with a negative lateral spring of stiffness $h = -4$ with and without an elastic foundation $-\sigma^{*2}$ as shown. All numbers are non-dimensional.

Eigen No.	$-\sigma^{*2}$	λ
1	0	-4.28331
2	0	469.958
3	0	3790.65
1	20	313.530
2	20	899.904
3	20	4931.45

The new frequencies are thus higher when the beam is vibrating on an elastic foundation of positive stiffness and the first eigenvalue is positive.

References

- [1] Howson, W.P.; Watson, A.: On the provenance of hinged-hinged frequencies in Timoshenko beam theory. *Computers and Structures*, Vol. 197, pp. 71–81, 2018.
- [2] Howson, W.P.; Williams, F.W.: Natural frequencies of frames with axially loaded Timoshenko members. *Journal of Sound and Vibration*, Vol. 26, pp. 503–515, 1973.
- [3] Howson, W.P.; Banerjee, J.R.; Williams, F.W.: Concise equations and program for exact eigensolutions of plane frames including member shear. *Advances in Engineering Software*, Vol. 5, pp. 137-141, 1983.
- [4] Howson, W.P.: A teaching analysis and design program for the complete eigensolution of plane frames using microcomputers. In *International Conference on Education, Practice and Promotion of Computational Methods in Engineering Using Small Computers (EPMESC)*, 1985.

Influence of temperature on metamaterial structure dynamics: an experimental study

Antonio Zippo^{*}, Moslem Molaie^{*}, Francesco Pellicano^{*}

^{*} Dept. of Engineering Enzo Ferrari, Centre Intermech MoRe
University of Modena and Reggio Emilia
V. P. Vivarelli 10 Modena, 41125, Italy
antonio.zippo@unimore.it, francesco.pellicano@unimore.it,
moslem_molaie@unimore.it

Summary

This study explores the vibrational behavior of sandwich structures made from metamaterials using experimental methods. The focus is on honeycomb plate structures, with specimens fabricated via 3D printing to incorporate chiral geometries and a negative Poisson's ratio within their cores. The aim is to evaluate dynamic properties—such as natural frequencies and damping—and how these characteristics vary with temperature. The core layers, constructed from polylactic acid (PLA), were produced using 3D printing. Two distinct core designs were examined to compare their dynamic responses. The experimental procedures include impact hammer tests and sinusoidal excitations. The former are used to identify natural frequencies and mode shapes, while the latter are carried out on a shaking table inside a climate chamber to simulate realistic thermal conditions. Temperature plays a critical role in affecting the elastic and damping properties of the materials, as well as the specific mechanical response of the metamaterial structures.

Spacecraft and aircraft experience intense dynamic loads during takeoff, landing, and critical flight conditions, driving the ongoing need for advanced material solutions. Modern flight vehicles increasingly rely on composite materials and sandwich panels—lightweight structures known for their high impact resistance [1], thermal insulation, and cushioning capabilities [2]. Metamaterials, which are artificially engineered to exhibit specific physical properties derived from their unit cell geometry rather than their chemical composition or crystal structure, are gaining significant attention. Integrating metamaterials with composite materials has led to the emergence of a new class of sandwich structures known as composite mechanical metamaterials (CMMs).

In this work, we investigate a sandwich plate composed of carbon fiber face sheets and a 3D-printed honeycomb metamaterial core. The core structure is formed by the periodic arrangement of chiral unit cells exhibiting auxetic behavior, characterized by a negative Poisson's ratio. After fabricating the test specimens, experimental modal analysis is performed using impact hammer tests to determine the structure's mode shapes, natural frequencies, and damping ratios. Additionally, a series of shaking table tests are conducted within a climate chamber to assess how varying temperature conditions influence the dynamic response of the plate.

We consider a sandwich plate shown in Figure 1; the plate is made by 3 layers, the external ones are carbon fiber/epoxy resin (CFRP) composites of thickness $t_1 = t_3 = 0.5$ mm, with a 0/90° weft and warp stacking sequence. The intermediate layer, i.e. the core, has thickness $t_2 = 5$ mm.

Two core patterns are considered, see Figure 2.

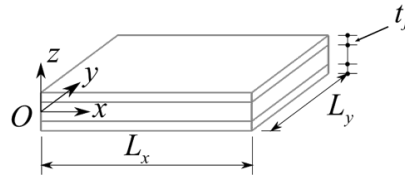


Figure 1. Dimensions of the sandwich panel.

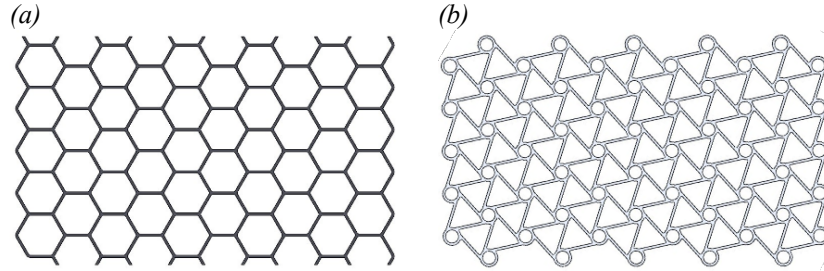


Figure 2. Patterns of the core layer: (a) regular hexagonal and (b) hexachiral core layers.

The experimental setup is shown in Figure 3, cantilever boundary conditions (CFFF) were imposed by rigidly clamping the lower edge of the plate using a vibration table adapter (VTA). Before conducting the shaking table tests, an impact modal analysis was carried out to identify the mode shapes of the samples. For this purpose, a PCB microhammer (model 086D80) with a vinyl tip was used to excite the structure, while a PCB monoaxial accelerometer (model 352C22) measured the response. Specifically, a 20-point grid was marked on the sandwich panel, and the roving hammer technique was employed to obtain the frequency response functions (FRFs).



Figure 3. Test setup.

Samples with identical unit cell densities exhibited similar mode shapes, regardless of core topology, see Figure 4a. The first mode shape corresponds to the fundamental cantilever beam mode, while the second displays a torsional behavior. Variations are observed in the FRF amplitude, with the sandwich featuring a regular honeycomb core demonstrating higher damping ratios.

Figure 4b summarizes the variation of natural frequencies and damping ratios as functions of test temperature. All samples exhibit a consistent trend, with natural frequencies decreasing monotonically as temperature increases. The damping ratio reaches its minimum at 0°C for the

sandwich with a regular core, and at 20°C for the sandwich incorporating a hexachiral intermediate layer. The key differences lie in the absolute values: the sandwich plate with an auxetic core shows higher natural frequencies but lower damping ratios compared to the sandwich with a regular honeycomb core

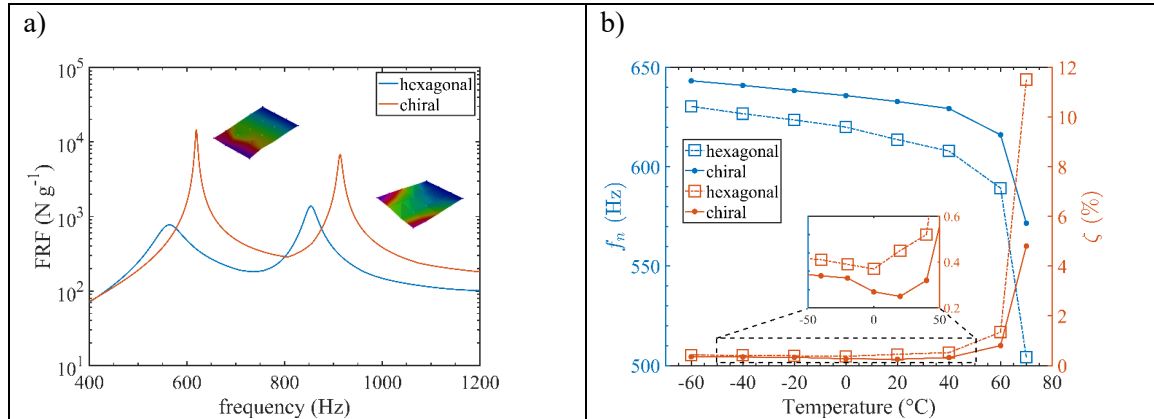


Figure 4. Dynamic characteristics: a) room temperature tests, frequency response functions for hexagonal and chiral cores; b) natural frequencies and damping dependence on temperature.

Conclusions


This study presents an experimental investigation into the dynamic response of sandwich panels featuring both auxetic and non-auxetic cores. Detailed descriptions of the test specimens and the experimental setup—used for modal analysis and shaking table tests across various temperature conditions—are provided. Under cantilever boundary conditions, the mode shapes were identified. Shaking table tests performed in controlled thermohygrometric environments revealed clear distinctions in natural frequencies and damping ratios between the samples. Notably, the sandwich panel with an auxetic core demonstrated greater stiffness and lower damping compared to its counterpart with a regular honeycomb core.

Acknowledgement: COMETA G6176

References

- [1] Karsandik, Y., Sabuncuoglu, B., Yildirim, B., and Silberschmidt, V. V., 2023, “Impact Behavior of Sandwich Composites for Aviation Applications: A Review,” *Composite Structures*, 314(January), p. 116941.
- [2] Gibson, L. J., and Ashby, M. F., eds., 1997, “The Mechanics of Honeycombs,” *Cellular Solids: Structure and Properties*, Cambridge University Press, Cambridge, pp. 93–174.
- [3] Pellicano, F. Cannillo, V. Iarriccio, G. Molaie, M. Zippo, A. Effect of temperature on the dynamics of metamaterial structures: experimental analysis. *ASME International Mechanical Engineering Congress and Exposition, Proceedings (IMECE)*, 2024, 5, V005T07A050.

Bio-sketch

<p>Prof. Haim Abramovich Faculty of Aerospace Engineering Technion, I.I.T., 32000, Haifa, ISRAEL. Email: haim@technion.ac.il; abramovich.haim@gmail.com Tel : +972 544 696566</p>	
-----------------------------------------------------------------------------------------------------------------------------------------------------------------------------------------------------------------------------------------------------------------------------------------------	------------------------------------------------------------------------------------

Obtained his B.Sc., M.Sc. and Ph.D. degrees from the Faculty of Aerospace Engineering, Technion, in 1975, 1979 and 1983, respectively.

His Ph.D. thesis was entitled “The behavior of the Blade of a Darrieus Wind Turbine”, while his M.Sc. thesis title was “Correlation between Vibrations and Buckling of Stiffened Shells with Realistic Boundary Conditions and Combined Loading”.

He has been with the Technion since 1987, and currently he is the head of the Aerospace Structures Laboratory.

He spent three years with the Israeli industry and between 1996-1998 he was Guest Professor at ETH Zurich Institut für Leichtbau und Seilbahntechnik, Switzerland, while from March-September 2018, he was at the Faculty of Aerospace Engineering, TU Delft, the Netherlands.

His main fields of interest are: static and dynamic stability of thin walled structures, piezoelectric materials, laminated composite structures, dynamic buckling of thin walled structures, smart structures technologies, structural mechanics and energy harvesting using piezoelectric and pyroelectric materials .

He has published more than 107 papers in well-known international journals on these quoted subjects. He is the author of 10 patents on piezoelectric harvesting devices. He is also the author of two new books with another one in progress:

1. H. Abramovich, *Intelligent Materials and Structures*, © 2016 Walter de Gruyter GmbH, Berlin/Boston, 386 p.
2. H. Abramovich, *Stability and Vibrations of Thin Walled Composite Structures*, © 2017 Woodhead Publishing Limited, 540 p.
3. H. Abramovich, *Advanced Aerospace Materials – Aluminum-based and Composite Materials*, in progress, to be published by Walter de Gruyter GmbH, Berlin/Boston.

Since 2017, Editor-in-Chief of The Open Aerospace Engineering Journal, Bentham Open.
Since 2013, editorial board member of the International Journal of Composite Materials
Since 2014, editorial board member for International Journal of Aeronautical Science & Aerospace Research (IJASAR).
Since 2018, editorial board member for Actuators, MDPI.



CV of Igor ANDRIANOV, RWTH Aachen University

The academic history of Igor Andrianov consists of the following steps: 1971- MSc, Mechanics, Dnepropetrovsk State University (DSU); 1975 - PhD, Physics and Mathematics, DSU; 1990 – DSc, Mechanics of Solids, Moscow Institute of Electronic Engineering; 1991 -Professor; 1996 - Soros Professor.

He worked at DSU, Dnepropetrovsk Civil Engineering Institute, RWTH Aachen University.

Co-author of 19 monographs published by various leading publishers. Editor of 3 books. Author or co-author of more than 300 papers in leading international journals. Speaker, invited speaker at numerous international conferences, organizer a large number of mini-symposiums. Recipient of scientific grants from the USA, Germany, the Netherlands, England. He supervised 25 PhD students.

Scientific interests: Asymptotology, Nonlinear Dynamics, Composite Materials, Mechanics of Solids, Science popularization.

Professor J R Banerjee, Emeritus Professor of Structural Dynamics

School of Science and Technology, City St George's, University of London, United Kingdom

Professor Ranjan Banerjee received his Bachelor's and Master's degrees in mechanical engineering from the University of Calcutta (1969) and the Indian Institute of Technology, Kharagpur (1971) respectively. He joined the Structural Engineering Division of the Indian Space Research Organisation, Trivandrum and worked there for four years (1971-75) first as a Structural Engineer and then as a Senior Structural Engineer. He was involved in the research and development of multistage solid propellant rocket structures with particular emphasis on dynamic response. Later in the year 1975 he was awarded a Commonwealth Scholarship by the Association of Commonwealth Universities to study for a PhD degree at Cranfield University where he researched within the areas of structural dynamics and aeroelasticity. He completed his PhD in 1978. An important spin-off from his PhD work is the development of an aeroelastic package called CALFUN (CALculation of Flutter speed Using Normal modes) which has been extensively used as a teaching and research tool in aeroelastic studies.

Professor Banerjee joined the University of Cardiff as a Research Associate in 1979 and worked there for six years on vibration and buckling characteristics of space structures using the dynamic stiffness method. He worked in close collaboration with NASA, Langley Research Center, and was principally involved in the development of the well-established computer program BUNVIS (BUckling or Natural Vibration of Space Frames) which was later used by NASA and other organizations to analyse spacecraft structures. He was promoted to the position of Senior Research Associate in 1982.

Professor Banerjee joined City, University of London in 1985 as a Lecturer in Aircraft Structures. He was promoted to Senior Lectureship and Readership in 1994 and 1998 respectively. In March 2003 he was promoted to Professorship. He was elected to the EPSRC Peer Review College in 1996 and served until 1999, and was re-elected in 2002, and is currently serving in the College. He has been conducting research within the technical areas of structural dynamics, aeroelasticity and composite materials for well over 40 years. To date he has published around two hundred and fifty papers in international journals and established conferences. In recognition of his research, he was awarded the degree of Doctor of Science (DSc) by City, University of London in 2017. Professor Banerjee is a Chartered Engineer and a Fellow of the Royal Aeronautical Society and the Institution of Structural Engineers and an Associate Fellow of the American Institute of Aeronautics and Astronautics.

Technion - Israel Inst. of Technology - Faculty of Civil Engineering

Moshe Eisenberger

July 2023

Degrees

B.Sc.	Civil Engineering, Technion, Haifa	1977
M.Sc.	Civil Engineering, Stanford University, USA	1978
Engineer	Civil Engineering, Stanford University, USA	1979
Ph.D.	Civil Engineering, Stanford University, USA	1980

Academic Appointments

Lecturer	Civil Engineering, Technion, Haifa	1980
Senior Lecturer	Civil Engineering, Technion, Haifa	1985
Tenure Senior Lecturer	Civil Engineering, Technion, Haifa	1987
Associate Professor	Civil Engineering, Technion, Haifa	1993
Professor	Civil Engineering, Technion, Haifa	2003
Professor Emeritus	Civil Engineering, Technion, Haifa	2020

Publications and Supervision of Graduate Students

Published over 100 Journal papers and 100 Conference papers

Supervised 32 Ph.D. and MSc. Students

Research Interests

Main area is applied and computational mechanics including static, dynamic, and stability analysis of structures. In the last 20 years I have been working on Dynamic Stiffness Analysis of various elements. Recent years were devoted to the exact solution for plate and shell vibrations.

Personal Interests

I am an active cyclist both road and mountain, and hiker. In the last years before retirement I was on sabbatical leave in Argentina and Brazil.



Matteo Filippi is a Associate Professor of the Department of Mechanical and Aerospace Engineering at Politecnico di Torino, Turin, Italy. received a Bachelor's degree in Aerospace Engineering in 2009, followed by a Master's degree in 2011. He subsequently obtained his Ph.D. from the same university in 2015. His research primarily focuses on the development of high-fidelity finite elements for stress and dynamic analyses of structures made of advanced materials, axial rotors, and rotary-wing configurations, as well as coupled thermoelastic formulations and geometric and dynamic stability analyses. Matteo has co-authored more than 100 scientific papers on these topics, which have been published in peer-reviewed international journals. He serves as editorial member of *Mechanics of Advanced Materials and Structures* and *Shock and Vibration*.



Alexander Humer is an Associate Professor at the *Institute of Technical Mechanics* (chaired by Prof. Michael Krommer) at *Johannes Kepler University* (JKU) Linz, Austria. He completed his doctoral studies under the supervision of Prof. Hans Irschik, focusing on nonlinear problems in the dynamics and stability of beams, and received his PhD in 2013. Following a brief excursion into non-university research, Alexander began his tenure as assistant professor at JKU and was awarded the *venia docendi* (habilitation) in engineering mechanics in 2020. In parallel with his academic career at JKU, he has been lecturing for over a decade at the University of Arts Linz, where he teaches fundamentals of engineering mechanics to design students.

His research spans a wide range of topics in structural and continuum mechanics as well as the development of numerical methods. Notably, he has developed a generalized sliding beam formulation to describe dynamic problems in structures exhibiting motion relative to their supports—work inspired by the classical “spaghetti problem.” He also contributes to the continuum modeling of electro-mechanically coupled systems, including the constitutive modeling of poling processes in ferroelectric materials and the development of mixed finite elements for thin-walled piezoelectric structures.

In the field of numerical methods, his recent work includes extending mixed finite element formulations to problems in elasto-plasticity and creating low-regularity shell elements for simulating viscoelastic plates and shells. His research further encompasses the design and synthesis of compliant mechanisms capable of large deformations, utilizing multi-objective optimization. A hybrid structural/continuum approach integrates computational efficiency and accuracy. Another focus of Alexander’s work lies in structural health monitoring, particularly the real-time localization of impacts on thin-walled composite structures using state-of-the-art AI techniques.

He serves on the editorial advisory board of *Acta Mechanica* and is an associate editor for *CMES – Computer Modeling in Engineering & Sciences*. Since 2024, he has been a scientific board member of the international conference on *Design, Modelling and Experiments of Advanced Structures and Systems*. He was member of the organizing committee of the *11th ECCOMAS Thematic Conference on Smart Structures and Materials* (SMART 2025), which was hosted by the Institute of Technical Mechanics in July 2025.

Sinniah Ilanko, The University of Waikato/Te Whare Wananga o Waikato

Ilanko was born in the north of Sri Lanka (Jaffna), and according to the common Tamil practice, he does not have/use a family name. Ilanko is his given name and Sinniah is his late father's given name, and conveniently remains informal as 'Ilanko'.

He graduated from the University of Manchester (U.K) with a BSc in civil engineering and also obtained an MSc from the same university under the supervision of late Dr S.C. Tillman, investigating the effect of initial imperfections on in-plane loaded rectangular plates. He commenced doctoral studies at the University of Western Ontario under the supervision of Professor S.M. Dickinson, continuing on the same topic. Soon after completing his PhD, he worked as a postdoctoral fellow at the UWO briefly before joining the University of Canterbury (NZ) in 1986. He continued his academic career at Canterbury for nearly 20 years, in various positions, as lecturer, senior lecturer and associate professor until he joined the University of Waikato in 2006. In 2012 he became a full professor. He has served as the Chairperson and later the Head of School of Engineering from January 2013 to December 2015. He has also previously served as the Head of Mechanical Engineering Department at Canterbury (2001-2202). He retired from his professorial position at the University of Waikato, but continue to be associated with it as an Honorary Professor, working on joint research with colleagues and research students.

His research areas include vibration and stability of continuous systems, numerical modelling and adaptive mechanisms. His most recent research projects include active control for adaptive stiffness foundations for earthquake isolation and crack detection using frequency measurements in structures with roving test bodies possessing rotary inertia. He has published 46 journal papers and in 2014 authored a book "The Rayleigh-Ritz Method for Structural Analysis" jointly with Dr Luis Monterrubio and Dr Yusuke Mochida. He has served as the Subject Editor for Journal of Sound and Vibration (2009-2020), for analytical methods for linear vibration and since 2021 he has been serving as a Receiving Editor/Deputy Editor-in-Chief. He has secured two major grants, a [Marsden grant](#) for research into vibration analysis of complex structures and a [grant](#) by the New Zealand government's Ministry of Business Innovation and Employment (Category Smart Ideas) to conduct research on the development of an omnidirectional base isolator.

His current research topics include adaptive vibration isolation from vertical seismic excitation and crack detection. He is also interested in computer-aided learning and has developed and used several interactive lectures and tutorials for teaching Mechanics of Materials and Vibration, as well as computer-based interactive tutorials and games for learning/teaching Tamil language.

ZHAO JING

Personal Data

Professor Zhao Jing was born on 20th, January, 1989. Currently work at School of Aeronautics, Northwestern Polytechnical University. Hobbies include basketball, swimming, and hiking.



Email: jingzhao@nwpu.edu.cn

Website: <https://teacher.nwpu.edu.cn/2019010151.html>

Google Scholar Profiles: <https://scholar.google.com/citations?user=UHKpbYEAAAAJ&hl=zh-CN>

EDUCATIONAL BACKGROUND

09/2011 – 01/2017 D.Eng. in Aircraft Design, Northwestern Polytechnical University

03/2015 – 03/2016 Joint PhD training in Mechanical Engineering, Loughborough University, UK

09/2007 – 06/2011 B.S. in Aircraft Design & Engineering, Northwestern Polytechnical University

WORK EXPERIENCE

07/2019- Present

Associate Professor, School of Aeronautics, Northwestern Polytechnical University

01/2017-06/2019

Postdoctoral, Department of Mechanics, Huazhong University of Science and Technology

RESEARCH INTERESTS

His research spans a wide range of challenges lying at computational solid mechanics, mechanics of variable stiffness structures, composite structures optimization, aircraft structural design and lightweighting, plate and shell structural analytical methods and numerical techniques.

He combines mathematics, experiments, mechanics theory, computer programming and simulations to develop innovative numerical methods and optimization techniques for simulations of structural behaviors with complex geometries and optimizations of large-scale composite structures. Currently working on developing a new numerical method, energy element method (EEM) /discrete Ritz method (DRM), combining extended interval integral, Gauss quadrature, variable stiffness, energy elements, and a global trial function to address the mechanical variational problems of structures on complex geometric domains. Simultaneously, he has developed several optimization algorithms based on mechanics of composite materials, i.e. two and three-dimensional sampling optimization algorithms, sequential permutation search, variable stiffness optimization algorithm, and global-shared layer blending method for design and optimization of large-scale composite structures.

MAJOR ACCOMPLISHMENTS

Hosted the two National Natural Science Foundations, Qin Chuangyuan Construction of Two-Chain Integration Special Project, Aeronautical Science Foundation of China, Natural Science Foundation of Shaanxi Province, two Foundations of Central Universities. Published more than 40 papers and authorized 5 national invention patents. Give more than 20 talks at int. conferences.

In 2023, he obtained the Digital Simulation Youth Science and Technology Award (China Digital Simulation Society) for solving the problem that Ritz method (a variational method) could not be applied on complex geometric domains. In 2022, he obtained the first prize of the Shaanxi Higher Education Institutions Science and Technology Research Outstanding Achievements Award, the second prize of the China Composite Materials Association Science and Technology Award, and the 2019 Shaanxi Province Excellent Doctoral Thesis and Excellent doctoral thesis from Northwestern Polytechnical University, for his research on large-scale composite structures optimization.

Reviews of Journal papers

AIAA Journal; Computer methods Applied in Mechanics and Engineering; Computers & Structures; Thin-walled Structures; Composite Structures; International Journal of Mechanical Science; Engineering Analysis with Boundary Elements; International Journal of Structural Stability and Dynamics; Structures; Engineering Structures; Mathematics.

SELECTED KEY PUBLICATIONS

1. **Jing, Z.*** (2024): Energy Element Method for Three-Dimensional Vibration Analysis of Stiffened Plates with Complex Geometries. *AIAA Journal*. 62(11): 4189-4206.
2. **Jing, Z.*** Liu Y, Duan L, et al. (2025): Three-dimensional buckling analysis of stiffened plates with complex geometries using energy element method. *International Journal of Solids and Structures*. 306: 113105.
3. **Jing, Z.***, (2023): Variable stiffness discrete Ritz method for free vibration analysis of plates in arbitrary geometries. *Journal of Sound and Vibration*. 553, 117662.
4. **Jing, Z.***, Duan, L. (2024): Free vibration analysis of three-dimensional solids with arbitrary geometries using discrete Ritz method. *Journal of Sound and Vibration*. 571, 118132.
5. **Jing, Z.***, Duan, L., (2023): Discrete Ritz method for buckling analysis of arbitrarily shaped plates with arbitrary cutouts. *Thin-Walled Structures*. 193, 111294.
6. **Jing, Z.***, (2022): Lamination Parameter-Based Two-Dimension Sampling Optimization Method for Stacking Sequence Design of Composite Laminates. *AIAA Journal*. 60(5), 3225-3250.
7. **Jing, Z.***, (2020): Semi-analytical Optimal Solution for Maximum Buckling Load of Simply Supported Orthotropic Plates. *International Journal of Mechanical Sciences*. 187: 105930.
8. **Jing, Z.***, Duan, L., Wang, S., (2024): Buckling optimization of variable-stiffness composite plates with two circular holes using discrete Ritz method and potential flow. *International Journal of Solids and Structures*. 297: 112845.



Dr. Moslem Molaie Emamzadeh is a researcher in mechanical engineering with a strong focus on nonlinear dynamics, mechanical transmissions, and structural vibrations. He earned his Ph.D. in Mechanical Engineering from the University of Modena and Reggio Emilia, Italy, where he developed advanced models on the nonlinear dynamics of spiral bevel gears under the supervision of Prof. Francesco Pellicano.

Prior to his doctoral studies, Dr. Molaie completed his M.Sc. and B.Sc. in Mechanical Engineering at Shahid Bahonar University of Kerman, Iran, specializing in applied mechanics and solid mechanics. His early research included simulation-based optimization of gear systems and advanced material processing in large-scale industrial settings, such as the Sarcheshmeh Copper Complex.

Dr. Molaie has contributed to several international research projects in Italy and Iran, ranging from Industry 4.0 predictive maintenance platforms to gear life prognostics using advanced simulation tools like KISSsoft and Romax. He is currently involved in research projects on electromechanical actuators for e-mobility and sustainable retrofitting of industrial machinery.

He is the author of over 20 peer-reviewed journal articles and numerous international conference papers, and has received honors such as the “Sir James Lighthill Student Best Paper Award” and the “CM 2024 Conference Attendance and Travel Award.” Dr. Molaie is also active in teaching and mentoring. He has served as a teaching assistant in subjects such as Vehicle Mechanics and Prognostics and Diagnostics, and previously worked as a lab manager for dynamics and vibration courses.



Dr. Fan Mu is an Associate Researcher at the College of Aerospace Engineering, Nanjing University of Aeronautics and Astronautics. He earned his Ph.D. in Engineering Mechanics from Nanyang Technological University, Singapore, and his bachelor's degree in Aircraft Design from Harbin Institute of Technology. On December 7, 2020, he was elected as a member of the Academic Committee of the American Society of Mechanical Engineers "Dynamics and Control of Systems and Structures (DCSS)", and in December 2022, he was elected as a member of the Academic Committee of the International Conference on Adaptive Structures and Technology of ICAST. He has published more than 50 academic papers, including mainstream journals in the fields of AIAA Journal, ASME Trans. JVA, JIMSS, etc. He hosted several coupling special sessions at the IMECE conference of the American Society of Mechanical Engineers (2019~2023) and co-organized the IDETC-CIE "Structural Electronic Systems and Precision Drives" WORKSHOP. He was approved for the Ministry of Science and Technology's High-end Foreign Experts Introduction Program, the National Natural Science Foundation (General, Youth), and the Jiangsu Natural Science Foundation. He participated in a number of cooperative technology development projects with scientific research institutes such as the First, Second, and Third Academy of Aerospace, and participated in 2 major national scientific and technological research projects. The research group currently has 6 graduate students. Most of the graduated students are employed in aerospace research institutes and central/state-owned enterprises.

Yoshi (Yoshihiro Narita)

Hokkaido University (Prof. Emeritus), Sapporo, Japan

I am a retired professor of Mechanical Engineering at Hokkaido University (HU) Sapporo Japan and other institutions. I started my research on vibration of continuous systems when I was a PhD student under adviser Prof. Irie of HU in 1976, and had a chance to study one year in 1978-1979 under Prof. Leissa at the Ohio State University. I have attended all the ISVCS's except for only once. I am very delighted to see old and new friends in Austria. I also hope to enjoy hiking this time (in 2024, I took surgeries to replace both of my knees with artificial mechanical joints).



Let's enjoy!

<career>

1951	Born in Sapporo, Japan (now, age 74)
1980	PhD Hokkaido University
1980-2004	Hokkaido Institute of Technology (Sapporo)
2004-2017	Hokkaido University (Sapporo)(now, Professor Emeritus)
2017-2020	JICA (Japan Intl. Corp. Agency) advisor for universities in east Indonesia
2020-2023	Yamato University (Osaka)
2023-present	Board chairman of Hokkaido Lutheran Institution (running four kindergartens)



Alfonso Pagani is Professor in the Department of Mechanical and Aerospace Engineering at the Politecnico di Torino. He earned a PhD in Fluid Dynamics (Aeroelasticity) from the Politecnico di Torino in 2015 and later a PhD in Aerospace Engineering from City University of London.

Dr. Pagani is associate editor for *AIDAA Aerotecnica Missili & Spazio*, *Advances in Aircraft and Spacecraft Structures* and the *International Journal of Dynamics and Control*. He conducts his research on Carrera Unified Formulation (CUF), structures, space mechanisms and advanced materials mechanics at the MUL2 Lab (www.mul2.com). He has published over 200 scientific articles in leading international journals, contributing to both fundamental and applied aspects of aerospace engineering and structures. Recognizing his contributions to the

field, he has indeed garnered several prestigious awards, including a Wiley Best Paper Award in 2023 and the Ian Marshall's Award in 2013.

Dr. Pagani is the PI of the EU-H2020 ERC-StG project PRE-ECO, which aims to explore a novel approach to addressing the challenges associated with the design of variable stiffness structures for aerospace applications (www.pre-eco.eu). Additionally, he is the deputy for Spoke 8 in the Extended Partnership "Space It Up!", a program funded by the Italian Space Agency that focuses on advancing human and robotic space exploration.

In 2018, Alfonso joined the California Institute of Technology as a Visiting Associate to work on the acoustics of metamaterials. He has also conducted research at Purdue University in 2016, where he worked on the micromechanics of fiber-reinforced composites; at RMIT in Melbourne in 2014; and at the University of Porto in 2013.

Since 2013 in Courmayeur, Alfonso has been a regular attendee of the ISVCS.

Biography

of Francesco Pellicano

Francesco Pellicano is Aeronautical Engineer and Ph.D. in Theoretical and Applied Mechanics, he is currently Full Professor, Head of the Centre Intermech MoRe and was committee president of 2 BsC and 2 MsC programmes. He was coordinator (PI or local) of several projects: COMETA, NATO (composite metamaterials), METaGEAR POR-FESR (Gears, Materials, Robotics), INDGEAR, EU-Fp7 (condition monitoring) and HPGA Fortissimo, EU-Fp7 (applications of high performance computing). He published 2 Books, more than 80 Journal papers and more than 100 conference papers. Bibliometry: 176 papers on Scopus, h-index 36, more than 3000 citations.

His research activities are:

Fluid-structure interaction: cooperating with Prof. Amabili and Païdoussis developed models for vibration and stability analyses of shells interacting with incompressible heavy fluids, compressible and supersonic fluids; recently interactions with non-Newtonian fluids were investigated.

Gear stress and vibration modelling and testing, the research was focused on vibration aspects of gears including non-smooth dynamics and chaotic vibration, optimization using Genetic Algorithms, Diagnostics and Prognostics.

Vibration control using active passive techniques: active control through piezo-electric actuators, active control of suspension through variable stiffness for earthquake applications; linear and nonlinear dynamic absorbers and applications to railways bridges; quasi-zero stiffness suspension for earthquake applications; origami isolators and applications to automotive.

Shell dynamics and stability: modal interactions, nonlinear random responses and synchronization phenomena, thermal effects and their impact on the dynamic scenario.

Vibration of carbon nanotubes: development of new continuous shell models for investigating the vibration characteristics of single and multiwalled nanotubes considering size effects and van der Waals interactions.

CV of Jakob Scheidl

**Institute of Mechanics and Mechatronics, Mechanics of Solids,
TU Wien**

Dr. Jakob Scheidl is a tenure track holder at the research unit Mechanics of Solids at the Institute of Mechanics and Mechatronics at TU Wien, Austria.

He obtained his master's and doctoral degrees in mechanical engineering at TU Wien. His primary field of expertise is structural mechanics, with particular focus on dynamics and quasistatics of moving structures, distributed frictionless and frictional contact of thin structures with solid counterparts, and structures that exhibit in-elastic material behaviour such as plasticity.



Jakob Scheidl currently leads a nationally funded research project on the simulation of continuous roll forming of thin metal sheets. For this sake, special algorithms are combined with an application-oriented shell finite element model, including contact and plasticity, to facilitate the efficient simulation of the continuous forming process.

As a prospective member of the editorial board, Jakob Scheidl frequently acts as a reviewer for Acta Mechanica. He has organised mini-symposia with regards to dynamics and large deformations of structures and acts as local co-organiser of this years ISVCS symposium in Austria.



Bio: Dr. Jiong Tang is the Pratt & Whitney Chair Professor in Design and Manufacturing at School of Mechanical, Aerospace, and Manufacturing Engineering, University of Connecticut (UConn), USA. Dr. Tang's principal teaching and research interests are in the general areas of dynamics and vibrations, control, sensing and automation. He received the B.S. and M.S. degrees in Applied Mechanics from Fudan University, China, in 1989 and 1992, respectively, and the Ph.D. degree in Mechanical Engineering from the Pennsylvania State University in 2001. Prior to joining UConn in 2002, he worked in GE Research Center as a research engineer. Dr. Tang's research has been supported extensively by federal agencies including NSF, DOD, NASA, DOT etc,

and by industries, with total amount exceeding \$30M. He has published over 270 journal articles and conference papers. Dr. Tang is a Fellow of the ASME and an elected member of the Connecticut Academy of Science and Engineering. He received the N.O. Myklestad Award of ASME in 2024, in recognition of major innovative contribution to vibration engineering.



Hornsen (HS) TZOU, Nanjing Univ. of Aeronautics and Astronautics, Nanjing, PRC; Univ. of Kentucky, USA.

Hornsen (HS) TZOU is an ASME Fellow, British RSA Life-fellow, ScholarGPS Highly Ranked Scholar worldwide #6 in Vibration Control and #10 in Piezoelectricity, Professor Emeritus of the University of Kentucky, the 1st-round Chinese QR Fellow of China (2008) and was the Director of Interdisciplinary Research Institute of Aero. & Astronautics in College of Aerospace Engineering at Nanjing University of Aeronautics and Astronautics, a Chair-Professor at Zhejiang University etc. He was among the pioneers in **“smart structures and structronic systems.”** His research and teaching interests encompass smart structures and structronic systems, multi-field photo/electro/magnetic/elastic/temp. coupling and distributed control, design and precision-actuation of devices, sensors and actuators, etc.

He worked/visited at IBM, Wright Laboratory, the Institute of Space and Astronautical Science (Japan), Tohoku University, the Otto-von-Guericke University of Magdeburg and German Aerospace Research Establishment (DLR), Amway Research R&D, Tokyo Institute of Technology, NASA-Levis, Harbin Institute of Technology, Natl. Taiwan University, etc. Dr. Tzou has won many *ASME/AIAA Best-Paper Awards*, *ASME Outstanding Service Awards* and *NASA Class-1 New Technology Disclosure Awards*, etc. He has published over 500 technical publications, authored ***Piezoelectric Shells (Sensing, Energy Harvesting and Distributed Control)***, ***Distributed Control of Nonlinear Structronic Shells*** and ***Design of Smart Structures, Devices and Structronic Systems***, and edited seven other books.

He was the Chair of ASME *Board on Technical Knowledge Dissemination*, Executive Member of *Technical Communities Operating Board* and Chair of the *Interdisciplinary Councils*, a founding member of the ASME *Adaptive Structures and Material Systems Committee* (now a *Division*), a life-member of ASME *Dynamics and Control of Structures and Systems committee*, ICASST IOC member, Chief-editor of *J. of Aerospace Sc. and Technology*, etc.





Prof. Yury Vetyukov

Biosketch

Yury Vetyukov studied applied mechanics at St. Petersburg State Polytechnical University, Russia and graduated in 2000 with distinction. His master thesis was devoted to large spatial deformations of thin curved rods. As a doctoral student of the same university he studied self-excited axial-torsional vibrations of rotating drillstrings at deep oilwell drilling and obtained his PhD in 2004. Between 2002 and 2004 he worked as a research assistant at the Johannes Kepler University Linz, Austria. From 2004 until 2008 he was an assistant professor in St. Petersburg. Here he started his career as a university teacher and independent

researcher, focusing on nonlinear mechanics of thin-walled structures (elastic shells, rods and thin-walled rods). In 2008 he returned to Linz as a post-doctoral researcher and stayed there until 2015, working in various basic and industrial research projects. A monograph entitled “Nonlinear mechanics of thin-walled structures: asymptotics, direct approach and numerical analysis” was published by him in 2014 at Springer. Since 2015 Yury Vetyukov is working at the Institute of Mechanics and Mechatronics at Technische Universität Wien (formerly known as Vienna University of Technology), Austria. Here he received his *venia docendi* in 2017. Having started as a post-doctoral researcher, in 2021 he was appointed as a full university professor and is currently the head of division of mechanics of solids.

Research interests of Yury Vetyukov comprise various aspects of structural mechanics and thin-walled structures. He actively puts into practice analytical methods based on direct tensor calculus, asymptotic techniques and analytical mechanics. Problem specific novel numerical approaches also stay in the focus of his basic and applied research. In the recent years, he mainly deals with axially moving structures such as flexible belts, elevator cables or moving metal sheets during forming processes. Nonlinear effects of material inelasticity, various contact phenomena and dynamics along with the motion of the structure across various qualitatively different domains make respective problem formulations often inaccessible for conventional methods of analysis or by means of commercial software. Along with several novel analytical solutions, Yury Vetyukov and his colleagues are developing problem-specific numerical approaches featuring non-material kinematic description in the framework of mixed Eulerian-Lagrangian formulation.

Andrew Watson
Lecturer of Aerospace Structures
Department of Aeronautical and Automotive Engineering
Loughborough University, United Kingdom

Andrew obtained his undergraduate and higher degrees from Cardiff University. His PhD looked at the stability analysis and optimisation of light weight structures. After two post-doctoral appointments at Cardiff Andrew joined Loughborough University as a member of academic staff in 2004.

His research includes buckling and postbuckling of aerospace panels and vibration of Timoshenko beams. Buckling and vibration problems can be approached by using the Dynamic Stiffness Method along with the Wittrick-Williams algorithm. Vibrating structures can be modelled as quantum graphs and Andrew is currently researching higher order graphs to obtain the spectral results of tree shaped graphs all using the DSM.

Outside of this research Andrew has been looking at fossil fuels and other finite resources. To facilitate this he is developing analytical methods to optimise structures where the objective function can be mass, energy costs or environmental degradation. Jaguar Land Rover are funding a research studentship looking at thermal management of electric vehicles.

In his spare time he likes to keep up with current affairs and enjoys walking and swimming.

Professor **Antonio Zippo** is a mechanical engineer with PhD in "Advanced Mechanics and Vehicle Techniques", he is currently an Associate Professor of Mechanism and Machine Theory, Applied Mechanics and Mechanical Vibration since 1 June 2023 at "Enzo Ferrari" Department of Engineering, University of Modena and Reggio Emilia - UNIMORE.

He has received the following funding for research activities:

- FAR2022 - Identification, modelling and analysis of nonlinear EMG signals of pathological tremor - University Research Fund 2022 for financing departmental development plans in the field of research. 27/07/2022 €10,000
- Funding from CONSORZIO FUTURO IN RESEARCH for research on "MODELLING AND EXPERIMENTAL MEASUREMENTS OF NON-LINEAR COMPLEX SYSTEMS AIMED AT THE ACTIVE CONTROL OF ESSENTIAL AND PARKINSONIAN TREMOR" 01/05/2022 €30870
- Project "International Higher Education School in NVH for Industry 4.0 Higher Education school in NVH for Industry 4.0" from 22/11/2021 to 31/12/2023 13750 €
- Individual funding of 3000€ for basic research activities REFERRED to ARTICLE 1, PARAGRAPHS 295 AND FOLLOWING OF LAW NO. 232 OF 11 DECEMBER 2016

He has participated in various international, European and national research projects:

- 2019 "DiaPro4.0 Diagnostic-Prognostic multi-sensor cost-effective system integrated in mechanical drives of Industry 4.0", POR-FESR 2014-2020ER
- 2018 "Omnidirectional earthquake isolation system", Ministry of Business, Innovation & Employment (New Zealand);
- 2016 "Integrated platform for the design and advanced production of industrial gearboxes - MetAGEAR" (PG/2015/732270) POR-FESR 2014-2020ER
- 2014 "FORTISSIMO, Experiment: HPGA", FP7 (applications for high performance computing);
- 2013 INDGEAR, FP7-SME (condition monitoring);

He teaches the courses of multibody dynamics in the master's degree course in mechanical engineering (industry 4.0 curriculum), Mechanical Vibration in the master's degree course Advanced Automotive Engineering and Mechanics of the Vehicle in the bachelor's degree course in vehicle engineering.

He has published 85 articles, has an h-index of 13 with 445 citations, and was nationally qualified for Full Professor in 2023

His research activities are in experimental tests, modelling and numerical simulations in complex nonlinear dynamics, linear and nonlinear vibration analysis of mechanical systems and nonlinear vibrations of structures and control. His research focused on chaos and nonlinear time series analysis, non-smooth dynamics, diagnostic, prognostic, predictive maintenance and condition monitoring of complex systems, fluid-structure interaction, the effect of thermal gradients and bioengineering. He is part of the Vibration, NVH and Powertrain Laboratory of the Department of Engineering "Enzo Ferrari".